J. M. P. Q. Delgado *Editor*

Hygrothermal Behaviour and Building Pathologies

Springer

Building Pathology and Rehabilitation

Volume 14

Series Editors

Vasco Peixoto de Freitas, University of Porto, Porto, Portugal

Aníbal Costa, Aveiro, Portugal

João M. P. Q. Delgado , University of Porto, Porto, Portugal

This book series addresses the areas of building pathologies and rehabilitation of the constructed heritage, strategies, diagnostic and design methodologies, the appropriately of existing regulations for rehabilitation, energy efficiency, adaptive rehabilitation, rehabilitation technologies and analysis of case studies. The topics of Building Pathology and Rehabilitation include but are not limited to - hygrothermal behaviour - structural pathologies (e.g. stone, wood, mortar, concrete, etc…) - diagnostic techniques - costs of pathology - responsibilities, guarantees and insurance - analysis of case studies - construction code - rehabilitation technologies - architecture and rehabilitation project - materials and their suitability - building performance simulation and energy efficiency - durability and service life.

More information about this series at http://www.springer.com/series/10019

J. M. P. Q. Delgado
Editor

Hygrothermal Behaviour and Building Pathologies

Editor
J. M. P. Q. Delgado
CONSTRUCT-LFC, Department of Civil
Engineering
University of Porto
Porto, Portugal

Preface

The hygrothermal behaviour of a building component or material exposed to weather is an important aspect of the overall performance of a building. In the case of a material, the hygrothermal behaviour can be defined as the change in functional properties that occur as a result of simultaneous heat and moisture exchange (with the surrounding environment) and storage within the material. The knowledge of the physical processes that define hygrothermal behaviour allows for the prediction of a building response to climatic solicitation and for the selection of envelope solutions that will lead to required feasibility.

Building pathologies originated by moisture are frequently responsible for the degradation of building components and can affect users' health and comfort. The solutions for treating moisture-related pathologies are complex and, many times, of difficult implementation. Several of these pathologies are due to innovative techniques combined with new materials of poorly predicted performance and the eventual identification of potential hidden defects is extremely useful, which can compromise the building's performance and, if identified late, can have very costly repairs or be out of warranty terms.

The main purpose of this book, *Hygrothermal Behaviour and Building Pathologies*, is to provide a collection of recent research works to contribute to the systematization and dissemination of knowledge related to construction pathology, hygrothermal behaviour of buildings, service life and diagnostic techniques and, simultaneously, to show the most recent advances in this domain. It includes a set of new developments in the field of building physics and hygrothermal behaviour, durability and numerical models applied to building materials analysed. The book is divided into six chapters that intend to be a resume of the current state of knowledge for benefit of professional colleagues, scientists, students, practitioners, lecturers and other interested parties to network. At the same time, these topics will be going to the encounter of a variety of scientific and engineering disciplines, such as civil, materials and mechanical engineering.

Porto, Portugal   J. M. P. Q. Delgado

Contents

Wetting and Drying Patterns in a Wet Moisture Reference Year Identified Using the Weinert's Index: Station Versus Gridded Data

Sneha Das and Kaustav Sarkar

Abstract Hygrothermal simulation of building elements requires consideration of pertinent meteorological parameters which can be accounted by apt identification of a Moisture Reference Year (MRY). There are different indices available for the identification of MRY which depend on the availability of relevant data which are often not available in the desired quality and quantity for the location of interest. This study describes the utility of Weinert's Index and gridded data for the identification of wet-MRYs across 10 locations in India. Weinert's Index indicate that the locations pertaining to the cold and hot-dry region of India exhibit the highest and the least severity respectively. The study subsequently compares the wetting and drying pattern exhibited by gridded and station records over the duration of the wet-MRY and its annual wet-spell. A novel wet-spell severity index has been developed to quantify the severity of encompassed wetting and drying patterns. Results reveal that gridded data offer a conservative representation of wet conditions at a location with the severity tending to differ in places bearing complex topography. The values of wet-spell severity index attributes the highest and lowest wetting drying severity to the locations considered in the warm-humid and hot-dry region respectively.

Keywords Moisture reference year · Weinert index · Gridded data · Wetting and drying pattern · Severity

S. Das · K. Sarkar (✉)
School of Engineering, Indian Institute of Technology Mandi, Kamand, Mandi 175005, Himachal Pradesh, India
e-mail: srkr@iitmandi.ac.in

S. Das
e-mail: D16031@students.iitmandi.ac.in

1

1 Introduction

The performance of built facilities is affected by the ambient conditions to which they get exposed to. Designing a structure for a desired level of service therefore requires the consideration of pertinent climatic variables, such as precipitation, solar radiation, temperature and relative humidity cycles, and wind. The persistent action of these variables on building elements compel a gradual change and eventually conjure deterioration in one form or the other based on their physical and chemical constitution (Parrott 1994; Neville 1995; Rozière et al. 2009; Charola 2000; Hobbs 1998; Li et al. 2009). The ambient moisture conditions in particular play an important role in regulating the weathering process (Andrade et al. 1999; Ryu et al. 2011). An appropriate identification of the exposure boundary conditions is, therefore, fundamental to the simulation of the hygrothermal performance of a building element and the prediction of its service life.

A typical reference year (TRY) or a typical meteorological year (TMY), conventionally constituted by averaging the available records of meteorological data is often considered adequate for estimating the long-term performance of an element. It, however, offers a deficient impetus if the goal is to study the impact of peak moisture influences (Kočí et al. 2014; Bilbao et al. 2004; Chan et al. 2006). Even though there are no fixed standards for the identification of a moisture reference year (MRY), it is a common consensus that an MRY should capture the climatic variability at a location and also the most severe wet and dry moisture conditions that may manifest on a structure (Cornick et al. 2003; Djebbar et al. 2001). The goal can be achieved with the direct use of pertinent meteorological variables or by working up their meaningful combinations to index the severity of individual years and select a wet, dry or an average MRY thereafter.

The magnitudes of annual rainfall, wind-driven rain, moisture carried by air in general or in excess of a specific threshold or its deficit with respect to that corresponding to saturation, have been widely used as simple indicators of ambient moisture loads (Lacy 1965; Narula et al. 2018; Blocken and Carmeliet 2004; Sanders 1996; Geving 1999). Indices based on the combination of two or more factors have also been used towards the indexing of ambient wetness and identification of MRY (Kočí et al. 2014; Cornick et al. 2003; Hagentoft and Harderup 1996; Salonvaara et al. 2010; Schindelholz and Kelly 2012; McCabe et al. 2013; Mukhopadhyaya et al. 2006). For instance, the temperature-humidity complex prescribed by Mukhopadhyaya et al. (2006), accumulates the product of the deviations in temperature and relative humidity with respect to their specified thresholds for mold growth, whenever both the deviations are simultaneously positive. In this case, the year with the highest value of the index would qualify as the MRY. The moisture index model given by Cornick et al. (2003) is further evolved in terms of the number of involved meteorological variables. The model is analogous to the calculation of a load resultant from its rectangular components as it applies a square root function to the sum of squares of normalized annual moisture loads corresponding to rain and humidity. These two components are calculated using the hourly deviations of rainfall and partial vapor

pressure with respect to the benchmark state of no rainfall and fully saturated air. A higher value of this moisture index, corresponds to a greater degree of ambient wetness and vice versa. The indices described hitherto primarily quantify ambient wetness and hence can be used to satisfactorily identify a wet-MRY. A dry-MRY corresponding to the lowest values of these indices would, however, be deficient in forming a critical drying scenario, since the indices do not incorporate the important influencing factors of solar radiation and wind speed.

A better representation of all the meteorological factors can be found in an index being referred to as the Weinert's index hereafter. The Weinert's index was originally constituted with the objective to classify the moisture severity in the context of the degradation of rocks and roads in South Africa (Weinert 1961, 1965, 1980). This index is, in fact, the ratio of potential evaporation of the warmest month of the year to the total annual rainfall. The numerator, therefore, implicitly accounts for the factors of temperature, relative humidity, solar radiation and wind speed. A higher value of this index is indicative of drier ambient conditions and vice versa.

The applicability of any of the above-mentioned approaches towards the identification of an MRY depends upon the availability of abundant meteorological data. More often than not, station records are not available for all locations and even when available are marred with the problem of missing data points. These shortcomings constitute a serious bottleneck for the designer who intends to compare the severity of moisture exposure over a region of interest. A viable solution to these shortcomings can be found in gridded datasets. These are spatially and temporally continuous interpolated products constituted by using ground observations and/or observations obtained from other sources like ships and satellites. Owing to the inherent strength of continuity, gridded data offers itself as a lucrative resource to enable the mapping of general moisture severity, especially over a region expected to present climatic diversity, and to identify the MRYs for all locations situated within the area. The reliable application of gridded data is, however, conditional to its efficiency in matching the overall severity and weather patterns exhibited by the nearby stations. In a tropical country, like India, an important weather pattern manifests in the form intermittent rains. The wetting and drying cycles concomitant to the exposure play a critical role in aggravating the evolution of moisture-induced degradation phenomena (Li et al. 2009; McCarter and Watson 1997).

2　Scope

The present study uses the Weinert's Index to identify MRYs for 10 different grids in India using datasets of 1° resolution spanning over the 30-year period of 1986–2015. As shown in Fig. 1, the chosen grids are distributed equally among the 5 climatic zones of the country (BIS 2005). Figure 1 also names the 10 stations, each located within a separate grid, which have been selected to facilitate the grid-to-point comparisons of overall severity and wetting and drying pattern concomitant to intermittent rains and Table 1 summarizes the geographical coordinates of station
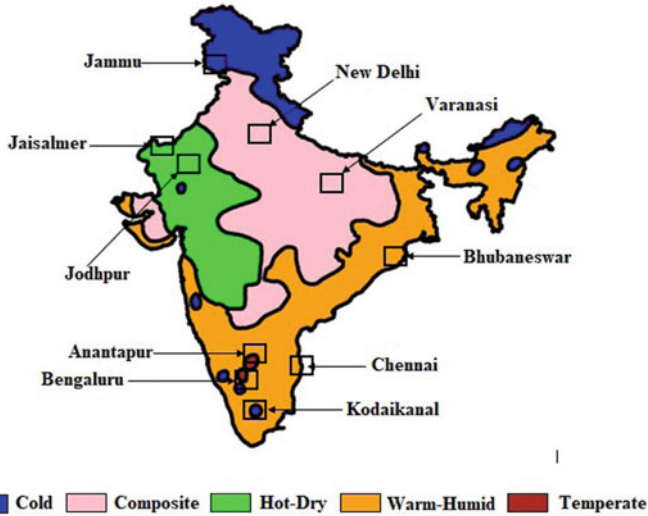
Fig. 1 Grid locations across different climatic zones along with the names of the enclosed stations

Table 1 Geographical Coordinates of stations and grids

S. No	Station name	Station lat./long.	Grid lat./long.	Grid-to-point distance (kms)
1.	Jammu	32.72/74.85	32.5/74.5	41
2.	Kodaikanal	10.23/77.48	10.5/77.5	30
3.	New Delhi	28.61/77.21	28.5/77.5	31
4.	Varanasi	25.31/82.97	25.5/82.5	52
5.	Jaisalmer	26.91/70.90	26.5/70.5	60
6.	Jodhpur	26.28/73.02	26.5/73.5	54
7.	Bhubaneswar	20.29/85.82	20.5/85.5	41
8.	Chennai	13.08/80.27	13.5/80.5	53
9.	Anantapur	14.68/77.60	14.5/77.5	23
10.	Bengaluru	12.97/77.57	12.5/77.5	53

and grids. For each grid-point pair, the evaluation has been carried out for the period of the entire year and for the annual wet-spell, the latter being especially important for tropical climates wherein the majority of rainfall events manifest in a distinct temporal cluster.

The grid-to-point comparison of wetting and drying patterns exhibit a better match over the period of a full year than in the annual wet-spell. Nevertheless, the mismatch is only caused due to conservative representation offered by gridded data wherein a larger number of days in the wet-spell appear as wet-rainy days. Furthermore, a novel wet-spell severity index was developed to quantify the difference in severity of the annual wet-spell in a grid-station pair. The wet-spell severity index identifies

Chennai (Warm-Humid) and Jaisalmer (Hot-Dry) grids to be on the highest and the lowest extremes of wetting and drying among the considered cases.

3 The Genesis of Weinert's Index

Weinert's index was originally developed in an attempt to quantify the severity of meteorological influences driving the degradation of natural rock formations and roads typically requiring the use of decomposed or disintegrated rock matter in South Africa (Weinert 1961, 1965, 1980). Field observations made on the weathering and performance characteristics of rocks and pavements revealed the existence of two distinct zones in the country separated by a North-South boundary running between 26°E and 27°E. The western part of this divide was noted to exhibit greater effects of weathering. Meteorological observations on air pressure, precipitation, temperature, relative humidity, and calculated values of potential evaporation, were used to compile separate contour plots with an intent to identify a climate border that would be in consonance with the delineated weathering and performance boundary. The isohyets of potential evaporation to precipitation ratio, $R = E_J/P_J$, corresponding to the warmest month (January) and of the annual precipitation (P_a), were found to succeed in achieving the goal. The intensity of natural weathering was, therefore, indexed using these parameters.

The summer rain was considered to be a more active agent of weathering relative to the winter rain. It was also necessary to account for the fact that stronger evaporation during summer reduces the period of moisture-induced deterioration. Thus, to constitute the index, the ratio R was weighted by a factor set to assume greater values in cases where the summer rain was dominant, $D = 12P_J/P_a$. The Weinert's index was, thus, constituted as, $N = R * D$, leading finally to the expression, $N = 12E_J/P_a$. The index assumed smaller values for a more severe moisture-exposure. It was suggested that potential evapotranspiration (PET) could be used in lieu of potential evaporation for the calculation of N as it would only change the numerical values of the index with no change in the pattern of the contours.

4 Methodology

The analysis was carried out in four steps. The first step was to identify a wet-MRY using gridded data. The second step involved the identification of annual wet-spell for the location using gridded and station data separately. In the third step, the similarity of wetting and drying pattern of the grid-MRY and its annual wet-spell were assessed with respect to the observations made at the encompassed station during the same year. The fourth step was implemented to ascertain if dissimilarity of the grid-MRY's annual wet-spell pattern was in the direction of a relatively greater or lesser severity

with respect to the station observations. This was facilitated by the development of a novel severity index.

4.1 Identification of a Wet-MRY

Since Weinert's *N* represents the moisture severity of prevailing climate and was constituted to effectively capture the weathering patterns on ground, it offers a strong criterion for the identification of MRY required to analyse the performance of exposed building elements. For the present study, the Weinert's *N* was defined as, $N = 365*$ PET_w/P_a. Here, PET_w refers to the PET of the warmest month in a given year - the month with the highest mean of daily average temperatures. *N* was calculated separately for all the years in the 30-year period of 1986–2015 at each of the 10 considered grids. Wet-MRY at each location was subsequently chosen as the year with the lowest value of *N*.

4.2 Identification of Annual Wet-Spell

The annual wet-spell is defined as the period of the year during which most of the rainfall occurs in tropics. The methodology proposed by Sarkar and Bhattacharjee (Sarkar and Bhattacharjee 2017) was used to facilitate the identification of the annual wet-spell. Firstly, a daily average rainfall series was generated by using daily records pertaining to the period of 1991–2011. The choice of this period was based on the availability of station data with the authors. The wet-spell was subsequently identified as the period which included the maximum number of rainy days (rainfall > 0 mm) while limiting the number of dry days to less than 2% of the wet-spell duration.

4.3 Wetting and Drying Patterns in a Wet-MRY

The similarity in wetting and drying patterns were evaluated in terms of the Sokal-Michener similarity index and its modified conservative form (Das et al. 2020). For this, the identified grid-MRY and the observations made at corresponding encompassed station for the same year were converted into binary series of '1 s' and '0 s', with '1' representing a wet-rainy day and '0' representing all other cases. A day was classified as wet-rainy if the amount of rainfall was greater than or equal to 2.5 mm. The threshold value of 2.5 mm was adopted based on the fact that an approximate evapotranspiration of 5 mm/day takes place under Indian exposure conditions (Singh 1986). The Sokal-Michener index and the modified Sokal Michner index are stated in Eqs. 1 and 2 respectively.

$$\text{Sokal-Michener Index:} \left[\frac{a+d}{a+b+c+d} \right] \tag{1}$$

$$\text{Modified Sokal-Michener Index:} \left[\frac{a+b+d}{a+b+c+d} \right] \tag{2}$$

where, a, b, c, d are the frequencies of '1-1', '1-0', '0-1', and '0-0' instances in a grid-station pair respectively. While Eq. 1 considers exact matches of rainfall pattern, Eq. 2 takes the case of '1-0' frequency as a favourable match as it allows for a conservative manifestation of rainfall events. Both the indices stated in Eqs. 1 and 2 lie in the range of [0, 1] with 1 representing an exact match of rainfall patterns. For each grid-point pair, the evaluation was carried out for the period of the entire year as well as for the annual wet-spell. For cases in which the start- and end-dates of the wet-spell were different across gridded and station datasets, the comparison was carried out for the duration between the earliest start-date and the latest end-date identified for the location.

4.4 Severity of Wetting-Drying Pattern

A novel index was developed for the assessment of severity of the wetting and drying pattern of an annual wet-spell as stated in Eq. 3.

$$\text{Severity Index:} \left(\frac{W+D}{365} \right) \times \left(\frac{W}{W+D} \right) \times p_{11} \tag{3}$$

where D and W are the total number of dry days and wet days in a wet-spell respectively, p_{11} is the conditional probability of consecutively manifesting wet-rainy days and can be calculated as $p_{11} = n_{11}/(n_{11} + n_{10})$, where, n_{11} and n_{10} are the number of consecutively occurring wet-rainy days and a dry day following a wet-rainy day in the annual wet-spell respectively.

In Eq. 3, the first term accounts for the duration of wet-spell in a given year. The longer the wet-spell, greater is the severity. The second term is a measure of the number of wet-rainy days during the wet-spell. Higher the value of this ratio, greater is the severity of the wet-spell on account of a greater number of rainfall events. The conditional probability term accounts for the tendency of wet-rainy days to manifest in the form of clusters. The larger the value of p_{11} greater would be the odds for wet-rainy days to form contiguous blocks leading to greater severity. The index would assume values in the range of [0, 1] with greater values representing a higher severity of wetting and drying in the location.

5 Data

The data used in this study were obtained from two different sources. The gridded records of rainfall and temperature were obtained from the India Meteorological Department (IMD), the public meteorological service of the country. Hourly records of rainfall for the 10 selected stations were also obtained from the IMD. PET data were obtained from the archives of the Climate Research Unit (CRU) running under the aegis of University of East Anglia, United Kingdom, on account of its unavailability from IMD. Further details of the data are summarized in the following sections.

5.1 Rainfall Data

The gridded dataset has been developed using the Shephard's Inverse Distance Weighing method (Shepard 1968) applied to a fixed network of 2140 stations for which a minimum of 40 years' of observations with less than 10% missing entries were available. In this method, a grid value is interpolated as the weighted average of observations from neighbouring stations located within a circular search area. The initial search radius (2°) was contracted or expanded so as to limit the number of contributing stations within a suitable range (1–4). The rainfall dataset being used in this study covers the entire Indian mainland with 357 square grids of 1° spatial resolution (~100 km) and has a daily temporal resolution over the period of 1951–2015 (Rajeevan et al. 2005).

The amounts of daily rainfall at the chosen stations were calculated using the hourly records obtained for the 21-year period of 1991–2011. To begin with, the missing data points in the hourly records were imputed barring those months in which more than 50% of the data points were missing and were deemed unfit for the present analysis. A two-pronged approach was adopted. If the data corresponding to the immediately preceding and succeeding hours of a missing entry were available, then, the mean of the two values was imputed at the missing point. In other cases, the missing data was substituted with the mean of all available observations corresponding to that hour of the year determined over the period of 1991–2011.

5.2 Temperature Data

The gridded dataset has been developed using the modified Shephard's angular distance algorithm applied to data obtained from 395 stations, for which a minimum of 10 years of daily records, each with at least 300 days of observations, were available. In this method, a grid value is interpolated as the weighted average of observations from neighbouring stations located within a circular search area constructed based on a correlation length scale. The search radius was contracted or expanded so

as to limit the number of contributing stations within a suitable range (4–10) (Srivastava et al. 2009). The temperature dataset being used in this study covers the entire Indian mainland with 357 square grids of 1° spatial resolution (~100 km) and has a daily temporal resolution over the period of 1951–2018.

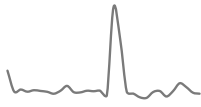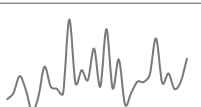## 5.3 Potential Evapotranspiration Data

PET is defined as the maximum possible amount of water vapor loss under a given climate from a clipped grass surface of height 0.12 m and a bulk surface resistance of 70 s m^{-1} (Allen et al. 1994). PET data used in this study is a derived parameter calculated at a station using a variant of the Penman-Monteith method (Harris et al. 2014). The gridded PET data for the chosen locations was obtained from CRU TS v4.03 which covers the entire globe, excluding the Antarctic region, at a spatial resolution of 0.5° (~50 km) for the period of 1901–2018. (Harris et al. 2014, 2020). The dataset has been developed by applying an angular distance weighing algorithm to stations for which 75% of the monthly values of mean daily PET were available in each decade starting from 1901 (Harris et al. 2020). The method interpolates a grid value as the weighted average of eight nearest stations lying within a correlation decay distance (Harris et al. 2014, 2020). The dataset was converted to 1° spatial resolution using bilinear interpolation to match the rainfall and temperature gridded datasets.

6 Results and Discussions

6.1 MRY

The grid specific minimum and maximum values of N, their variation over the 30-year period of 1986–2015, and the wet-MRYs are summarized in Table 2. It can be observed that the grids pertaining to the Cold region exhibit the highest level of severity. This can be attributed to the slower drying and higher precipitation in this region. This is followed by the Warm-Humid locations of Chennai and Bhubaneswar. The severity at these locations is due to heavy rainfall owing to their proximity to the coast. The locations belonging to the Composite and Temperate zones reflect similar level of severities. The least severity is exhibited by locations in the Hot-Dry regions on account of high temperature leading to faster drying, and low rainfall conditions.

Table 2 Characteristics of MRYs across 10 grids

Location	Climate zone	N		Variation of N over 1986–2015	Wet-MRY
		Min	Max		
Kodaikanal	Cold	0.47	29.08		2007
Jammu	Cold	0.76	3.19		2015
Chennai	Warm-Humid	1.00	5.22		2005
Bhubaneswar	Warm-Humid	0.98	2.85		1990
Bengaluru	Temperate	1.62	5.78		2005
Anantapur	Temperate	2.57	7.18		2007
Varanasi	Composite	1.95	11.41		1990
New Delhi	Composite	2.37	16.45		2003
Jodhpur	Hot-Dry	4.91	27.98		1997
Jaisalmer	Hot-Dry	6.36	70.94		2006

6.2 Wetting and Drying Pattern and Its Severity

The wetting and drying patterns in the wet-MRYs as identified in Table 2 could be compared for similarity at only 6 stations (Jaisalmer, Anantapur, Jodhpur, New Delhi, Kodaikanal, Chennai), due to unavailability of rainfall data for the corresponding years at other stations. The annual wet-spells needed to facilitate the comparison are shown in Fig. 2 wherein, the vertical bars at the top depict the wet-rainy days. It can be observed from Fig. 2 that the temporal manifestation wet-spell varies considerably across climatic zones. The Hot-Dry region exhibits the least wet-spell duration owing to scarce rainfall. On the other hand, Kodaikanal and Chennai show longer wet-spells.

The results of Sokal-Michener and the modified Sokal-Michner similarity indices are summarized in Table 3. Observations reveal that the strict similarity quantified by the Sokal-Michener index during the span of the year is better as compared to the annual wet-spell. The residual mismatch is contributed by n_{10} and n_{01} with the
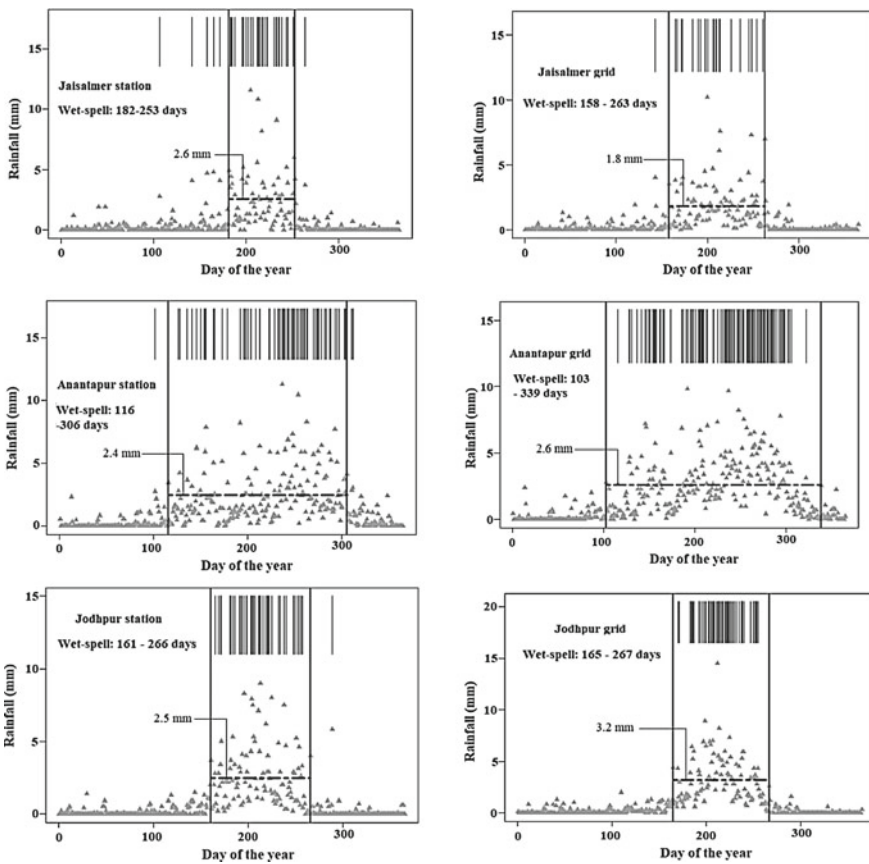
Fig. 2 Wet-spell characteristics
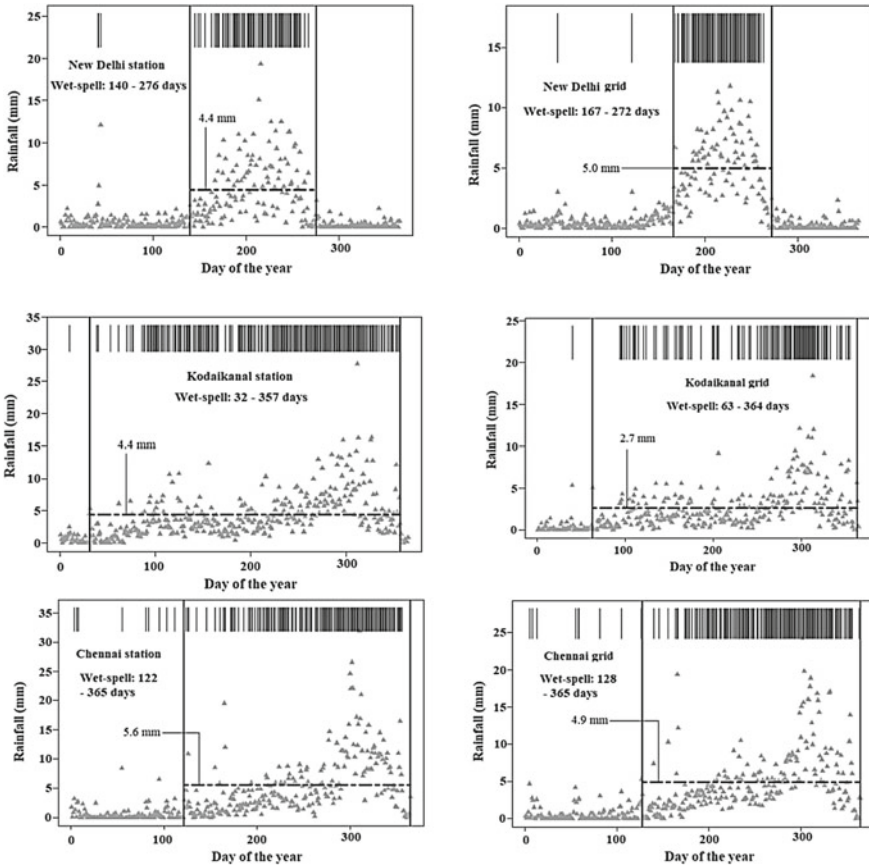
Fig. 2 (continued)

Table 3 Similarity indices

Location	Climate zone	Full year		Annual wet-spell	
		Sokal-Michner index	Modified Sokal-Michener index	Sokal-Michner index	Modified Sokal-Michener index
Jaisalmer	Hot-Dry	0.95	0.98	0.78	0.89
Anantapur	Temperate	0.90	0.94	0.86	0.93
Jodhpur	Hot-Dry	0.89	0.96	0.81	0.94
New Delhi	Composite	0.87	0.95	0.72	0.88
Kodaikanal	Cold	0.77	0.81	0.77	0.82
Chennai	Warm-Humid	0.65	0.87	0.50	0.83

Table 4 Severity index

Location	Climate zone	Severity index		Difference between grid-station
		Station	Grid	
Jaisalmer	Hot-Dry	0.019	0.011	−0.008
Anantapur	Temperate	0.055	0.052	−0.003
Jodhpur	Hot-Dry	0.016	0.036	0.019
New Delhi	Composite	0.058	0.068	0.011
Kodaikanal	Cold	0.124	0.044	−0.080
Chennai	Warm-Humid	0.107	0.216	0.110

former exceeding the latter in 5 out of 6 cases. Hence, the values of the modified index which are in the range of [0.81, 0.98], offers a conservative representation of wetting and drying.

The values of wet-spell severity indices for grid-station pairs of 6 locations are compared in Table 4. It can be observed that in 3 locations the severity assessed by the gridded dataset is higher whereas in the remaining 3 locations station dataset captures higher magnitude of severity. The maximum differences in severity in a grid-station pair are observed at Kodaikanal and Chennai. Here it is worth mentioning that Kodaikanal and Chennai have special topographic conditions. While the former is a hill station, the latter is coastal city. The observation indicates that topography can cause a significant difference among the gridded and station records. The wet-spell severity index applied to station and gridded datasets identifies Chennai (Warm-Humid) and Jaisalmer (Hot-Dry) grids to be on the highest and the lowest extremes of wetting and drying among the considered cases.

7 Summary and Conclusion

The objective of this study was to identify wet-MRYs by combining Weinert's Index with gridded data and to subsequently compare their wetting and drying patterns and the severity of annual wet-spell with respect to the station data. A novel wet-spell severity index was developed to quantify the severity of the wetting and drying pattern. The developed index accounts for the length of the annual wet-spell, the number of wet-rainy days contained in that period, and the conditional probability of occurrence of wet-rainy days on consecutive days. The main findings and conclusions of this study are summarized as follows:

- Since Weinert's Index cumulates the effect of various meteorological factors contributing towards the wetting and drying of building elements, the index could be effectively used towards the identification of MRY.
- The calculated values of Weinert's Index indicate that the locations pertaining to the cold region of India have the highest severity while those pertaining to the

hot-dry regions exhibit least severity. The other three climatic zones, temperate, warm-humid, and composite are intermediate between these two extremes.

- The grid-to-point comparison of wetting and drying patterns exhibit a better match over the period of a full year than in the annual wet-spell. Nevertheless, the mismatch is only caused due to conservative representation offered by gridded data wherein a larger number of days in the wet-spell appear as wet-rainy days.
- It was observed that the annual wet-spell severity of gridded and station records tends to differ significantly in locations with special topographic conditions. However, the direction of the deviation was observed to be random.
- The wet-spell severity index identifies Chennai (warm-humid) and Jaisalmer (hot-dry) grids to be on the highest and the lowest extremes of wetting and drying among the considered cases.

References

Allen RG, Smith M, Perrier A, Pereira LS (1994) An update for the definition of reference evapotranspiration. ICID Bull 43(2):1–34

Andrade C, Sarría J, Alonso C (1999) Relative humidity in the interior of concrete exposed to natural and artificial weathering. Cement Concr Res 29(8):1249–1259

Bilbao J, Miguel A, Franco J, Ayuso A (2004) Test reference year generation and evaluation methods in the continental mediterranean area. J Appl Meteorol 43(2):390–400

Blocken B, Carmeliet J (2004) A review of wind-driven rain research in building science. J Wind Eng Ind Aerodyn 92(13):1079–1130

Chan AL, Chow TT, Fong SK, Lin JZ (2006) Generation of a typical meteorological year for Hong Kong. Energy Convers Manag 47(1):87–96

Charola AE (2000) Salts in the deterioration of porous materials: an overview. J Am Inst Conserv 39(3):327–343

Cornick S, Djebbar R, Dalgliesh WA (2003) Selecting moisture reference years using a moisture index approach. Build Environ 38(12):1367–1379

Das S, Narula P, Sarkar K (2020) Design of intermittent rainfall-pattern for structures with gridded data: validation and implementation. J Build Eng 27:100939

Djebbar R, van Reenen D, Kumaran MK (2001) Indoor and outdoor weather analysis tool for hygrothermal modelling. In: 8th conference on building science and technology, Toronto, Ontario, pp 139–157)

Geving S (1999) Moisture design of building constructions: hygrothermal analysis using simulation models

Hagentoft CE, Harderup E (1996) Climatic influences on the building envelope using the Π factor. In: IEA-Annex 24 Hamtie Task 2, environmental conditions

Harris IPDJ, Jones PD, Osborn TJ, Lister DH (2014) Updated high-resolution grids of monthly climatic observations—the CRU TS3. 10 dataset. Int J Climatol 34(3):623–642

Harris I, Osborn TJ, Jones P, Lister D (2020) Version 4 of the CRU TS monthly high-resolution gridded multivariate climate dataset. Sci Data 7(1):1–18

Hobbs DW (1998) Minimum requirements for durable concrete: carbonation-and chloride-induced corrosion, freeze-thaw attack and chemical attack

Kočí J, Maděra J, Černý R (2014) Generation of a critical weather year for hygrothermal simulations using partial weather data sets. Build Environ 76:54–61

Lacy RE (1965) Driving rain maps and the onslaught of rain on buildings. In: Proceedings of the CIB/RILEM symposium on moisture problems in buildings, Helsinki

Li K, Li C, Chen Z (2009) Influential depth of moisture transport in concrete subject to drying–wetting cycles. Cement Concr Compos 31(10):693–698

McCabe S, Brimblecombe P, Smith BJ, McAllister D, Srinivasan S, Basheer PAM (2013) The use and meanings of 'time of wetness' in understanding building stone decay. Q J Eng Geol Hydrogeol 46(4):469–476

McCarter WJ, Watson D (1997) Wetting and drying of cover-zone concrete. Proc Inst Civil Eng-Struct Build 122(2):227–236

Mukhopadhyaya P, Kumaran K, Tariku F, Van Reenen D (2006) Application of hygrothermal modeling tool to assess moisture response of exterior walls. J Archit Eng 12(4):178–186

Narula P, Sarkar K, Azad S (2018) Indexing of driving rain exposure in India based on daily gridded data. J Wind Eng Ind Aerodyn 175:244–251

Neville A (1995) Chloride attack of reinforced concrete: an overview. Mater Struct 28(2):63

Parrott LJ (1994) A study of carbonation-induced corrosion. Mag Concr Res 46(166):23–28

Rajeevan M, Bhate J, Kale JD, Lal B (2005) Development of a high resolution daily gridded rainfall data for the Indian region. Met Monogr Climatol 22:2005

Rozière E, Loukili A, El Hachem R, Grondin F (2009) Durability of concrete exposed to leaching and external sulphate attacks. Cem Concr Res 39(12):1188–1198

Ryu DW, Ko JW, Noguchi T (2011) Effects of simulated environmental conditions on the internal relative humidity and relative moisture content distribution of exposed concrete. Cement Concr Compos 33(1):142–153

Salonvaara M, Sedlbauer K, Holm A, Pazera M (2010) Effect of selected weather year for hygrothermal analyses. In: Proceedings of thermal performance of the exterior envelopes of whole buildings XI. Atlanta: American Society of Heating, Refrigerating and Air-Conditioning Engineers, Inc

Sanders C (1996) Environmental conditions, final report. Task 2. In: International energy agency. Energy conservation in buildings and community systems, Annex, p 24

Sarkar K, Bhattacharjee B (2017) Modeling of tropical rainfall exposure for the study of moisture penetration in porous building materials. J Hydrol Eng 22(8):04017017

Schindelholz E, Kelly RG (2012) Wetting phenomena and time of wetness in atmospheric corrosion: a review

Shepard D (1968) A two-dimensional interpolation function for irregularly-spaced data. In: Proceedings of the 1968 23rd ACM national conference, pp 517–524

Singh N (1986) On the duration of the rainy season over different parts of India. Theoret Appl Climatol 37(1–2):51–62

SP I (2005) 7: national building code of India. Bureau of Indian Standards, New Delhi

Srivastava AK, Rajeevan M, Kshirsagar SR (2009) Development of a high resolution daily gridded temperature data set (1969–2005) for the Indian region. Atmos Sci Lett 10(4):249–254

Weinert HH (1961) Climate and weathered Karroo dolerites. Nature 191(4786):325–329

Weinert HH (1965) Climatic factors affecting the weathering of igneous rocks. Agric Meteorol 2(1):27–42

Weinert HH (1980) Natural road construction materials of Southern Africa. CSIR

Knee Point Detection in Water Absorption Curves: Hygric Resistance in Multilayer Building Materials

A. C. Azevedo, J. M. P. Q. Delgado, A. S. Guimarães, I. Ribeiro, and R. Sousa

Abstract The moisture transfer process in multilayered building components with an interface is very different than the moisture transfer considered when having different materials/layers separately. Quantifying moisture transfer in multi-layered systems through numerical simulations is essential to predict the real behaviour of those building materials in contact with moisture, which depends on the climatic conditions. Unfortunately, the contact phenomenon is neglected in numerical simulations which compromise the feasibility of the results. In this work, the moisture transfer in multi-layered building components is analysed in detail, for perfect contact and hydraulic contact interface. The "knee point" was detected, numerically, in water absorption curves and the moisture-dependent interface resistance was quantified and validated for transient conditions. The methodology proposed to detect the "knee point" can be also used in the future for different multilayer materials with an interface, in order to obtain more correct maximum hygric resistance values, to be used in future numerical simulations.

Keywords Moisture transfer · Water absorption · Knee point · Interface · Hygric resistance · Numerical simulations

---

A. C. Azevedo · J. M. P. Q. Delgado (✉) · A. S. Guimarães · I. Ribeiro
Departamento de Engenharia Civil, Universidade Do Porto, Rua Dr. Roberto Frias, S/N, 4200-465 Porto, Portugal
e-mail: jdelgado@fe.up.pt

A. C. Azevedo
e-mail: antonio.costaazevedo@fe.up.pt

A. S. Guimarães
e-mail: anasofia@fe.up.pt

I. Ribeiro
e-mail: iribeiro@fe.up.pt

R. Sousa
Universidade Do Porto, Rua Dr. Roberto Frias, S/N, 4200-465 Porto, Portugal
e-mail: rtsousa@inesctec.pt

17

1 Introduction

Moisture transfer in construction building components is fundamental for the durability of built elements, influencing the thermal behaviour and consequently the energy consumption in the building and occupants' health by the air quality. There are such demonstrative problems due to moisture like frost/defrost damage in facades, mould on interior surfaces, fungus in floors and walls by rising damp, deterioration in floors and walls by flood occurrences, degradation of walls and roofs by internal condensations, etc.

For example, the study of rising damp phenomenon allowed the investigation of a technique to solve this problem that can already be used, with the necessarily revisions, to treat building walls after a flood (Delgado et al. 2016; Barreira et al. 2016 Guimarães et al. 2012, 2013; Freitas et al. 2011. In Portugal we have historical buildings near water courses with degraded walls by the permanence of water. Moisture in buildings can have different origins and rising damp is probably the most current one. Floods are extreme occurrences but can introduce large amounts of water in the walls. In conclusion, rising damp, because of its high occurrence frequency, and floods, because of the seriousness of their consequences, represent both a high risk in terms of building humidity.

The analysis of moisture migration in building materials and elements is crucial for its behaviour knowledge also affecting its durability, waterproofing, degradation and thermal performance. A building wall, generally, consists of multiple layers, and thus the investigation of the moisture transfer presumes knowledge about the continuity between layers. de Freitas (1992, 1996) considered three different interfaces configurations:

1. Perfect contact—when there is contact without interpenetration of both layers porous structure;
2. Hydraulic continuity—when there is interpenetration of both layers porous structure;
3. Air space interface—when there is an air box of a few millimetres wide between layers.

In resume, the most common interfaces types are perfect contact (ex: blocks in contact), hydraulic contact (mortar between the masonry blocks) and air space. It is necessary to have thorough knowledge regarding the building constituent material (red clay, concrete, granite, etc.).

Derdour et al. (2000) analysed the effect of thickness, porosity and the drying conditions of several building materials on the drying time constant. Bednar (2002) studied the influence of the following properties: material size and insulation, and climate conditions on the liquid moisture transport coefficient during drying experiments. Karoglou et al. (2005) evaluated the effect of environmental conditions, such as air temperature, air relative humidity and air velocity, on the drying performance of 4 stone materials, 2 bricks and 7 plasters. However, the study of multilayered masonry walls with imperfect contact, as the hydraulic interface, is practically inexistence in literature.

Considering the contact phenomena in multi-layered building components, like brick-mortar composites, or even mortar-brick-isolation-mortar solutions, the moisture transfer process and the obtained values differs from the moisture transfer considered when having different materials/layers separately (de Freitas 1992). In fact, the interface promotes a hydric resistance which means that becomes a slowing of the moisture transport across the material interface. The study of liquid transport across this interface configuration (ceramic brick and mortar) implies the correct knowledge of the hygrothermal mechanical and thermal properties of the build materials employed.

There is still a high unawareness regarding the influence of the interfaces between layers. Some studies which have been carried out conclude that it is important to analyse and consider the interface correctly. In the hydraulic contact like, for example, a mortar joint, it is important to understand that in the curing process water will be transported (Davison 1961; Groot 1995; Holm et al. 1996; Brocken et al. 1998; Hendrickx et al. 2009; Derluyn et al. 2011) which contributes to the modification of mortar properties. More, there is an interpenetration between the solid structural material that is in contact with the mortar which means that occurs changing in the pore structure of the material in contact (Brocken et al. 1998; Derluyn et al. 2011), in a certain thickness. This result in the continuity of the pore structure, i.e., the thermal and hydric flows that go out by layer 1 is the same that go in layer 2. There is continuity in capillary pressure but the water content in the first layer is different from the water content in the second layer.

In numerical simulations, some authors include hydraulic contact phenomena. As example, Brocken (1998) calculates only a change in the mortar properties neglecting the change in contact properties by assuming a perfect hydraulic interface contact. Qiu et al. (2003) and de Freitas et al. (1992) only consider an interface resistance, however, Derluyn et al. (2011) consider both cases, a change in mortar properties and an interface resistance.

Thus, the interface resistance can be calculated experimentally by the mass variation curve as a function of time, in a water absorption test, and correspond to the curve pendant after hit the discontinuity, i.e. the interface. The problem is to correctly detect the pendant which can be made if the "knee point" (transition) can be reached.

In this paper, the moisture transfer in multi-layered building components is analysed. The existence of different types of interfaces (perfect contact and hydraulic contact interface) contributes to different means of moisture transport when compared to a monolithic porous element. As examples, the "knee point" was detected in water absorption curves of multi-layered building components with different interfaces. It was presented a "knee point" measurement procedure, which is automatic and has proved to be accurate. To fully achieve this objective, herein it is proposed the use of an automatically changing point detection method to assist the water absorption analysis. In fact, the manual procedure can be highly time-consuming. In addition to the time saved, there is, as well, still an increase in accuracy, which does not depend on the result of the operator. This methodology to detect the "knee point" can also be used in the future for different materials with interfaces.

Finally, the moisture-dependent interface resistance between brick building components was quantified and validated for transient conditions which mean that can be used for future numerical simulations.

2 Moisture Transfer Across Material Interfaces

Moisture transfer across material interfaces is influenced by a number of phenomena and directly depends on the interface type. In the hydraulic contact like, for example, a mortar joint, it is important to understand that in the curing process water will be transported (Davison 1961; Groot 1995; Holm et al. 1996; Brocken et al. 1998) which contributes to the modification of the mortar properties. Concurrently, there is an interpenetration between the solid structural material that is in contact with the mortar which means that occurs changing in the pore structure of the material in contact with mortar (Hendrickx et al. 2009; Derluyn et al. 2011), in a certain thickness. This results, for hydraulic contact, in a continuity of the pore structure where the thermal flow that goes out in the layer 1 is the same that goes in the layer 2, there is continuity in temperature profiles, the hygric flow that goes out in the layer 1 is the same that goes in in the layer 2 and there is continuity in capillary pressure but the moisture content in the first layer is different from the moisture content in the second layer ($W_1 \neq W_2$). In hydraulic contact phenomena, the equality of the capillary pressure ($P_{c1} = P_{c2}$) allows the determination of a relation between the moisture content of both materials ($W_1 = R.W_2$), in the interface, through a function $R(P_c)$ that can be determined as sketched in Fig. 1.
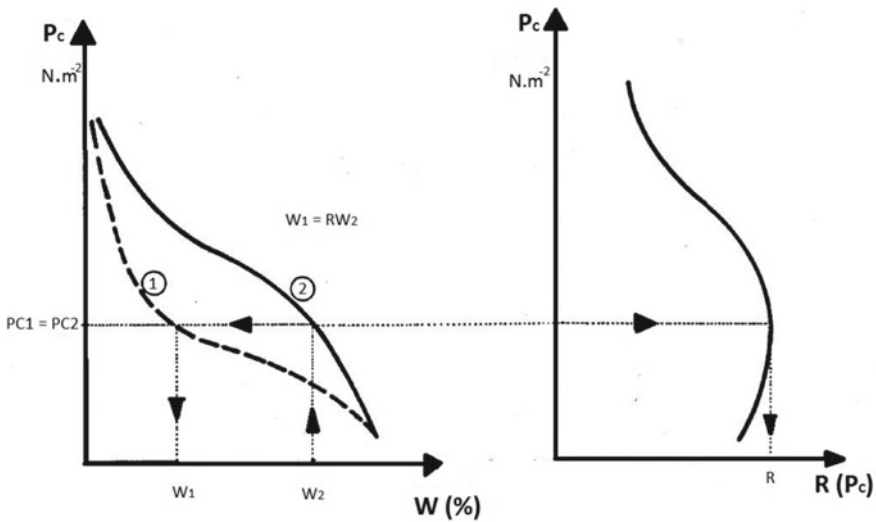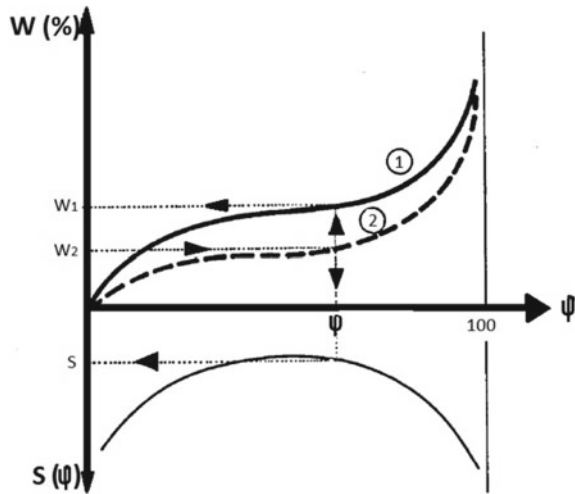

Fig. 1 Function R determination

Fig. 2 Function S
determination

In the air space interface where two solid layers are separated by an air space with some millimetres it can be considered that, in isothermal regime, the hygric flow that goes out in the layer 1 is the same that goes in in the layer 2 being this value limited by the maximum vapour value transported by the air space that depends on the vapour pressure of both surfaces and on the air thickness. In addition, if the water content of the layer with higher value is lower than the critical water content (W_{cr}) there is continuity in the relative humidity in the air space interface $\varphi_1 = \varphi_2$, if the water content of one layer is higher than the Wcr the other layer presents a water contact that goes to the critical value of that material. The equality of the relative humidity $\varphi_1 = \varphi_2$ means that it can be established a relation between the water content in the interface ($W_1 = S.W_2$) considering a function S that can be determined as described in Fig. 2.

In numerical simulations, when more than one consolidates material is separated by air space there is a capillary break that avoids the transport of liquid water being all the transport made in the vapour phase. In the perfect contact, i.e., a contact without interpenetration of both layers' porous structure, it can be assumed that there is continuity of temperature and equality of thermal flows at the entrance and exit, on the interface. About the humidity, experimental studies showed that the discontinuity of the porous structure generates a hygric resistance that imposes a maximum flow transmitted, FLUMAX, $Fhum_1 = Fhum_2 \leq$ FLUMAX. In addition, the capillary pressure is different in both interface materials.

In numerical simulations, it must be considered a hygric resistance that imposes a maximum flow transmitted, FLUMAX, which should be calculated experimentally. In practice, however, commonly neither a change in material properties nor interface resistances are taken into account in the current numerical simulations. Only a limited number of studies have determined an interface resistance (Qiu et al. 2003; Brocken 1998) or analysed the change in mortar properties (Derluyn et al. 2011; Brocken

1998; Vereecken and Roels 2014) while both are probably strongly case-dependent; furthermore, those studies all assume a constant value for the interface resistance. Particularly, in perfect contact and hydraulic contact interface a limited number of studies have determined an interface resistance considering the difficulty and time consuming experimental test that should be made to estimate this parameter.

3 Materials and Methods

The water absorption curve increases over time and then presents instants (points of change) where the rate of absorption seems to decrease significantly. These instants correspond to the contact of the water with a different material (contact with the interface). Only one point of change is expected for the interfaces in perfect contact and air space interface (see Fig. 3a), different from what happens with for the hydraulic interfaces (see Fig. 3b) where we can observe two discrete knees, one before the interface and another when the interface is saturated.

This study can be applied to other cases of interfaces. This generalization will be presented later. Since the goal is to address the effect of the interface in water absorption, the water resistance is measured immediately after the first changing point, which is the time interval of interest. The final measurement is performed by calculating each Hygric Resistance (RH). Figure 4 depicts how the several values are measured.

Considering this measuring procedure, it is important to detect the exact time instant of the "knee point" automatically and with some precision. In the literature, there are several methods of knee or jump point detection (Ville Satopaa et al. 2011; Wang and Tseng 2013; Zhao et al. 2008a, b; Christopoulos 2014; Du et al. 2014). The following three methods were taken into consideration to develop the algorithm presented in this work. The choice of these methods took into account the fact that there are discrete methods, intuitive and easy to implement, available in the literature. The following two methods were considered to develop the algorithm presented in this work:

- **1st Method**: This method considers a line which passes through the two extreme points observed (x_0 and x_n). It also considers a set of line segments perpendicular
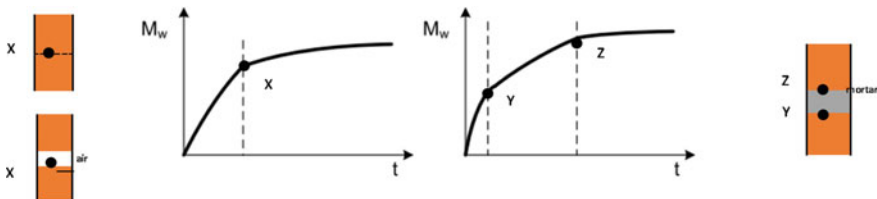
Fig. 3 Water absorption curve and the changing instant, knee point
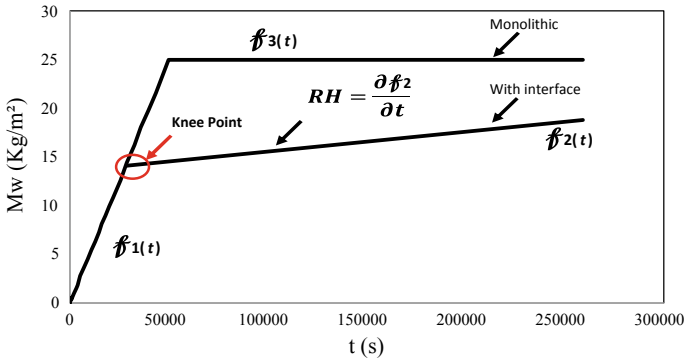
Fig. 4 Method for hygric resistance measurements

Fig. 5 Knee point determination by the 1st method
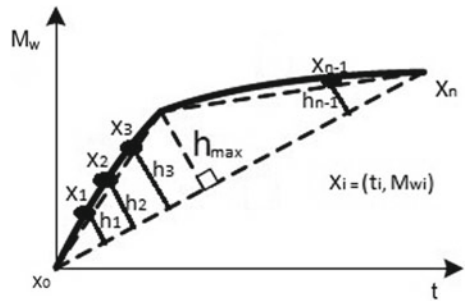
to this line, where each line segment begins at an observed point ($x_i = (t_i, Mw_i)$) and ends at a point of the line. The knee point is defined as the point related to the greater segment (Ville Satopaa et al. 2011), as described in Fig. 5 and Annex 1—SEC.Program (an algorithm developed by the authors).

- **2nd Method**: In this method, the point where the pair of lines that best approaches the curve is called "knee". For its determination, it is necessary to perform, for each point ($x_i = (t_i, Mw_i)$) of the curve, two linear fittings, one for all points to the left of x_i and one for all points to the right of x_i. The knee is considered the point that minimizes the sum of the errors for the two fittings. This method is implemented in Matlab in a function called "knee-pt.m".

- **3rd Method**: This method is a combination of the two methods previously presented. Since the main goal of the algorithm proposed is to find the "knee" point of a set of points $x_i = (t_i, M_{wi})$, $i = 1, 2, …, n$ obtained in the measuring procedure, where the data errors should be taken into account, the combination of the two previously presented methods can give a better knee point.

- The steps of this algorithm are (see Annex 2—Hybrid.program, an algorithm developed by the authors):

1. Use the 1st Method to calculate, for each point obtained in the measuring procedure, the length of the line segment that is perpendicular to the line that connects the two extreme points of the set. Sort the length of perpendicular line segment by a decreasing order. Let $M1$ be the set of indices of the points corresponding to this ordering.

2. Use the 2nd Method to determine the sum of the errors for the two linear fittings found for each point obtained in the measuring procedure. Sort the sum of the errors for the two linear fittings by an ascending order. Designate by $M2$ the set of indices of the points associated with this ordering.

3. Determination of the knee point. Find the point $x_i = (t_i, M_{wi})$ whose index, i, occupies the best positions in sets M_1 and M_2, using the following algorithm:

   – **Step 0**—Let $k = 1$ be the position of an element in a set, $i = 1$ an index position and n the total number of points obtained in the measuring procedure.
   – **Step 1**—If $i > k$, let $j = 1$ and go to **Step 3**.
   – **Step 2**—If $M1(k) = M2(i)$, the knee point is $(t(M1(k)), Mwi(M1(k)))$ and **Stop** the algorithm. Otherwise, let $i = i + 1$ and return **Step 1**.
   – **Step 3**—If $j \geq k$, go to **Step 5**.
   – **Step 4**—If $M2(k) = M1(j)$, the knee point is $(t(M2(k)), Mwi(M2(k)))$ and **Stop** the algorithm. Otherwise, let $j = j + 1$ and return **Step 3**.
   – **Step 5**—Let $k = k+1$. If $k > n$, an error message must be sent. Otherwise, let $i = 1$ and return **Step 1**.

4 Experimental Setup

The experimental procedure has been described to guarantee consistent measurements of hygric resistance in multilayer building materials and to "knee point" detection in water absorption curves. The hygric resistance was determined after the knee point of several curves, and for each curve, it was computed several dispersion measures to evaluate the consistency. The measures were the coefficient of variation.

In this work, two different ceramic blocks of red brick were tested with a sample similar size: ceramic A with $4 \times 4 \times 10$ cm and ceramic B with $5 \times 5 \times 10$ cm (see Fig. 6). Several standards can be applied for the experimental determination of bulk density, as ISO 10545-3 (1995) for ceramic tiles, EN 12390-7 (2009) for concrete, EN 772-13 (2000) for masonry units. The samples must be dried until a constant mass is reached. The samples volume was calculated based on the average of three measurements of each dimension.

Porosity or void fraction is a measure of the void spaces in a material, and is a fraction of the volume of voids over the total volume, between 0 and 1 (see Fig. 7). The standard ISO 10545-3 (1995) for ceramic tiles was used to measure the bulk porosity. The building materials porous characteristics have an important influence on the mechanisms of moisture transfer. The porous network, formed by cavities and channels, is the medium through which a fluid (liquid or vapour) are propagated. This
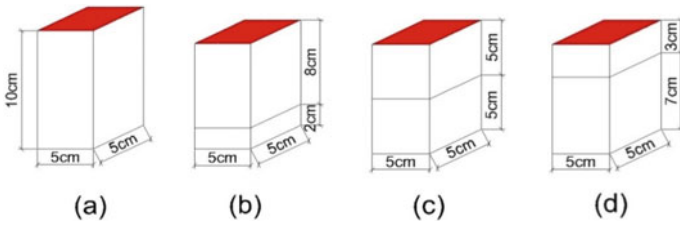
Fig. 6 Specimen's designation and configuration—water absorption tests

Fig. 7 Material porous structure
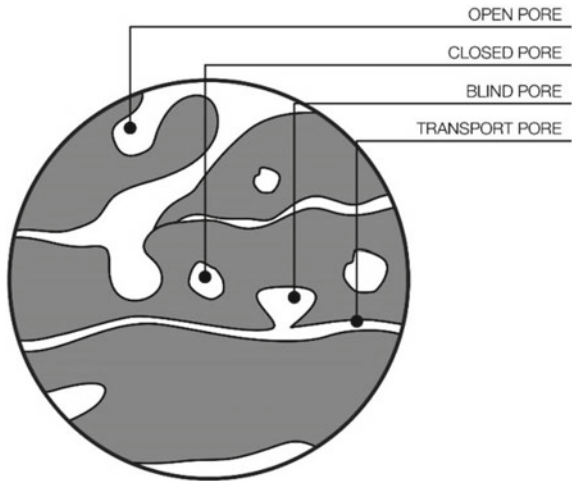
type of porosity, called open porosity, is characteristic of most building materials. In this study, it was used an automated mercury porosimeter (Poremaster-60 Quantachrome) and a helium pycnometer The mercury porosimeter allowed to determine the pore size distribution up to 0.0035 micrometres in diameter, as well as the total surface area normalized to the sample mass and bulk density.

It is important to be noted that there is a relation between the mortars and the sample properties in the masonry performance related to water penetration resistance. The mortar properties considered in the study include compressive strength, workability, water retention, and porosity. The properties of masonry elements include surface texture; porosity and the initial rate of absorption (Ghosh and Melander 1991).

Since the building walls present mortars with average values of porosity and a large number of pores that allow the capillary action and movement of water inside the coating system, the presence of moisture can be observed, mainly in the lower part of the walls. Mortars are characterized by the presence of voids within the materials (pores), which may vary according to the water/cement ratio, as well as the granulometry of the aggregates used in the mortar.
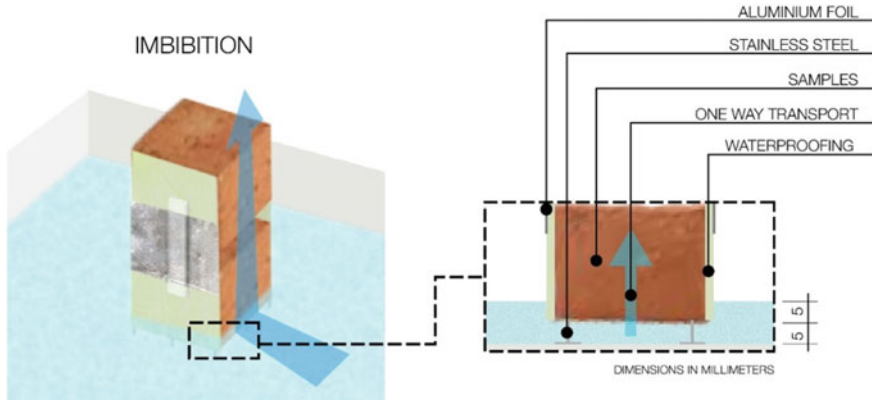
Fig. 8 Imbibition model used in the research

The moisture transport is strongly dependent on the complex morpho-optic aspect of the porous space. The pores, free spaces distributed inside the solid structure, characterize the permeability of the medium, allowing the fluid flow (Mendes and Philippi 2005).

The experiments to determine the interface influence, conducted in this study, are guided by the outline of the partial immersion method as explained by the standard ISO 15148 (2002). Specimens of two different red bricks, A and B, were tested (see Fig. 8). During the tests, the temperature and the relative humidity was also measured (see Fig. 8).

$$T(°C) \approx 23 \text{ and } \varphi\,(\%) \approx 50$$

All the specimens were sealed in the lateral faces with an epoxy coating to avoid the evaporation through these sides and assure the unidirectional moisture flow from the bottom to the specimens' top surface.

Capillary absorption data were obtained by placing samples in distilled water. Their base was submerged only a few millimetres (~1–5 mm) in order to avoid build-up of hydrostatic pressure. The environmental laboratory conditions were approximately 23 °C of temperature and 50% of relative humidity (φ), during the experiments duration. Experiments were conducted for immersion periods from several minutes to about 20 days. The samples were placed in a constant-temperature water bath controlled within ±0.5 °C to avoid changes in liquid viscosity that might affect the absorption rate (Mukhopadhyaya et al. 2002; Delgado et al. 2006; Guimarães et al. 2018). After soaking, the moisture content of samples was calculated based on the increase in the sample weight at corresponding times. For this purpose, at regular time intervals, ranging from 5 min at the beginning to 12 h during the last stages of the process, the samples were rapidly removed from the water bath and superficially dried on a large filter paper to eliminate the surface liquid. The samples were then weighed

to determine the moisture uptake. The samples were subsequently returned into the analysed solution via wire mesh baskets and the process was repeated, consequently.

5 Results and Discussion

In this study, two different ceramic blocks of red brick were tested with similar size samples: ceramic A with $4 \times 4 \times 10$ cm^3 and ceramic B with $5 \times 5 \times 10$ cm^3. The density and porosity of the tested materials were measured carefully and the obtained values are summarized, in Table 1. Also, Table 1 presents the absorption coefficients obtained, i.e., 0.10 kg/m^{2}s$^{0.5}$ and 0.19 kg/m^{2}s$^{0.5}$, for the monolithic samples of red brick type "A" and "B", respectively (see Fig. 8). The absorption coefficient of red brick type "B" is approximately two times higher, an expectable result as the density of this material is greater than the density of red brick type "A". The water vapour diffusion resistance factor, μ, is given by $\mu = \delta_p / \delta_a$, where δ_a is the vapour permeability of the air. The results obtained showed that the average values of the water vapour diffusion resistance factor for ceramic block A samples were in the order of 33.1 (corresponding to 5.94×10^{-12} kg/msPa) for drycup, while for ceramic block "B" samples it was 21.4 (corresponding to 9.07×10^{-12} kg/msPa) for the drycup. For these values, it is possible to conclude that the ceramic block "B" samples always presented lower values of water vapour diffusion resistance factor when compared to the ceramic block "A" samples.

Table 1, also, described the experimental results obtained for the physical and hygrothermal characterization of cement mortar and lime mortar samples analysed.

Table 1 Properties of red brick A, red brick B and mortars tested

Physical properties	Red brick A	Red brick B	Cement mortar	Lime mortar
Density, ρ (Kg/m^3)	1800	1600	1878	1810
Porosity, ε (m^3/m^3)	0.32	0.38	0.20	0.21
Water absorption coefficient, A (kg/m^2 s$^{1/2}$)	0.10	0.19	0.15	0.12
Water vapour permeability, δ_p (kg/msPa)	5.94×10^{-12} (dry) 7.98×10^{-12} (wet)	9.07×10^{-12} (dry) 12.3×10^{-12} (wet)	1.07×10^{-11} (dry) 1.15×10^{-11} (wet)	1.47×10^{-11} (dry) 1.50×10^{-11} (wet)
Water vapour diffusion resistance factor, μ (-)	33.1 (dry cup) 24.9 (wet cup)	21.4 (dry cup) 15.6 (wet cup)	17.9 (dry cup) 16.6 (wet cup)	13.1 (dry cup) 12.7(wet cup)
Diffusion-equivalent air-layer thickness, s_d (m)	0.61 (dry cup) 0.48 (wet cup)	0.3 (dry cup) 0.29 (wet cup)	0.38 (dry cup) 0.35 (wet cup)	0.27 (dry cup) 0.26 (wet cup)
Moisture content, w (kg/m^3)	$w_{80\%} = 15.51$ $w_{\text{sat.}} = 261.38$	$w_{80\%} = 9.75$ $w_{\text{sat.}} = 233.07$	$w_{80\%} = 38.16$ $w_{\text{sat.}} = 228.59$	$w_{80\%} = 8.16$ $w_{\text{sat.}} = 186.61$

The results showed that the two mortars tested present similar values of bulk density and porosity, however, cement mortar presents highest values of moisture content, $w_{80\%}$ and w_{sat} and lower values of water vapour permeability.

The average mass variation per contact area in the capillary absorption process for the mortar samples tested. The experimental assessment of the water absorption coefficients showed a slight difference of values between the two mortars tested. The averages values obtained are 0.153 ± 0.012 kg/m^2 s$^{0.5}$ and 0.124 ± 0.002 kg/m^2 s$^{0.5}$, for cement mortar and lime mortar, respectively. The coefficient of variation found for each set of identical samples was approximately 7.8% for cement mortar and 1.4% for lime mortar.

A schematic plot of the increase in weight of the test specimen versus the time indicates that the specimen weight increases before it comes close to the saturation limit (see Figs. 9 and 10). These Figures show that the samples with perfect contact and hydraulic contact interface present similar behaviour, before the interface, with the monolithic samples, however, when water reaches the interface a water resistance is verified, reducing the absorption rate. As expected, the results showed a decrease of the absorption rate for samples with hydraulic contact (cement mortar and lime mortar) and perfect contact, in comparison with the monolithic samples. Also, it is possible to observe a decrease of the absorption rate for samples with cement mortar interface comparatively to the lime mortar materials (Guimarães et al. 2018). As described by Nunes et al. (2017) the changing of porosity in mortar near the transition zone of brick-mortar can be attributed to the flow of water from fresh brick during the bonding process. In the beginning, small binder particles can be transported to the mortar-brick interface and the plaster becomes more compact (enriched in binder) in the interface.

Another conclusion observed was as further away from the base is located the interface, higher is the water absorbed. The interface could significantly retard the flow of moisture transport. i.e., the discontinuity of moisture content across the interface indicated that there was a difference in capillary pressure across the interface.

For the gravimetric method analyse the "knee point" is determined manually and the hygric resistance (RH) is calculated experimentally (during a water absorption test) by the slope of the mass variation curve as function of time, after the knee point:

$$RH = \frac{\Delta M_w}{\Delta t} \tag{1}$$

where Δt and ΔM_w are the variation of the time and water absorption immediately after the knee point, respectively. Considering this measuring procedure, it is important to detect this instant with precision and automatically. To fulfil this propose, it is intended to use a changing point automatic detection method to assist the water absorption analysis.

The three methods presented above were applied to the experimental data reported with the interface at three different heights (at 2 cm of the base, at 5 cm and at 7 cm) of perfect contact and hydraulic contact interface and two types of bricks. The results for the determination of the "knee point" of 20 cases showed:
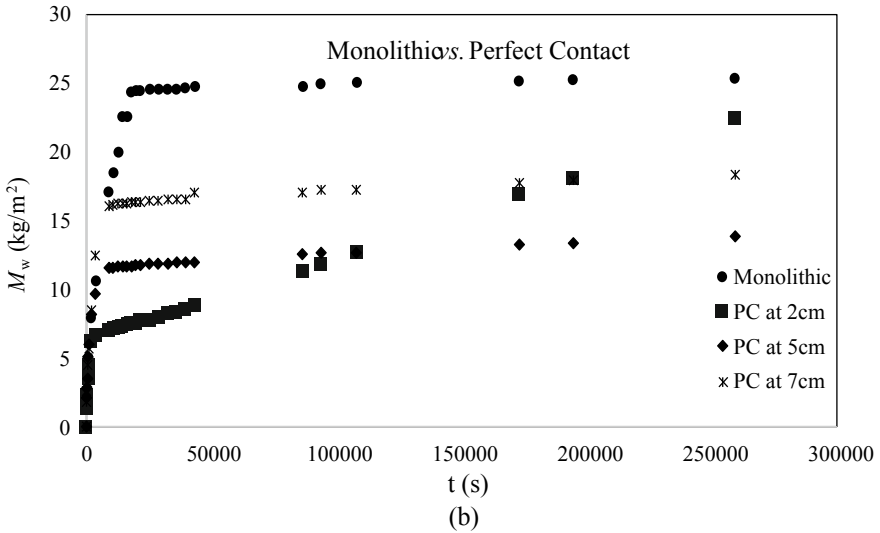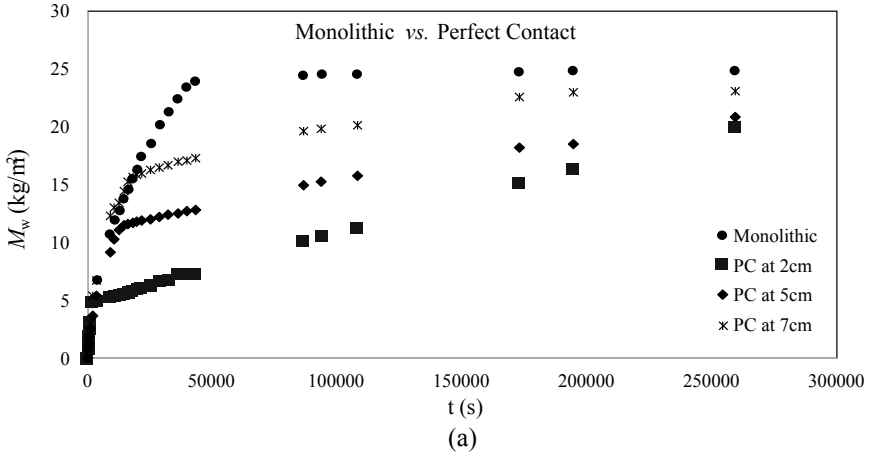
Fig. 9 Water absorption curves of the monolithic sample and samples with perfect contact: **a** for red brick type "A" and **b** red brick type "B"

- In 3 cases, the three methods obtained the same knee point;
- In 10 cases, each method obtained a distinct point as a knee;
- In 1 cases, the 2nd and 3rd methods obtained the same point as the knee, but the 1st method produced another distinct point;
- In 6 cases, the 1st and 3rd methods obtained the same point as knee but the 2nd method produced another distinct point;
- No cases were observed in which the 1st and 2nd methods obtained the same knee point and the 3rd method produced another distinct point.

(a)

(b)
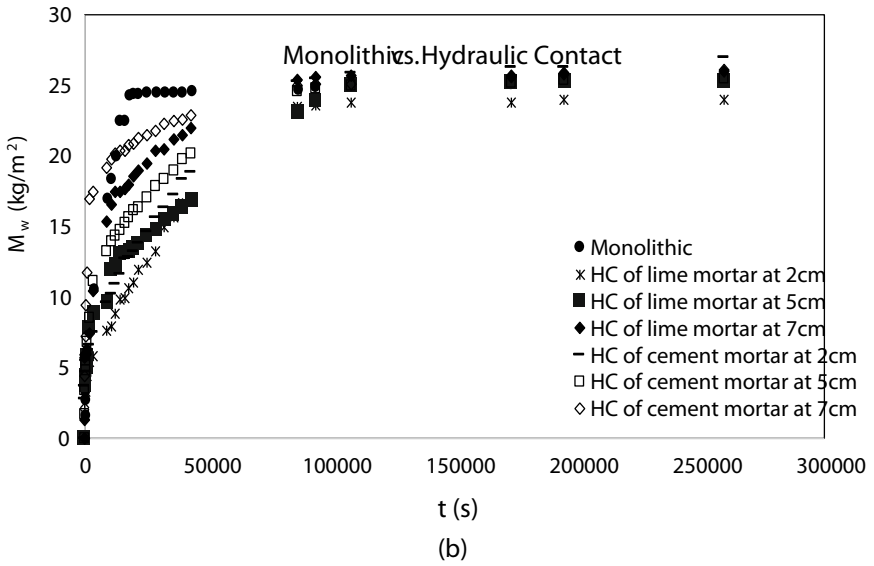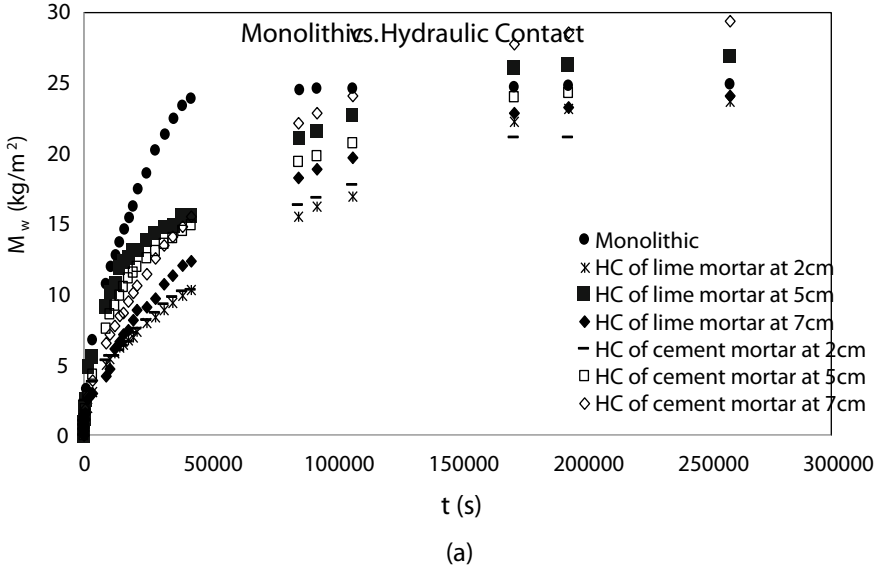
Fig. 10 Water absorption curves of the monolithic sample and samples with hydraulic contact (cement and lime mortar): **a** for red brick type "A" and **b** red brick type "B"

Figure 11 shows some particular cases. In this figure, black asterisks represent all points obtained in the measuring procedure, magenta circle denotes the knee attained by the 1st method, red square symbolizes the knee determined by the 2nd Method and blue diamond characterizes the knee reached by the 3rd method.

It should be noted that when the three methods do not obtain the same knee, the point determined by the 2nd method is always to the left of the point calculated by the 3rd method. Meanwhile, the point obtained by the 1st method is always to the right of the point attained by the 3rd method.

The 3rd method is an optimization of the existent ones, 1st and 2nd, and showed to be the best method in the experimental cases analysed, with a good detection of the knee point. It is important to keep in mind that in this type of analyse is, usually, used with experimental data, which means that there are "discrete" points, and not
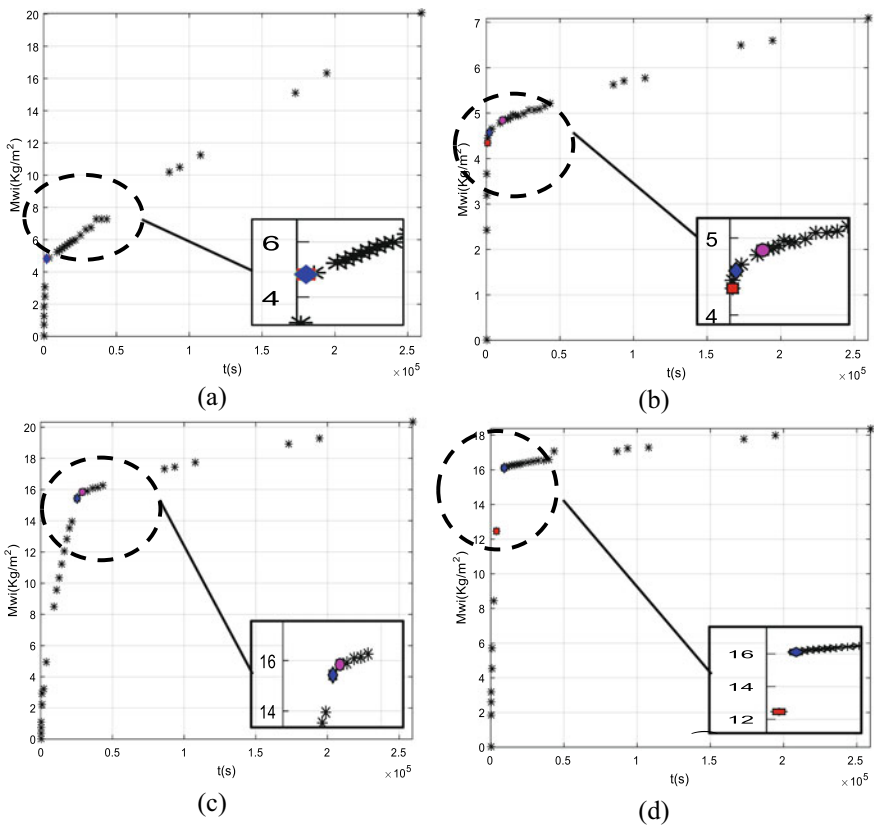
Fig. 11 **a** The three methods obtained the same knee point; **b** each method obtain a distinct point as a knee; **c** only the 2nd and 3rd methods obtained the same point as the knee; and **d** Only the 1st and 3rd methods obtained the same point as the knee (magenta circle—knee attained by the 1st method, red square—knee determined by the 2nd method and blue diamond—knee reached by the 3rd method)

a curve, with some possible outliers that sometimes contribute to wrong solutions using other methodologies. Finally, the gravimetric method includes 12 with an error ratio lesser than 20% in relation to the new methodology. When speaking of an error ratio in the order of 30%, the cases increase to 14 for gravimetric method (GM) compared to new method (NM).

The results presented in Table 2 shows good accordance similarity between the hygricv resistance values obtained by gravimetric method and the new methodology

Table 2 Hygric resistance values determined by gravimetric method and the new methodology proposed

| Material	Sample/(interface type)	Hygric Resistance (kg/m^2 s)	
		Gravimetric method (GM)	New method (NM)
Red brick type "A"	Perfect contact (2 cm)	6.6×10^{-5}	6.2×10^{-5}
	Perfect contact (5 cm)	4.3×10^{-5}	3.8×10^{-5}
	Perfect contact (7 cm)	2.4×10^{-5}	2.3×10^{-5}
	Hydraulic contact (cement mortar at 2 cm)	7.9×10^{-5}	7.7×10^{-5}
	Hydraulic contact (cement mortar at 5 cm)	7.1×10^{-5}	6.9×10^{-5}
	Hydraulic contact (cement mortar at 7 cm)	4.2×10^{-5}	5.7×10^{-5}
	Hydraulic contact (lime mortar at 2 cm)	7.9×10^{-5}	7.6×10^{-5}
	Hydraulic contact (lime mortar at 5 cm)	5.8×10^{-5}	7.5×10^{-5}
	Hydraulic contact (lime mortar at 7 cm)	5.4×10^{-5}	6.5×10^{-5}
Red brick type "B"	Perfect contact (2 cm)	7.3×10^{-5}	6.5×10^{-5}
	Perfect contact (5 cm)	5.0×10^{-5}	2.0×10^{-5}
	Perfect contact (7 cm)	2.9×10^{-5}	1.3×10^{-5}
	Hydraulic contact (cement mortar at 2 cm)	7.9×10^{-5}	6.6×10^{-5}
	Hydraulic contact (cement mortar at 5 cm)	3.8×10^{-5}	4.0×10^{-5}
	Hydraulic contact (cement mortar at 7 cm)	3.2×10^{-5}	2.6×10^{-5}
	Hydraulic contact (lime mortar at 2 cm)	7.9×10^{-5}	7.1×10^{-5}
	Hydraulic contact (lime mortar at 5 cm)	4.2×10^{-5}	4.8×10^{-5}
	Hydraulic contact (lime mortar at 7 cm)	4.2×10^{-5}	3.6×10^{-5}

proposed. It is possible to observe that for higher positions of the interface the water absorbed is higher and the hygric resistance is lower. It was expected that considering an interface between layers the water absorption would become lower, and for the case of interfaces located in higher positions the absorption would become higher as the discontinuity is reached latter.

It is important to be in mind that if we place the interface at different distances from the wetting plane the beginning of the slowing of the wetting occurs in different time periods, as expected, however, from that moment onwards, there is an increase in mass that, in the limit, is constant for all cases.

6 Conclusions

In conclusion, the main achievements related to the new methodology proposed for "knee point" detection are the following:

- There is still a high unawareness regarding the influence of the building components interfaces between layers in moisture transfer processes;
- The existence of different types of interface (perfect contact, hydraulic contact, and air space interface) contributes to different ways of moisture transport when compared to a monolithic porous element;
- The "knee point" was detected in water absorption curves which mean the hygric resistance was measure in perfect contact multilayer building components. Moreover, when the contact between the different materials is hydraulic, i.e., there are two points of change, the user can define the time-space in which the knee is to be determined and run the program more than once if you want to determine the two knees;
- The moisture-dependent interface resistance between brick building components was quantified and validated for transient conditions which can be used for future numerical simulations;
- Two methodologies were studied to detect the knee point;
- A 3rd methodology is proposed, optimizing the other two, which showed to be the best method for cases presented;
- The proposed methodology is especially important considering that it is usually used in conjunction with experimental data which means that there are "discrete" points, and not a curve, with some possible outliers that sometimes contribute to wrong solutions using other methodologies;
- The proposed methodology to detect the "knee point" can be also used in the future for different materials;
- From the computational experimental performed, it is shown that the method developed in this work (3rd method) determines a point that best fits the definition of the knee;
- In order to make this process even more efficient and effective, the program allows the user to choose whether to define the time frame in which to determine the knee;
- Finally, in case there is an air space between the different materials, the procedure is the same that was presented for the perfect contact.

Annexes

SEC.Program

```
function [a,c]=FindKnee(idx,Segment)
a=1;
c=-1;
x1=idx(1);
x2=idx(end);
y1=Segment(1);
y2=Segment(end);
if((x1-x2)==0)
   x=x1;
   y=y1;
   c=0;
   return;
end
hmax=0;
x=0;
y=0;
hcum=[];
for i=1:length(Segment)
   %==================
x0=idx(i);
y0=Segment(i);
A=sqrt( (x1-x2)^2 + (y1-y2)^2 );
B=sqrt( (x0-x2)^2 + (y0-y2)^2 );
C=sqrt( (x0-x1)^2 + (y0-y1)^2 );
h=sqrt( B^2 - ( ( B^2 + A^2 - C^2 )/(2*A) )^2 );
%==================
if h>hmax
   hmax=h;
   x=x0;
   y=y0;
   a=i;
end
end
%Concavity
%============
u=y2+(y1-y2)*( B^2 + A^2 - C^2 )/(2*A^2);
if( u>y0 )
   c=1;
else
   c=0;
end
```

```
%FIGURE
%=======================================
figure(92554)
plot(idx,Segment);hold on;
plot(x1,y1,'*r');
plot(x2,y2,'*g');
plot(x,y,'r*');
hold off;
figure(45)
plot(idx,hcum);hold on;
plot(x,hmax,'*r');hold off;
pause;
%=======================================
end
```

Hybrid.Program

```
nRMC=0;
nMmC=0;
format compact
format long
disp('*************************')
disp('* Interface:          *')
disp('*   1 - Perfect contact  *')
disp('*   2 - Cement mortar    *')
disp('*   3 - Lime mortar      *')
disp('*   4 - Air space        *')
disp('*************************')
b=input('What kind of interface do you want?  \n');
if(all(b~=1:4))
    error('Wrong value')
end
%for b=1:1;
    for e=1:3;
        for d=1:3;
            for f=1:4 ;
                for a=1:5 ;
%disp([a,f,d,e,b])
M=Tnsr(b,e,d,f,a).M;

total=(e-1)*3*4*5+(d-1)*4*5+(f-1)*5+a;
if isempty(M);
%   disp('não existe')
    nn=nn+1;
    continue;
end
```

```
 if total==1
nop=input('Do you want to change the search time instants (Y or N)? \n', 's');
if all(nop~=['Y', 'N', 'y', 'n'])
   error(' You did not write the correct option: Y or N')
end
if any(nop == ['Y' 'y'])
   TT=input('What is the interval of instants of time that you intend to do the
research? [1st_value, 2nd_value] \n');
   if( any(TT) < 0 || TT(2)<TT(1))
       error(' Wrong interval of instants of time')
   end
   aux=find(M(:,1)<=TT(1));
   T(1)=aux(end);
   T(2)=find(M(:,1)>=TT(2),1);
else
   T(1)=1;
   T(2)=length(M(:,1));
end
end
t1=M(:,1); Mwi1=M(:,2);
t=M(T(1):T(2),1); Mwi=M(T(1):T(2),2);
pp=length(t);
figure(10)
plot(t1,Mwi1,'k:o');hold on;
xlabel('t(s)'); ylabel('Mwi(Kg/m^2)');grid on; hold off;
grid on;
axis([0 max(t1) 0 max(Mwi1)]);
xx=zeros(pp,1);
for i=2:pp
   xx(i-1)= (Mwi(i)-Mwi(i-1))/(t(i)-t(i-1));
%   if xx(i-1)<=aijtol;
%       xx(i-1)=0;
%   end
end
% Knee deviations
[idxn,~]=FindKnee_novo(t,Mwi);
[~,c11]=knee_pt1(Mwi,t);
```

```
  for i=1:pp
     k1=find(idxn(i)==c11(1:i));
     if ~isempty(k1)
       c111=k1;
        break
     end
     if any(c11(i)==idxn(1:i-1))
       c111=i;
        break
     end
  end
 end
 cm=c11(c111);
 kk=xx(cm+1);
 figure(10)
 plot(t1,Mwi1,'-bd','MarkerFaceColor','g');hold on;
 plot(t(cm),Mwi(cm),'k*');
 title([num2str(total), ' ' ,'Combination ', num2str(cm) , ' ',num2str(kk)])
 xlabel('t(s)'); ylabel('Mwi(Kg/m^2)');grid on; hold off;
 grid on;
 axis([0 max(t) 0 max(Mwi)]);
 if total==1
    pause(8)
 else
    pause(5)
 end
           end;
         end;
       end;
    end;
 %end
 disp([no Figure   ', num2str(nn)])
 disp([TD,TI,CM,CK,MK,nMmC, nRMC])
 % TD – All different
 % TI – All equals
 % CM – Combination equal to Matlab
 % CK - Combination equal to Knee-pt program
 % MK - Matlab equal to Knee-pt program
 % nMmC - knee number which in the Knee-pt program is below that obtained in
 the combination
 % nRMC - knee number which in the Knee-pt program is above that obtained in
 the combination
```

```
clc;clear;close all;warning off;
Path='.\TempoxMw_grama.xlsx';
OUT=Read_Data_File(Path,[],[]); DtSt=cell2mat(OUT.Dt); DtSt=DtSt(1:4159,:);
FctrIndx=[1:5];
[Tnsr,FctrLst]=Mtx2Tnsr(DtSt,FctrIndx);
aijtol=1.0e-6;
nn=0;
TD=0;
TI=0;
CM=0;
CK=0;
MK=0;
```

References

Barreira E, Almeida R, Delgado JMPQ (2016) Infrared thermography for assessing moisture related phenomena in building components. Constr Build Mater 110:251–269. https://doi.org/10.1016/j.conbuildmat.2016.02.026

Bednar T (2002) Approximation of liquid moisture transport coefficient of porous building materials by suction and drying experiments. demands on determination of drying curve. In: Proceedings of the 6th Symposium on Building Physics, Nordic Countries, Trondheim, Norway, pp 493–500

Brocken HJP (1998) Moisture transfer in brick masonry: the grey area between bricks, T.U. Eindhoven, The Netherlands, Ph.D. thesis

Brocken HJP, Spiekman ME, Pel L, Kopinga K, Larbi JA (1998) Water extraction out of mortar during brick laying: a NMR study. Mater Struct 31(1):49–57

Christopoulos DT (2014) Reliable computations of knee point for a curve and introduction of a unit invariant estimation. https://doi.org/10.13140/2.1.3111.5844

Davison JI (1961) Loss of moisture from fresh mortars to bricks. Mater Res Stand ASTM 1:385–388

de Freitas VP (1992) Moisture transfer in building walls—Interface phenomenon analysis, Faculdade de Engenharia da Universidade do Porto, Porto, Portugal, Ph.D. thesis [in Portuguese]

de Freitas VP, Abrantes V, Crausse P (1996) Moisture migration in building walls: analysis of the interface phenomena. Build Environ 31:99–108. https://doi.org/10.1016/0360-1323(95)00027-5

Delgado JMPQ, Ramos NMM, Freitas VP (2006) Can moisture buffer performance be estimated from the sorption kinetics? J Build Phys 29(4):281–299. https://doi.org/10.1177/1744259106062568

Delgado JMPQ, Guimarães AS, de Freitas VP, Antepara I, Kočí V, Černý R (2016) Salt damage and rising damp treatment in building structures. Adv Mater Sci Eng 2016:13, Article number ID 1280894. https://doi.org/10.1155/2016/1280894

Derdour L, Desmorieux H, Andrieu J (2000) A contribution to the characteristic drying curve concept: application to the drying of plaster. Dry Technol 18(1–2):237–260

Derluyn H, Janssen H, Carmeliet J (2011) Influence of the nature of interfaces on the capillary transport in layered materials. Constr Build Mater 25(9):3685–3693

Du W, Leung SYS, Kwong CK (2014) Time series forecasting by neural networks: a knee point-based multi-objective evolutionary algorithm approach. Expert Syst Appl 41(18):8049–8061. https://doi.org/10.1016/j.eswa.2014.06.041

EN ISO 10545-3 (1995) Ceramic tiles—Part 3: determination of water absorption, apparent porosity, apparent relative density and bulk density. Geneva, Switzerland

EN ISO 12390-7 (2009) Testing hardened concrete. Density of hardened concrete. Geneva, Switzerland

EN ISO 772-13 (2000) Methods of test for masonry units. Determination of net and gross dry density of masonry units (except for natural stone)

Freitas VP, Guimarães AS, Delgado JMPQ (2011) The HUMIVENT device for rising damp treatment. Recent Patents Eng 5:233–240. https://doi.org/10.2174/187221211797636863

Ghosh SK, Melander JM (1991) Air content of mortar and water penetration of masonry walls. Masonry Information, Portland Cement Association

Groot CJWP (1995) Effects of water on mortar-brick bond. Heron J 40:57–70

Guimarães AS, Delgado JMPQ, Freitas VP (2012) Rising damp in building walls: the wall base ventilation system. Heat Mass Transf 48:2079–2085. https://doi.org/10.1007/s00231-012-1053-3

Guimarães AS, Delgado JMPQ, Freitas VP (2013) Rising damp in walls: evaluation of the level achieved by the damp front. J Build Phy 37:6–27. https://doi.org/10.1177/1744259112453822

Guimarães AS, Delgado JMPQ, Azevedo AC, Freitas VP (2018) Interface influence on moisture transport in buildings. Constr Build Mater 162:480–488. https://doi.org/10.1016/j.conbuildmat.2017.12.040

Hendrickx R, Van Balen K, Van Gemert D, Roels S (2009) Measuring and modeling water transport from mortar to brick. Building materials and building technology to preserve the built heritage. In: 1st WTA-international Ph.D. symposium, vol 33, pp 175–194

Holm A, Krus M, Künzel HM (1996) Feuchtetransport über Materialgrenzen im Mauerwerk. Rest Build Monum 2(5):375–396

ISO 15148 (2002) Hygrothermal performance of building materials and products–Determination of water absorption coefficient by partial immersion. Genève, Switzerland

Karoglou M, Moropoulou A, Maroulis ZB, Krokida MK (2005) Drying kinetics of some building materials. Dry Technol 23(1–2):305–315

Mendes N, Philippi PC (2005) A method for predicting heat and moisture transfer through multilayer walls based on temperature and moisture content gradients. Int J Heat Mass Transf 48(1):37–51

Mukhopadhyaya P, Goudreau P, Kumaran K, Normandin N (2002) Effect of surface temperature on water absorption coefficient of building materials. Report NRCC-45369, Institute for Research in Construction, National Research Council, Ottawa, Canada

Nunes C, Pel L, Kunecký J, Slížková Z (2017) The influence of the pore structure on the moisture transport in lime plaster-brick systems as studied by NMR. Const Build Mater 142:395–409. https://doi.org/10.1016/j.conbuildmat.2017.03.086

Qiu X, Haghighat F, Kumaran K (2003) Moisture transport across interfaces between autoclaved aerated concrete and mortar. J Therm Envel Build Sci 26(3):213–236

Vereecken E, Roels S (2014) A numerical study of the influence of the hydraulic interface contact on the hygric performance of multi-layered systems. In: Proceedings of XIII IDBMC conference, São Paulo, Brazil

Ville Satopaa JA, Irwin D, Raghavan B (2011) Finding a "Kneedle" in a Haystack: detecting knee points in system behaviour. https://doi.org/10.1109/icdcsw.2011.20

Wang Z, Tseng SS (2013) Knee Point search using cascading top-k sorting with minimized time complexity. Sci World J 10, Article ID 960348. https://doi.org/10.1155/2013/960348

Zhao Q, Hautamaki V, Fränti P (2008) Knee Point detection in BIC for detecting the number of clusters. In: Blanc-Talon J, Bourennane S, Philips W, Popescu D, Scheunders P (eds) Advanced concepts for intelligent vision systems. ACIVS 2008. Lecture Notes in Computer Science, vol 5259. Springer, Berlin, Heidelberg. https://doi.org/10.1007/978-3-540-88458-3_60

Zhao Q, Xu M, Fränti P (2008) Knee point detection on Bayesian information criterion. In: Proceedings of 20th IEEE international conference on tools with artificial intelligence, Dayton, Ohio, USA. https://doi.org/10.1109/ictai.2008.154

Adhesion of Gypsum Plaster Coatings: Experimental Evaluation

A. C. Azevedo, J. M. P. Q. Delgado, T. H. C. Neves, and A. J. Costa e Silva

Abstract Nearly 95% of the Brazilian production of natural gypsum comes from the state of Pernambuco, from the Araripe Gypsum Center. Of the 95%, that is to say, of the 1.3 million ton/year production, 61% is allotted to the making of blocks and plates, 35% for coverings, 3% for ceramic moulding, and 1% for other uses. The Gypsum Center generates nearly 12,000 jobs directly and approximately 60,000 jobs indirectly, and has an annual invoicing of US$300M per annum. In civil construction, the use of gypsum increases continually, because plaster paste is seen by builders as a low cost, quality alternative material to be applied as coatings to internal walls. The reduced cost results in higher productivity on the part of the craftsperson due to the speed of application as well as providing a good final finish. Paint can be applied without needing to apply putty. Bases commonly used for these types of finishes are ceramic and concrete substrates. These materials are known for their excellent mechanical strength and low thermal conductivity. The superior surface quality on both sides of these materials makes them suitable for any thickness of plaster paste. This study evaluates experimentally the adhesion strength of coatings made with gypsum paste, considering different substrates and application heights. There are four types of blocks (ceramic and concrete, non-structural and structural blocks), two types of slice cutting (superficial and penetrating to the substrate) and three application heights (up to 0.6 m, between 0.6 and 1.2 m and above 1.2 m). The

A. C. Azevedo · J. M. P. Q. Delgado (✉)
Civil Engineering Department, Faculty of Engineering, University of Porto, 4200-465 Porto, Portugal
e-mail: jdelgado@fe.up.pt

A. C. Azevedo
e-mail: antonio.costaazevedo@fe.up.pt

T. H. C. Neves
Instituto Federal de Ciências de Educação e Tecnologia de Pernambuco (IFPE), Brazil, USA
e-mail: engthcneves@gmail.com

A. J. Costa e Silva
Civil Engineering Department, Universidade Católica de Pernambuco, Brazil, USA
e-mail: angelo@tecomat.com.br

41

results indicated the strong influence by the base and depth of cut on the adhesion, but there was no influence on adherence attributed to the height of application.

Keywords Gypsum paste · Ergonomics · Adhesion strength

1 Introduction

Adhesion is one of the most important properties for the performance of the compound, especially as it is responsible for securing the gypsum to the base over the years, including under any conditions to which it might be subjected. Adhesion can be used to describe the strength and the extent of contact between the mortar and the base (Argamassas 2010; Flores-Colen et al. 2009; Freitas et al. 2014; Melo et al. 2019).

Given this scenario, the contribution stemming from scientific and technological research is important in the elucidation of beliefs and factors that lead to empiricism. The application of knowledge acquired through research is capable of providing appropriate conditions for material development, as well as perfect construction techniques, contributing to the more significant rationalization of materials, productivity gains and, above all, a decrease in the incidence of pathological manifestations, as the potential is known, and the weaknesses of the system can be worked out (Scartezini 2002).

In this sense, this work is designed to provide an evaluation of the influences of two of the main types of bases (ceramic and concrete blocks, both structural and non-structural) based on the results obtained at different application heights of the gypsum plaster coating. For a more enriched discussion, the influence of some generating conditions on the overall behaviour will be evaluated, starting with the analysis of the depth of the cut used in the implementation of the test, as well as the ergonomics.

The construction industry is responsible for a high level of extraction of natural resources from the planet. Because of this, the emergence of new materials, as well as new construction systems, occur as a result of the need for more excellent production, in less time, with high quality and lower costs.

Gypsum plaster coatings, widely used as a protective layer for buildings and masonry work, are responsible for protection, impermeability, beautification, and user comfort. The lack or loss of adhesion of the coatings leads to economic losses and, especially, to diminished liability, directly interfering with the course of human life.

The application techniques of gypsum plaster, unlike cement mortars, are not done by roughcasting, but by compressing the paste into the base, with the aid of a trowel. Thus, this can imply an influence on the ergonomics as well as on the variations of the results found. This difference in the execution technique can also influence the final finish; therefore, we will evaluate the surface adhesion as well as deep adhesion.

There are currently several studies regarding the lack of adhesion in cementitious materials, which is something that does not occur in the area of gypsum coatings. Given this scenario, the study that guides the qualitative and quantitative analysis of coatings made with gypsum plaster becomes essential. Therefore, this work proposes to experimentally evaluate the adhesion capacity of layers made with gypsum plaster, considering different substrates and different heights of application.

The objective of this work is to evaluate, utilizing an experimental study, the influence of the base and the execution conditions on the adhesion strength of plaster paste coatings and acquire a better knowledge of the impact of base properties on the adhesion of plaster paste. This study also presents the effect of ergonomics from a comparative evaluation at different times of the test, as well as a comparative analysis the importance of the final finish, starting with surface and deep adhesion resistance of gypsum plaster.

2   Plasters in Civil Construction

Plaster stands out among the materials that have been growing in use over a long period. It can be considered the oldest binder known to man. Samples of this material have been found in abundance in constructions of ancient Egypt, the Keops Pyramid (2800 BC). It is also found among the ruins of the ninth millennium BC in Turkey and the ruins of the sixth millennium BC in Jericho (Baltar et al. 2005).

Also, according to these authors, the techniques for using this material, such as calcination, and its hydraulic properties were known to these ancient peoples. This knowledge spawned a variety of uses, from the making of decorative objects like statues to construction processes which are so well-known in today's engineering, such as wall coverings in the form of mortars and pastes. Lavoisier, in 1768, published the first scientific study of the phenomena related to plaster preparation. From 1885, the use of plaster in the construction industry has been stimulated by the discovery of a process which facilitates the delay in bonding time.

Plaster is present all over the world. Its largest producers and consumers are undoubtedly the countries of the American continent (see Table 1). Currently, the world's largest producers of gypsum are United States (17%), Iran (10%), Canada (8%), Mexico (7%) and Spain (6.8%), followed by other countries like Brazil, Chile, and Uruguay (Peres et al. 2008; Paula and Delgado 2017; Paula et al. 2017).

Gypsum exploration in Brazil is located, for all practice purposes, in the northeast (see Fig. 1). Currently, the largest producing locality is found in the Araripina micro-region in Pernambuco (comprised of the municipalities of Araripina, Trindade, Ipubi, Ouricuri, Bodocó, Morais and Exu) which generates more than 90% of the national production (Peres et al. 2008).

These authors also point out that the second most important locality in production is Grajaú, in Maranhão; the third is Codó, which is also in the municipality of Maranhão. Gypsum production exists in Nova Olinda, Ceará as well. Gypsum mining in Brazil is conducted in open-pit mines, with amphitheatre-shaped mine fronts and

Table 1 World gipsite production, in million tons

Country	2002	2003	2004	2005	2006	%PM
Australia	4268	4066	4325	3857	400	3.2
Germany	1761	1748	1579	1644	1650	1.3
Brazil	1633	1529	1472	1582	1600	1.3
Canada	8809	8378	9339	9400	9500	7.6
China	6850	6850	7000	7300	7500	6.0
Egypt	2000	2000	2000	2000	2000	1.6
U.S.A.	15700	16700	17200	21100	21100	16.9
Spain	11218	11500	12534	13000	13200	10.6
France	4900	5600	5700	4902	4800	3.9
Total (09)					61750	52.4
Worldwide total					125000	100

Fig. 1 Araripe plasterboard pole

ore benches ranging in thickness of around 15 m. Despite having increased in recent years, the per capita consumption of plaster in Brazil is quite low when compared to other South American countries (see Table 2), which is a promising indicator of potential market growth in the country in the next few years.

The state of Pernambuco, which has abundant gypsum reserves in the Sertão do Araripe region, encompassing the municipalities of Araripina, Bodocó, Ipubi, Ouricuri, and Trindade, is responsible for 95% of Brazilian production. Araripe

Table 2 Annual consumption in Chile, Argentina and Brazil

Country	Annual consumption (kg/hab.)
Chile	41
Argentina	21
Brazil	9.3

reserves are considered to contain the best quality ore in the world and have excellent mining conditions (Baltar et al. 2005)

According to information from the Sindusgesso (Union of Extraction and Processing Industries of Gypsum, Limestone, Gypsum Derivatives and Non-Metallic Minerals of the State of Pernambuco), the Pernambuco Gypsum Center contains 18 active mines, 69 industrial calcination units, and 250 precast industries, providing about 12,000 direct jobs and about 60,000 indirect jobs (Luz et al. 2001). The production of Gypsum Pole, in 2001, was 1.8 million ton/year, of which about 1.3 million of the manufacturing of plaster, about 500 thousand tons, is used in the production of cement (Luz et al. 2001).

Construction plaster is a powder material obtained by gypsum calcination and is composed of hydrated calcium sulphate, with basanite as its main component. The presence of anhydrite, gypsum, and aggregate impurities are also detected (Lyra 2002; Nita et al. 2004).

The production of natural plaster takes place basically in four stages (see Figs. 2 and 3): gypsum extraction, calcination preparation, calcination, and selection. Gypsum is a sedimentary rock which contains gypsum, anhydride, and some

Fig. 2 Gypsum, plaster raw material

Fig. 3 Casting powder obtained by calcination

impurities, usually mineral clay, calcite, dolomite, and organic materials (Barbosa et al. 2014).

Gypsum is a soft, compact, poorly soluble mineral, which is the primary material for the manufacturing of plaster. After extraction, gypsum undergoes some processing to suit the type of furnace where it will later be calcined. The processing stages are as follows: crushing, coarse grinding, stockpiling, drying, fine grinding, and packaging.

Calcination is the thermal process by which gypsum is dehydrated. The material is calcined at a temperature range of 140–160 °C, so that 75% of the crystalized water is removed from the structure to obtain the hemihydrate (Barbosa et al. 2014).

Calcination may be performed by dry or wet methods. If the gypsum is dry calcined under atmospheric or low pressure, beta hemihydrate is obtained. If calcination occurs under saturated water vapour pressure, alpha hemihydrate is obtained. The alpha plaster, due to its production process, is used for high-end applications (hospital plaster) and consequently is sold at higher prices. Beta plaster, with lower production cost, predominates in national construction plaster (Barbosa et al. 2014).

2.1 Concept of Adherence

The performance of plaster coatings is directly related to adherence and durability, as well as to other properties. Thus, regardless of the proportion of the plaster and the quality of the materials employed, it is imperative that optimum conditions of coating adherence at the base exist.

A concern for improved knowledge of the properties and phenomena that affect the detachment of the coatings can help avoid the disagreeable experience involved in reworking, dangerous accidents, and user dissatisfaction, as well as repair costs.

In buildings, one of the main reasons for coating mortar failure is related to the loss or lack of adhesion to the substrate. Thus, mortar's ability to achieve a complete, durable, and lasting adhesion to the base is perhaps the most critical property concerning the behaviour of said coating (Carasek 2007; Ioppi 1995).

Hardened coating adhesion is conceptualized as the "property of the coating to withstand normal or tangential stresses at the interface surface with the substrate" (Ioppi 1995).

2.2 Plaster/Substrate Adhesion Mechanism

In the case of plaster coatings, the term adhesion is used to describe the strength and extent of contact between the plaster and a porous base. This base, the substrate, is usually a type of masonry, which may be ceramic bricks, blocks, concrete blocks, structural concrete bricks, structural ceramic bricks, etc., as well as their in situ concrete structure mould.

Didactically, it can be said that adhesion derives from the combination of three properties of the mortar/substrate interface: the tensile bond strength, the shear bond strength, and the bond length, which is the ratio between the precise contact area and the total possible area to be joined (Carasek et al. 2001, 2011).

In addition to the need for strength and sufficient adhesion surface, the durability of the bond is essential for strong adhesion, which begins with the initial hardening of the mortar and continues throughout the service life of the coating. If cracks occur during or after the hardening of the mortar, adherence may be compromised (Carasek et al. 2001, 2011).

The adhesion of the hardened mortar to the substrate is essentially a mechanical phenomenon, basically due to the penetration of the binder paste or the mortar itself into the pores or between the roughnesses of the application base. When the mortar in the plastic state comes into contact with the absorbent surface of the substrate, part of the kneading water, which carries with it the binder components in dissolution or colloidal state, penetrates through the pores and cavities of this substrate (Carasek et al. 2001, 2011).

2.2.1 Influence of Base (Substrate) on Adhesion

Base adhesion is the foundation for the application of the coating layers. The most frequently used are masonry bases and concrete structure. The substrate, especially those that are not roughcast applied, can have a significant influence on the final quality of the coating due to the diversity of characteristics and texture: absorbent, waterproof, smooth, rough, rigid, and deformable (Santos 2008).

NBR 7200 (1998) specifies that the coating bases must meet the flatness, plumb and levelling requirements set in masonry and concrete structure standards. When the base is composed of different materials and is subjected to forces that generate considerable differential deformations—overhangs, eaves, and last floors, for example—a metallic, plastic or other similar substance should be used to join these materials, creating an area capable of withstanding movement. Alternatively, a joint may be required that separates the coating which spans over the two different elements, allowing each part to move separately.

Analysing the results presented in this work together with NBR 13749 (2013), which prescribes the tensile bond strength limits for plaster and monolayer coats, we can verify that the coatings applied to the substrates of rough or chipped ceramic brick, solid brick with and without splatter cast and rough concrete blocks met the requirements for application of internal wall and ceiling coatings, appropriate for the option of a painted finish or plaster base on interior surfaces, as they presented tensile strengths above 0.20 MPa as required by the standard.

2.2.2   Requirements and Performance Criteria

The dimensions of the blocks, the shape of the cross-section, the presence of coatings, the height/thickness of the wall, the characteristics of the mortar, the rigidity of the structure, and the presence of door and window gaps significantly influence the performance of the masonry (Costa e Silva et al. 2017).

In the case of walls, the compressive strength of the blocks, in addition to being a general indicator of their quality, will have a direct influence on the shear and compressive strength of walls required by imposed deformations of the structure. Blocks with a minimum compressive strength of 1.5 MPa can be used in light masonry filling walls. If the walls are subjected to imposed deformations or more significant occupancy loads, the blocks with a minimum resistance of 3 MPa should be chosen. The deformability of non-load bearing masonry of hollow ceramic blocks can be evaluated based on the values of their deformation module (Costa e Silva et al. 2017).

In special situations, such as buildings with more than 20 floors, longer walls, and walls with a considerable height (over 3 m), masonry must have adequate resistance to lateral loads, particularly those imposed by the wind. In this case, the bending moment acting on the wall shall be calculated based on the dynamic load, the wall dimensions, and its bonding conditions. At the same time, the dynamic stress shall not exceed the allowable masonry stress required for flexural traction. For masonry with fully filled lashing joints (horizontal joints and vertical joints) laid with mortars of compressive strength greater than or equal to 5 MPa (Costa e Silva et al. 2017).

Non-structural Ceramic Substrates

Hollow components, with prismatic holes perpendicular to the faces on which they are located, incorporating non-structural masonry interspersed in the spans of reinforced

Fig. 4 Structural blocks factory

concrete structures, steel or other materials are generally employed with the holes arranged horizontally and should resist only their weight and small occupancy loads.

Structural Ceramic Substrates

Hollow components, with prismatic holes perpendicular to the faces on which they are located, which incorporate masonry that makes up the sturdy framework of the construction, and are usually applied with the holes arranged vertically, can also be used in non-load bearing masonry.

Non-structural Concrete Substrates

Non-structural blocks and structural blocks made of concrete are apparently physically identical. However, structural blocks have thicker walls, which gives it increased resistance to compressive stresses and can, therefore, be used to support building constructions.

Structural Concrete Substrates

Structural concrete substrates have good compressive strength and range between the minimum 4.5 MPa required by current standards and 16 MPa. This higher strength is only available from some manufacturers, and this type of block weighs more. Compared to other units, the concrete block wall (see Fig. 4) performs the structure

and closing functions by eliminating columns and beams and reduces the use of reinforcement and cement forms. These are below the required 0.30 MPa.

2.3 Properties of Fresh Mortar

Initial adherence is the ability of the mortar to anchor itself to the base surface by penetration of the paste into the pores, recesses, and protrusions followed by the gradual hardening of the substance (Santos 2008).

The initial adherence, also called "tackiness," is the ability of the fresh mortar to initially bond to a base. It is directly related to the rheological characteristics of the binder paste, precisely its surface tension. Reducing the surface tension of the paste favours substrate "wetting" diminishing the contact angle between the surfaces and the implementation of adhesion. This phenomenon provides a more significant physical contact of the adhesive with the aggregate grains as well as with its base, thus improving adherence (Carasek 2007).

2.4 Properties of Mortar in a Hardened State

Adhesion is a property that the coating possesses in order to remain attached to the substrate through resistance to the standard and tangential stresses that arise at the base/coating interface. It is the result of tensile bond strength, shear bond strength, and mortar bond length. Adherence depends on the properties of the mortar in the fresh state, the coating performance procedures, the nature and characteristics of the base and the cleanliness of the surface. The pull-off test can be used to measure the tensile strength of the coating (Maciel et al. 1998).

The adhesion of the hardened mortar to the substrate is an inherently mechanical phenomenon due basically to the penetration of the binder or the mortar itself into the pores or into the roughness of the base to which it is applied. When the mortar in the plastic state comes into contact with the absorbent surface of the substrate, part of the kneading water, which contains the binder components in dissolution or colloidal state, penetrates through the pores and cavities of the substrate. Inside the pores there a phenomenon of precipitation occurs between the hydration products of cement and lime, and after some time, this initial precipitous intra-capillary action exerts an anchoring effect of the mortar to the base (Carasek 2007).

3 Experimental Campaign: Materials and Methods

3.1 Experimental Planning

The experiment was carried out from direct tensile bond strength tests performed on plaster pastes applied to ceramic and concrete, both structural and non-structural blocks (Naderi 2005). For improved visualization of these elements, the dependent and independent variables used are shown in Table 3.

In each of these bases, tests were performed on 120 samples, totalling 480 adherence tests, all performed at the age of 28 days. The choice of concentrating the tests only at one age was due to the preference for a more significant number of samples per study variable. The same stonemason raised the four (4) panels. These were divided into four bases with dimensions 1.50 m (width) × 1.80 m (height) and were constructed of the different aforementioned compositions. These were kept in a covered area of the Construction Materials Laboratory of the Catholic University of Pernambuco throughout the experiment. Industrialized block laying mortar was used for the raising of the walls, which the manufacturer indicated was a mortar suitable for multiple uses, using the mixture specified on the bag.

Seven days after having laid the blocks, measurements using *taliscas* was carried out in order to ensure uniformity of mortar thickness, set at 20 mm, followed by the application of plaster paste. For this step, the conventional application technique was used for this type of coating, which consists of manual compression of the paste on the base, with the aid of PVC trowel, and "slow" plaster, suitable for indoor use. The amount of water adopted was that indicated by the product supplier on the bag, and the mixing was done manually, with the craftsperson's trowel. For better orientation and understanding of the results, study families will be identified as described in Table 3.

On each of these bases, 120 samples were tested, totalling 480 adherence tests, all performed at 28 days of age. The choice of concentrating the tests only at one age was due to the preference for a more significant number of samples per study variable (see Fig. 5).

The four (4) panels were raised by the same stonemason and were divided into four bases of the following dimensions: 1.50×1.80 m^2 made of the different aforementioned materials, being exposed in an outside area of the Construction Materials

Table 3 Dependent and independent variables used in the study

Dependent variables		Independent variables	
Component Ceramic brick (Tc) Concrete block (Bc)	*Use* Structural (E) Non-structural (V)	*Test height* 0–60 cm (A1) 60–120 cm (A2) 120–180 cm (A3)	*Cut profundity* Superficial (S) Profound (P)

Example: Non-load bearing ceramic brick with a height from 0 to 60 cm and deep cut—TCVA1P

Fig. 5 General overview of the bases

Laboratory of the Catholic University of Pernambuco. For the elevation of the walls, industrialized block laying mortar was used, which the manufacturer indicated was a mortar suitable for multiple uses.

Seven days after laying the blocks, an initial plumb line was applied in order to ensure uniformity of the thickness of the mortar, established at 2 (two) centimetres, followed by the application of plaster paste. For this step, the conventional application technique for this type of coating was used, which consists of manual compression of the compound on the base, with the help of PVC trowel, and "slow" plaster, suitable for indoor use. The amount of water adopted was that indicated by the product supplier on the contents bag, and mixing was done manually with the craftsperson's trowel.

Before the application of the coating, no preparation of the base was performed except a surface brushing. All steps of the plaster paste execution were performed by the same stonemason in order to reduce operator influence on the results found (see Fig. 6).

3.2 Materials Used

The materials used in the experimental study performed in this dissertation, as well as their characteristics, are identified in this section. These materials are plaster, ceramic brick, structural ceramic brick, concrete block and structural concrete block, as detailed below.

Fig. 6 Structural block concrete with gypsum coating

Table 4 Results of the gypsum plaster characterization test

Tests		Results
Normal consistency		29.00 (a/g: 0.54)
Net content		14.20
Sieve size	Sieve 0.840 mm	0
	Sieve 0.420 mm	0.3
	Sieve 0.210 mm	6.98
	Sieve 0.840 mm	17.45
	Sieve 0.105 mm	75.27
Unit mass (g)		719.85
Fineness module		0.32 (thin plaster)
Compressive strength (MPa)		12.25
Catch time	Initial	00:26:38
	Final	00:48:10

3.2.1 Coating Plaster

Plaster was used for the manual coating, a material which is readily available in the region. Table 4 presents information concerning the tests of the physical and chemical characteristics of the product, involving standards and test methods.

3.2.2 Blocks

Ceramic and concrete, non-structural and structural blocks (see Fig. 7) were used in the experiments, all characterized by total water absorption, compressive strength, and dimension determination (see Table 5).
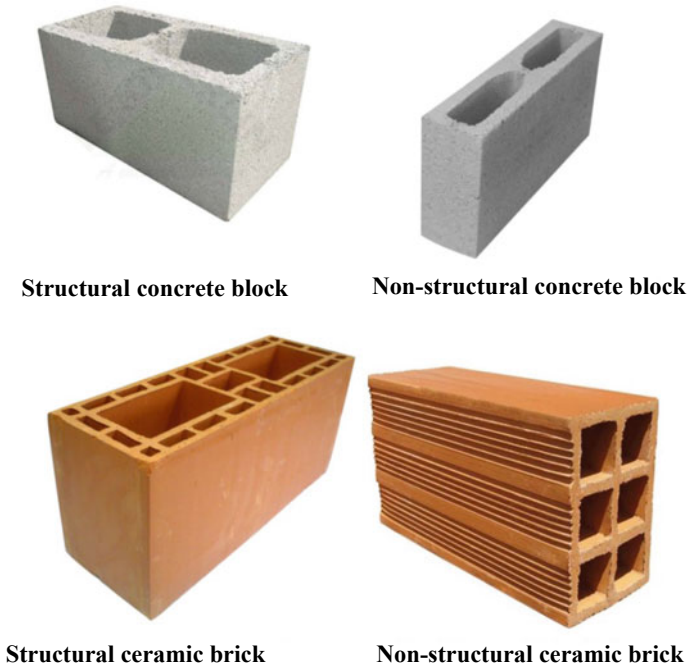
Structural concrete block   **Non-structural concrete block**

Structural ceramic brick   **Non-structural ceramic brick**

Fig. 7 Blocks used in the experimental campaign

Table 5 Results of the base characterization test

Characteristics	Standard	Ceramic bricks		Concrete blocks	
		Non-struct.	Structural	Non-struct.	Structural
Total water absorption (%)	NBR 7184 (1992)	18	12.5	8	6.5
Compressive strength (MPa)	NBR 6461 (2005)	1.2	2.7	3.4	6.6
Dimensions L × C × A (cm)	–	(9 × 19 × 19)	(14 × 39 × 19)	(19 × 19 × 19)	(9 × 39 × 19)

3.3 Experiment Description

For this experiment, masonry panels were prepared with ceramic and concrete blocks (non-structural and structural), coated with plaster paste. Tensile bond strength tests followed the procedure described in NBR13528 (NBR 1352), with 120 samples per substrate, totalling 480 tests. Initially, each base was divided into three heights (as sketched in Fig. 8), from 0 to 0.6 m; from 0.6 to 1.2 m and from 1.2 to 1.8 m. By

Fig. 8 Division of heights
tested
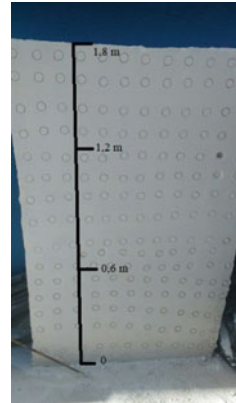
separating the panels in this way, it was possible to verify the influence of ergonomics utilizing a comparative evaluation.

A Bosch GSB-13RE impact drill was used to perform the cuts (see Fig. 9), together with a 53 mm internal diameter diamond cup saw, cutting the coating through to the substrate. After removing the dust, a metal lining was attached to the specimen produced by the cut to facilitate equipment attachment. Metal lining fixation was done by bonding with epoxy adhesive 24 h before the test.

For the blocks, the test was carried out precisely on the surface, bearing in mind that each wall had one hundred and twenty specimens, sixty with cuts to the substrate and the other sixty with superficial cuts, as shown in Fig. 10.

For the performance of the bond strength test, an Alfa Instruments brand force transducer (see Fig. 11), model Z2T, nominal range 2000 kgf was used; and Alfa Instruments brand digital associated electronic instrumentation, model 3105C, serial

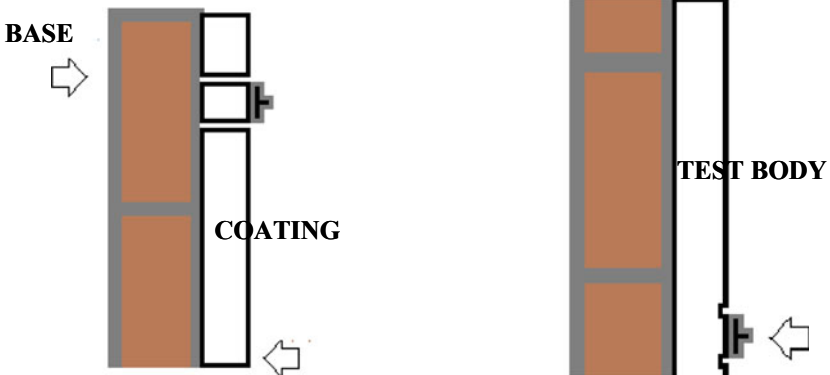**Cut 01 – Coating until substrate**   **Cut 02 – Superficial coating**

Fig. 9 Types of coating cuts

○ Corte 01 - Revestimento até o substrato
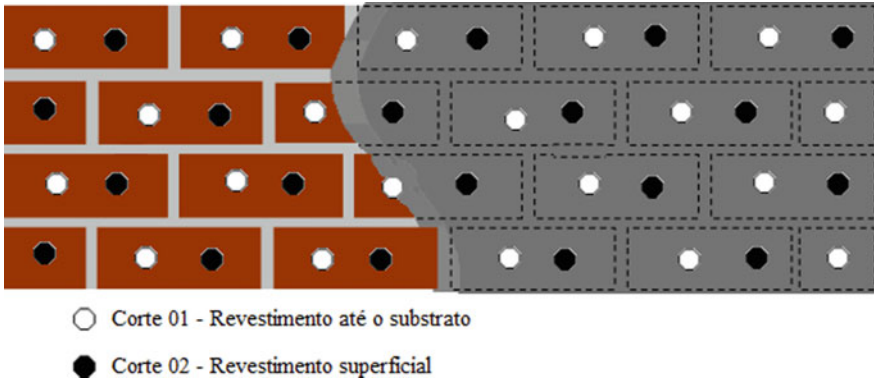
● Corte 02 - Revestimento superficial

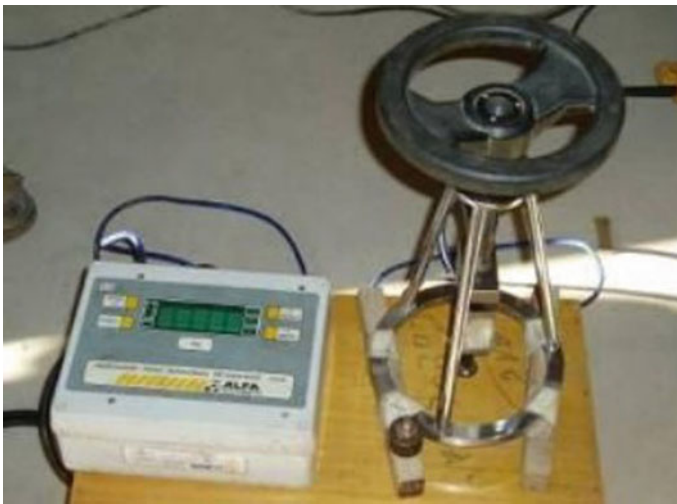**Fig. 10** Possible locations for determining tensile strength

**Fig. 11** Digital equipment used in experimental set-up

number 100BC9, five-digit nominal range and 1 point. This equipment measures the tensile stress through a load cell, which records the tensile stress at break. The traction stress is applied by the use of a manual device with operator-controlled speed.

For bonding the metal parts required for the adhesion test, the panels were divided into 3 different heights, to allow for the evaluation of the influence of ergonomics, with cuts being made to avoid coinciding with the horizontal joints of the panels, thus avoiding the impact of these elements on adherence. The depth of 20 mm of the cut was controlled by a mark made on the cup itself, while in the case of the superficial evaluation, the metal linings were bonded directly to the paste, without delimitation

Fig. 12 Cut of the coating using a cup saw

Fig. 13 Structural concrete
block with the coating all cut
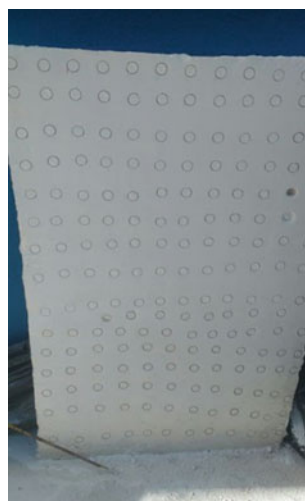
by cut, as recommended by NBR 13755 (2017) for this type of assessment (see
Figs. 12, 13 and 14).

4 Results and Discussion

This section presents the results obtained in the experimental program, which are
the foundation for the discussion based on initial expectations, previous research,
and existing literature. A statistical analysis (ANOVA) was performed, allowing for
a more detailed analysis of the values presented, with a 95% confidence level.

Fig. 14 Specimens for testing

To facilitate a better understanding, since there are many variables involved in the study, the results will be presented in a scaled manner, from macro analysis to more detailed discussions of influential factors.

Figures 15, 16, 17 and 18 show the results of the underlying statistical analysis performed with the tensile strength values obtained from the coating bases under study. After the calculation of the bond strengths, the existence of spurious values was statistically verified, and these were eliminated from the mean calculation. The individual results, together with the respective cut types and heights tested, are compiled in Annexes I, J, L, and M.
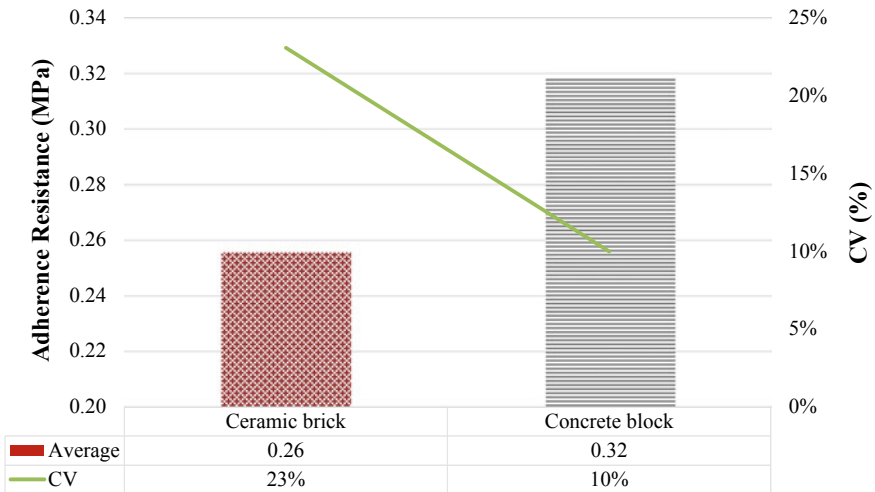

	Ceramic brick	Concrete block
Average	0.26	0.32
CV	23%	10%

Fig. 15 Overall results of the 480 samples tested

	TCV	TCE	BCV	BCE
Average	0.27	0.25	0.31	0.32
CV	22%	24%	8%	12%
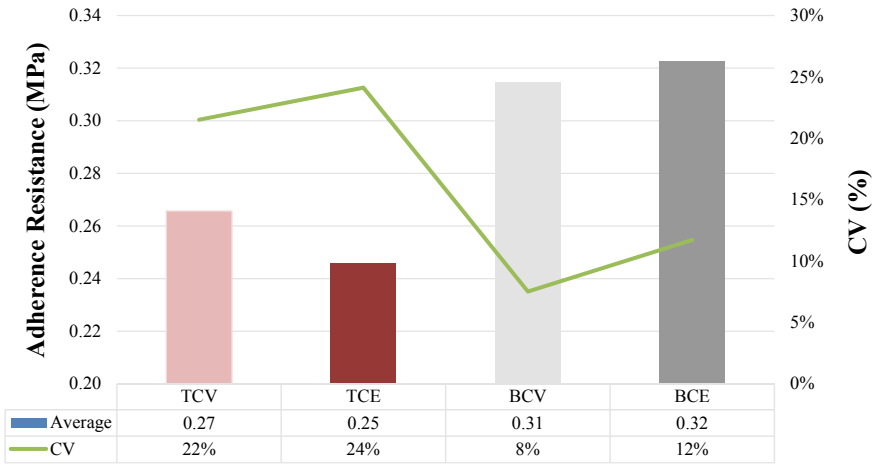
Fig. 16 Comparative results of the different bases

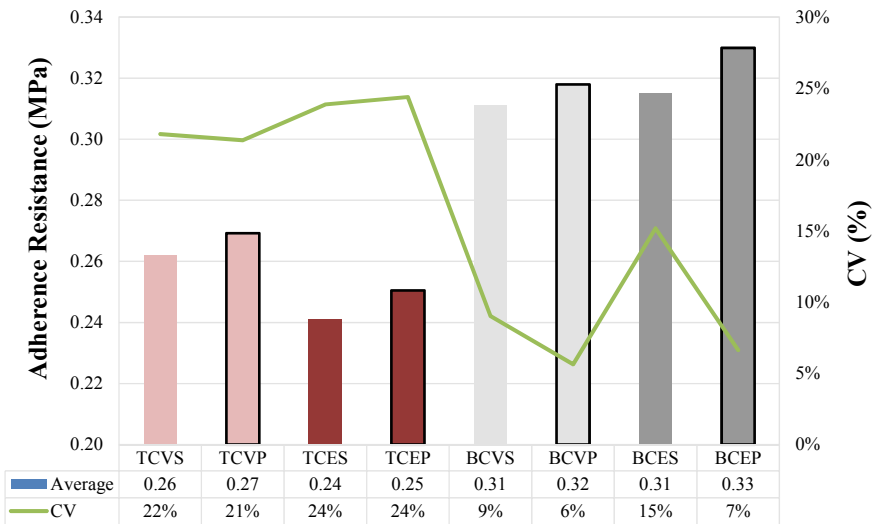|	TCVS	TCVP	TCES	TCEP	BCVS	BCVP	BCES	BCEP
Average	0.26	0.27	0.24	0.25	0.31	0.32	0.31	0.33
CV	22%	21%	24%	24%	9%	6%	15%	7%

Fig. 17 Adhesion results with different bases and depth of cut

4.1 Base Type Influence

Figures 15 and 16 show the values found in the 480 samples tested separated according to the type of component used in the base. As can be observed, the adherence values found in the samples tested on concrete blocks were higher than those obtained in the case of ceramic brick bases, a behavioural difference considered significant by statistical analysis ($F_{calculated} = 385 > F_{critical} = 3.86$).
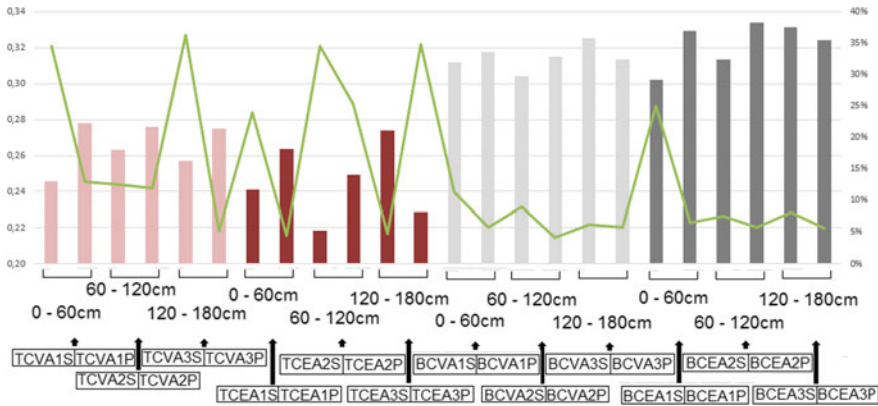
Fig. 18 Adherence results with different types of height

The better overall mechanical capacity between these bases can be credited to the higher roughness found in the concrete blocks, which helps in the macro anchoring of the plaster to the base while decreasing the contact area deficiencies. As for the coefficients of variation, higher values were found for the ceramic bricks, probably due to the naturally more significant heterogeneity of the manufacturing process of this type of component. It is crucial to keep in mind that the data analysed are from a set of 480 test samples, which corresponds to a number considered representative of the tests.

In this graph, each bar corresponds to a group of 120 samples and, in the case of ceramic bricks; a reduction in values can be observed when the tests were performed on structural components. For the ceramic blocks, an increase was observed when the test was performed with the structural elements. It is noteworthy that, in both cases, despite the close proximity between the absolute mean values, both are considered different by the analysis of variance at 95% (ceramic bricks: Calculated $= 8.42 >$ Critical $= 3.88$; concrete blocks: Calculated $= 12.01 >$ Critical $= 3.88$).

The difference in results between these bases can be credited to the increased roughness found in the concrete blocks, which helps in the macro anchoring of the plaster to the base and decreases the contact area deficiencies. It is crucial to keep in mind that in the case of concrete blocks, there was no significant difference observed whether they were structural or non-structural, unlike ceramic bricks, probably due to the naturally increased roughness of the concrete blocks.

In general, it is worth highlighting the predominantly adhesive rupture type in the samples (among those tested with paste cutting), especially in the bond between the paste and the base, which reinforces its influence on the adherence of the system. As for the coefficients of variation, higher values were found for the ceramic bricks, probably due to the naturally more significant heterogeneity of the manufacturing process of this type of component. It is important to be in mind that the data analysed are from a set of 480 test samples, which corresponds to a number considered representative of the tests.

4.2   Cut Profundity Influence

Figures 17 and 18 present the values found in the tested samples, separated according to the base type and profundity of the cut. The results showed a slight loss of adhesion resistance in the tested samples without making the cuts, which is, evaluating only the superficial layer, regardless of the base. This behaviour can be explained by the exposure of this surface layer after its execution, especially the presence of natural moisture, which tends to reduce the mechanical resistance of the gypsum plaster. Table 6 presents a summary of all rupture results obtained.

Table 6 Summary of rupture results

| Rupture form (%)					
Coating age: 28 days					
	A	B	C	D	E
Panel 01: Non-structural ceramic brick					
Cut 01	29.83	27.83	39.67	0.00	0.00
Cut 02	00.00	29.75	66.67	0.00	0.00
Average	14.92	28.79	53.17	0.00	0.00
Panel 02: Structural ceramic brick					
Cut 01	29.25	24.00	41.75	0.00	0.00
Cut 02	00.00	23.42	71.58	0.00	0.00
Average	14.63	23.71	56.67	0.00	0.00
Panel 03: Non-structural concrete block					
Cut 01	31.25	22.42	47.33	0.00	0.00
Cut 02	00.00	20.33	79.67	0.00	0.00
Average	14.63	23.71	56.67	0.00	0.00
Panel 04: Structural concrete block					
Cut 01	32.83	17.42	49.75	0.00	0.00
Cut 02	00.00	19.82	79.42	0.00	0.00
Average	16.42	18.17	64.58	0.00	0.00
Legend of rupture type			Legend of cut type		
Type A—Substrate rupture			Cut 01—Coating to substrate		
Type B—Rupture in substrate/mortar interface			Cut 02—Surface finish		
Type C—Mortar rupture					
Type D—Tear/glue interface rupture					
Type E—Glue/insert interface rupture					
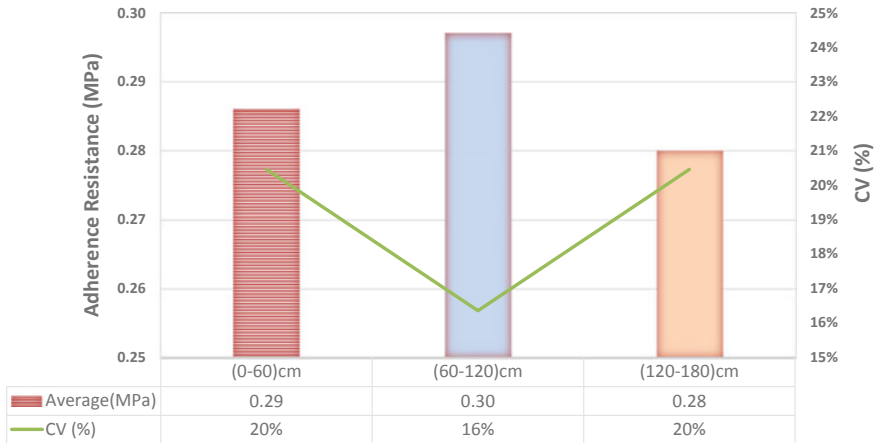
Fig. 19 Experimental results obtained at different heights

4.3 Influence of the Application Height

Figure 19 shows the values observed in the tested samples, separated according to the application time of the plaster paste.

In general, it was observed that there were no significant differences between the samples tested in the lower, central and upper planes with the plaster paste, regardless of the base to which it was applied. This fact stems from the technique of applying this coating, which is not made in a cast, as with the cement mortars (Scartezini 2002), which forces the applicator to push the mass against the wall and, thus, reduces the dispersions and the influence of ergonomics.

4.4 Analyse of the Factors that Influencing the Bond Strength

Although quite high, the variation coefficients of adhesion resistance obtained can be considered, for the most part, acceptable. This property measures the interaction between the mortar and the substrate and, therefore, depends on the characteristics associated with these two materials (Scartezini 2002).

In addition to the materials, it is essential to point out that other factors contribute to this high variation, such as the mortar application method, the craftsperson, and the intrinsic characteristics of the test method itself.

The obtained results lend themselves to the development of graphs that make more visible the interference of these variables: base type, cut type, and tested height, in relation to the tensile strength. The base type utilized had a significant influence on the values of bond strength of the coating, as seen in figures above. Regarding the cut type, a small decrease was noted in the results in all blocks where the cut was

performed superficially. Regarding heights, all bases in the heights between 0.6 and 1.2 m presented the best results, followed by heights between 1.2 and 1.8 m, and finally the heights between 0 and 0.6 m gave the worst results.

In general, lower values of adhesion were observed in ceramic blocks as compared to concrete blocks. Probably the more porous and rougher surfaces of the concrete blocks allowed for a more substantial amount of plaster paste pore penetration, contributing to the adhesion.

5   Conclusions

The bond strength test was found to have high variability due to the characteristics of the system and application themselves. The same is true with a large number of specimens tested (480 in the four bases) where the average coefficient of variation obtained was 41%.

Although some bond strength results stand out more than others, it can be observed that, compared to the requirements for cement mortar coatings, the plaster paste met the minimum required values.

The first point to note is the issue of the dispersion of the results. As expected, the application of plaster in concrete blocks presented a smaller dispersion than in the ceramic blocks; that is, it shows a greater homogeneity of the utility rendered.

For the ceramic block bases, the ruptures occur predominantly in the plaster layer, very close to the interface region, and therefore are characterized as a rupture due to cohesion failure.

For concrete block bases, ruptures almost invariably occur within the substrate due to the failure of block cohesion. This fact was denoted as a limiting factor in the bond strength value for this type of substrate.

The substrate type is mainly responsible for the variation in bond strength and is hugely significant. Concrete blocks provide bond strength much higher than the values produced by ceramic blocks.

The so-called "outer layer", which would be the first layer of the plaster coating, produced acceptable results in relation to the tests. An excellent professional together with superior materials and tools are vital aspects of perfect performance.

After testing and analysis of basic statistics, it was observed that the results in the concrete bases were more satisfactory, both in the surface cuts as well as in the cuts through to the base. This result is due to the higher porosity factor in the concrete bases than in the ceramic bases. However, all the tested specimens had positive results, demonstrating good adherence.

Adhesion is the property that the coating has to resist the tensions acting at the interface with the substrate, depending on the interaction between the layers that constitute the system for which the evaluation is intended (base, base preparation, and coating).

Several factors may influence the adhesion of the plaster coating, such as the dosage of the paste, the exposure conditions, the avidity for water, and the roughness

of the base. These are issues that have spawned several studies by different authors for a better understanding of the subject. Among these, one factor is of particular importance, which is the ergonomics of the operator during the application of the mortar to the wall, the height of which extends from the floor to the ceiling, as well as the application energy to the base, which varies according to its manual casting.

There was no marked variation regarding the height of the application of the plaster. The results in the extremities were inferior in all bases, albeit satisfactory.

In the centre of the panels, there was a tendency towards a more significant variation compared to the extremities, which indicates an excellent utility performance, since the median height enables more significant proximity of the craftsperson's arms to the work area, requiring less application effort, providing more homogeneity.

In the three casting conditions, the results showed that the height of the area to which the material is being applied influences significantly the craftsperson's ability in the performance of coating application, which could be verified by the higher resistance levels and the smaller dispersion values in the tested samples.

Ergonomics influenced the results obtained in the adhesion tests, the best results being observed in the samples tested in the centre areas (between 0.6 and 1.2 m) of the wall.

The experiments presented in this study, part of the author's master's dissertation, and highlight the influence of the base type (ceramic and concrete blocks, structural and non-structural) and the depth of the cut (deep or superficial) in the mechanical adhesion behaviour of the gypsum pastes used as a vertical internal coating.

It is noteworthy that, as already observed in other studies, the ergonomics of the craftsperson, evaluated in separate tests at different heights, was not relevant in the data studied. This element should come from an application technique using continuous pressure of the paste on the wall, as opposed to the energetic roughcasting commonly employed in mixed cement mortars.

In all cases, bond strength values higher than 0.20 MPa were found, which meet the requirements presented by NBR13281 (2005) for indoor use, the very situation in which plaster paste coatings were studied in this research.

It is important to note that the results presented should be restricted to the materials used in this research, and cannot be generalized in regard to all types of blocks and plaster used in construction work. Never-the-less, the significant amount of samples used (480 in total) represents a significant behaviour trend regarding this type of coating solution employed in interior building environments.

References

Baltar CAM, Bastos FF, Luz A (2005) Benvindo. Gipsita. Rio de Janeiro, Cetem

Barbosa AA, Ferraz AV, Santos GA (2014) Caracterização química, mecânica e morfológica do gesso β obtido do polo do Araripe. UNIVASF, Petrolina

Carasek H (2007) Materiais de Construção Civil e Princípios de Ciência e Engenharia de Materiais. São Paulo, IBRACON

Carasek H (2010) Argamassas. In Isaia GC (ed) Materiais de Construção Civil e Princípios de Ciência e Engenharia de Materiais. São Paulo: IBRACON, vol 2, Cap. 28, pp 893–944

Carasek H, Cascuco O, Scartezini LM (2001) Importância dos materiais de aderência dos revestimentos de argamasse. IV Simpósio Brasileiro de Tecnologias das Argamassas. Brasília, Beazil

Carasek H, Cascuco O, Santos MSJ, Lemos N (2011) Avaliação em obra da resistência superficial de revestimentos de argamassa. Rev ALCONPAT 1(2):118–140

Costa e Silva AJ, Cabral FMS, Neves TH, Lima BCSB (2017) Estudo comparativo da aderência de revestimentos de gesso aplicados por projeção mecânica e manual. XII Simpósio Brasileiro de Tecnologia das Argamassas, São Paulo

Flores-Colen I, Brito J, Branco F (2009) In situ adherence evaluation of coating materials. Exp Tech 33(3):51–60

Freitas VP, Corvacho H, Quintela M, Delgado JMPQ (2014) Assessing the durability of mortar tiles—A contribution for a prediction model. Eng Fail Anal 44:36–45

Ioppi PR (1995) Estudo da aderência das argamassas de revestimento em substratos de concreto. Florianópolis. MSc Thesis, Universidade Federal de Santa Catarina

Luz AB, Baltar CAM, Freitas EJG, Silva AP (2001) Mineração São Jorge. In: Sampaio JA, Luz AB, Lins FAF (eds) Usinas de Beneficiamento de Minérios do Brasil, pp 241–249

Lyra AC (1986) O mercado de gipsita e gesso no Brasil. Vortal Cadeia Produtiva do Gesso, 2002. http://www5.prossiga.br/gesso/index.html NOLHIER M. Construire en plâtre. França, L'Harmattan, 1986

Maciel LL, Barros MMS, Sabbatini FH (1998) Recomendação para Execução de Revestimentos de Argamassa para paredes de vedação internas e externa e tetos. São Paulo, Brazil

Melo A, Costa e Silva AJ, Torres SM, Delgado JMPQ, Azevedo A (2019) Influence of the contact area in the Adherence of Mortar—Ceramic tiles interface. Constr Build Mater (Accept)

Naderi M (2005) Friction-transfer test for the assessment of in situ strength and adhesion of cementitious materials. Constr Build Mater 19:454–459

NBR13281 (2005) Argamassa Para Assentamento e Revestimento de Paredes e Tetos. Rio de Janeiro, ABNT

NBR 13528 (2010) Revestimentos de paredes e tetos de argamassa inorgânicas—Determinação de resistência de aderência à tração. Rio de Janeiro, ABNT

NBR 13749 (2013) Render made of inorganic mortar walls and ceillings applications—Specification. Rio de Janeiro, ABNT

NBR 13755 (2017) Revestimentos cerâmicos de fachadas e paredes externas com utilização de argamassa colante — Projeto, execução, inspeção e aceitação — Procedimento. Rio de Janeiro, ABNT

NBR 7184 (1992) Hollow concrete masonry blocks—Compressive strenght testing. Rio de Janeiro, ABNT

NBR 7200 (1998) Render made of inorganic mortars applied on walls and ceilings—Procedure for application. Rio de Janeiro, ABNT

NBR 6461 (2005) Bloco cerâmico para alvenaria - Verificação da resistência à compressão. Rio de Janeiro, ABNT

Nita C, Pileggi RG, Cincotto MA, John WM (2004) Estudo da reciclagem do gesso de construção. I Conferência latino-americana de construção civil sustentável X encontro nacional de tecnologia do ambiente construído. São Paulo, Brazil

Paula P, Delgado JMPQ (2017) Hygrothermal performance of gypsum plaster houses. Diffus Found 14:128–157

Paula P, Vázquez da Silva M, Delgado JMPQ (2017) Numerical analysis of hygrothermal building performance of gypsum houses in different Brazilian climates. Diffus Found 10:132–148

Peres L, Benachour M, Santos VA (2008) Gesso produção e utilização na construção civil. Recife, SEBRAE

Santos HB (2008) Ensaio de aderência das argamassas de revestimento. MSc thesis in Civil Engineering of Escola de Engenharia da UFMG, Belo Horizonte

Scartezini LM (2002) Influência do tipo e preparo do substrato na aderência dos revestimentos de argamassa: Estudo da evolução ao longo do tempo influência da cura e avaliação da perda de água da argamassa fresca. Goiânia

Model to Estimate Concrete Carbonation Depth and Service Life Prediction

E. Possan, J. J. O. Andrade, D. C. C. Dal Molin, and José Luis Duarte Ribeiro

Abstract This chapter proposes a mathematical model for estimating the concrete carbonation depth and predicting the service life of concrete structures subject to CO_2 action, with easily obtainable input data. The input variables are divided into three groups: concrete properties (concrete compressive strength at 28 days, type of cement used, content and type mineral admixture); exposure conditions (a structure is indoors or outdoors, protected or not from rain) and environmental conditions (relative humidity and CO_2 content). The model was obtained by coupling the concrete conduct equations reported in the literature, especially the first Fick's Law. To adjust the model's coefficients and parameters, 1298 data obtained through experts' knowledge were used. The model determination coefficient was 0.9860, and the root-mean-square error (RMSE) was 0.3 mm. The model was validated using 298 data of the natural carbonation available in the literature, representing 87% of tested data. The results indicate that the model has the potential to predict the concrete carbonation depth for the boundary conditions that guided its development. It also presents itself as a potential tool for determining the concrete carbonation depth and service life prediction of new or existing structures.

Keywords Mathematic modeling · Concrete durability · CO_2 diffusion · Knowledge of experts

E. Possan (✉)
Federal University for Latin American Integration (UNILA), Foz do Iguaçu, Brazil
e-mail: epossan@gmail.com; edna.possan@unila.edu.br

J. J. O. Andrade
Pontifical Catholic University of Rio Grande Do Sul (PUC-RS), Porto Alegre, Brazil
e-mail: jairo.andrade@pucrs.br

D. C. C. Dal Molin · J. L. D. Ribeiro
Federal University of Rio Grande Do Sul (UFRGS), Porto Alegre, Brazil
e-mail: dmolin@ufrgs.br

J. L. D. Ribeiro
e-mail: ribeiro@producao.ufrgs.br

1   Introduction

The development of new technologies, constructive processes and construction materials associated with the sector's competitive requirements has fostered the construction of increasingly slim and economical buildings. However, edifications started to be exposed to extremely unfavorable environments due to industrial progress and the cities growth, and consequently, the increase in urban pollution. As a result, over time, many buildings began to show degradation levels higher than desired, presenting problems related to quality and durability, characterized by premature aging due, above all, to damages appearance.

Activities related to maintenance, repair and restorations of concrete structures and their parts correspond to 35% of total works volume in the civil construction sector and this number has been increasing in recent years (García-Alonso et al. 2007). It is estimated, in industrially developed countries, that 40% of total resources in the construction industry are destined to exist structures interventions and less than 60% in new constructions (Mehta and Monteiro 2014). This increment in costs involving structures replacement and the growing emphasis on Life Cycle Cost (LCC), more than the initial cost, is forcing engineers to pay more attention to durability issues (Mehta and Monteiro 2014). Organizations such as ACI (American Concrete Institute), Fib (Fédération Internationale Du Béton), RILEM (Reunion Internationale de Laboratoires D'essais et Materiaux), ISO (International Standards Organization), among others, have been working for years to improve this sector, inserting new concepts in Construction Industry (CI) for the benefit of durability and Service Life (SL) increasing of Reinforced Concrete (RC) structures. Several documents (Fib 53 2010; Fib 34 2006; Rilem 230-PSC 2015; ISO 13823 2008; ISO 16204 2012) published by these institutions have introduced by the years, relevant solutions both from an economic and durability viewpoint.

Regarding durability, the expectation that a structure can be durable or not can only be assessed using models that represent the deterioration processes in which it is susceptible, so that, for project assurances, the use of service life prediction (SLP) models are required (Fib 53 2010). To understand and model deterioration mechanisms, their kinetics and their action in RC structures, numerous studies have emerged from the technical-scientific community. As a result, several models to estimate the carbonated depth and SLP have been established in the literature (Hamada 1969; Ho and Lewis 1987; Papadakis et al. 1991; Jiang et al. 2000; Saetta and Vitaliani 2004; Thiéry 2005; Silva et al. 2014; Hills et al. 2015; Ta et al. 2016; Ekolu 2018, among others), which enabled considerable advances in understanding RC structures exposed to CO_2 over the time.

In RC structures, reinforcement corrosion is the main damage, caused mainly by chloride ions action (Tuutii 1982; Mehta and Monteiro 2014; Possan and Andrade 2014) and carbon dioxide penetration (Pasupathy et al. 2016; Andrade 2016; François et al. 2018). The global trend of increasing carbon dioxide (CO_2) emissions in the atmosphere (IPCC 2006; Mehta and Monteiro 2014; NOAA 2020), has direct consequences for structures inserted in urban environment, because carbonated depth

increases with gas concentration rise in the an environment (Saetta and Vitaliani 2004; Neville 2012; Ekolu 2018). This affects the life cycle (LC) of RC structures, reducing their durability and SL. According to Silva et al. (2014), the concrete carbonation is considered an important problem both in Civil Engineering and in Materials Science.

Many of models designed to determine the carbonated depth are based on simplified equations such as Fick's Law (Tuutii 1982; Pasupathy et al. 2016), which significantly limits the scope of its application (Marchand and Samsonb 2009). Others (Papadakis et al. 1991; Saetta and Vitaliani 2004; Thiéry 2005) require hard-to-obtain input data such as hydrates amount, crystals formed size and the CO_2 diffusion coefficient. The amount of hydrates and the CO_2 diffusion coefficient play an important role in the evaluation of carbonation kinetics. However, it is very difficult to obtain the CO_2 diffusion coefficient experimentally, due to time and cost limitations (Possan 2010a; Kwon and Song 2010).

Therefore, mathematical models in which input data are easy to obtain and have low acquisition costs (such as concrete compressive strength, cement type, mineral admixture content, among others) and which includes a probabilistic approach, can contribute to diffusion concrete degradation model by carbonation. In this way, this work presents a new mathematical model for predicting the concrete carbonation depth over time, developed with easily obtainable input variables.

2 Concrete Degradation Mathematical Modeling Due to Carbonatation

2.1 Influence Variable's Definition

The CO_2 ingress by concrete is linked to the porous structure of the material and it depends on the diffusion transport mechanism for it to occur (Houst and Wittmann 2002; Ishida and Maekawa 2001) and the concrete pores moisture (Steffens et al. 2002; Possan et al. 2017; Ekolu 2018).

According to Fig. 1, the literature states that the main factors affecting the carbonation phenomenon (Saetta and Vitaliani 2004; Papadakis et al. 1991; Hyvert 2009; Pauletti et al. 2007; Ekolu 2016; Chen et al. 2018) are related to:

(a) environmental conditions (CO_2 content, relative humidity and temperature);
(b) exposure conditions (indoor, outdoor, protected and unprotected from the rain); and,
(c) the concrete characteristics (binder chemical composition, compressive strength and adequate execution procedures).

These factors were considered in the proposed model, once the carbonation rate depends on its alkaline reserve and factors related to the concrete composition, such as water/binder ratio (w/b), cement type and content (Monteiro et al. 2012; Felix and
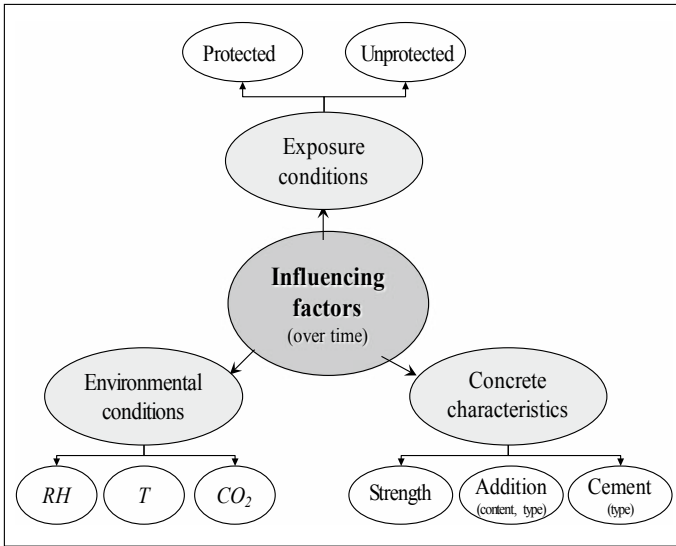
Fig. 1 Concrete carbonatation influencing factors with time variation

Possan 2018; Ekolu 2018). It's a slow process tending to attenuate over time (Parrot 1987; Neville 2012; Ekolu 2018), with a chemical reaction that depends on the porosity (Zhu et al. 2019), alkaline reserve, the cementing matrix's internal moisture and CO_2 availability in environment (Houst and Wittmann 2002; Ekolu 2018; Possan 2010b). Zhu et al. (2019) highlight that pore size distribution also presents a great influence on gas permeability.

2.2 Degradation Modeling

In the degradation process, there are always two simultaneous steps: transport and reaction (Andrade 2016). These need to be considered in modeling. Concerning the degradation modeling and the prediction of the structure's SL, Mehta (1994) presented that three key elements must be considered to establish a reliable model:

(a) a precise material definition (concrete);
(b) characterization of the environment; and
(c) a data file of accelerated durability results.

The author reports that the modeling of intervening parameters in different formulations to predict the SL of RC structures is difficult to be performed due to the existing complexity between the deterioration forms.

The carbonation front is controlled by CO_2 diffusion that occurs through the concrete's pores, which depends on concrete composition, environmental temperature, moisture content and carbon dioxide concentration. Therefore, the modeling of the carbonation within concrete is difficult because the process is very complex (Monteiro et al. 2012).

The studies based on probabilistic models of concrete degradation were intensified, existing some models that can foresee with a certain level of accuracy this process, which can provide contributions to the development of projects oriented to durability.

In general, there are two mains theoretical principles related to durability model development for SLP: one is empirical and the other is phenomenological or complex modeling. The first one is based on the acquired experience and results from performed tests, most of all applying statistical validation and data fit in modeling. This theoretical basis was used in the development of Hamada (1969), Ho and Lewis (1987), Jiang et al. (2000), Silva et al. (2014), Hills et al. (2015) models. Most of these models are based on Tuutti (1982) principle, represented by Eq. (1), which describes carbonatation as square root function of concrete exposed to CO_2, based on the diffusion law.

$$x = k\sqrt{t} \tag{1}$$

where, x is the carbonation depth (mm); k is the carbonation coefficient (mm/year$^{-0,5}$); t is the exposure time to CO_2 (year).

The second theoretical principle is based on the general nature laws—for carbonatation studies, physical and chemical laws and algebra inferences. Models resulted from this modeling type are developed according to the knowledge, mechanism analysis and kinetic degradation, highlighting the models presented by Papadakis et al. (1991), Saetta and Vitaliani (2004), Thiéry (2005) and others.

Both approaches present vantages and limitations. Although empirical modeling provides analytical solutions, it is not limited to a deep understanding of the degradation mechanisms involved, which makes extrapolation and generalization of the models difficult. Marchand and Samson (2009) report that the data basis used to generate these models is generally limited, which significantly restrain your application.

Complex modeling presents little practical application because most of its input parameters are very difficult to obtain. Besides, its application demands a large number of tests to determine the material properties (such as CO_2 diffusion coefficient, $Ca(OH)_2$ available, and others), requiring in most cases numerical solutions (Possan et al. 2018).

Thus, this work presents a new model aimed to estimate the carbonatation in real conditions with input parameters that are easy to obtain (like compressive strength, cement type and others), that included the main variables that influence in CO_2 ingress. The proposed model is designed to estimate the concrete carbonatation depth in natural exposure environments, allowing the use of simulations to predict the SL

of RC structures considering the corrosion initiation phase. Also, it can be used in carbon capture and storage (CCS) studies.

3 Proposed Model

The proposed model fits within the empirical modeling, which is based on data from experts of concrete degradation by carbonatation. However, physical-chemical laws that represent the carbonatation phenomenon were followed and are implicit in the model. Another important point is that the degradation data used in model validation is very significant, providing a major model application and generalization. Possan et al. (2018) provide additional information about the modeling process. Figure 2 shows the steps followed to develop the proposed model.

On the first step, data were collected using the focus group technique, carried out with experts in concrete durability. The second step covered carbonatation modeling where the equations that drive the degradation process were determined. Each influence variable was analyzed separately, the regression equations were found, coefficients and parameters were derived. On the last step, the model's coefficient and parameter adjustments were made, verifying its performance. If the model corresponded to the behavior of the carbonation phenomenon, it was validated using literature data. Otherwise, the previous steps were reviewed.

3.1 Data Collection

Due to the time required to perform long-term tests, experimental results of natural carbonation depth are few and fragmented in literature. This implies difficulties in generalizing and modeling the phenomenon, as well as in converting the results to real situations (Pauletti et al. 2007; Idorn 2005; Ekolu 2018). As experiment conduction which contemplates every influence variable on the concrete carbonatation would demand much time and resources, the data collection was based on the expert's knowledge using a focus group technique to collect model origin data.

Focus groups are forums that gather people in small groups to talk about a topic of interest. A focus group may be considered an interviewed group, with no alternation sense where a researcher and the interviewed answer. Instead, its essence is based on the interaction within the individuals, grounding on topics prompted by the researcher, who usually takes the role of a section moderator (Morgan 1997). The studies on the engineering field that applies this technique are scarce, lighting the scientific works of Bust et al. (2005) and Andrade et al. (2017).

In this study, the focus group meeting 11 concrete durability experts collaborated with it. Nine of them are Brazilian, one Mexican and one Spanish. During the meeting, it was discussed 118 scenarios arranged in 32 questions, which generated a data bank with 1298 pieces of information. Every requested information to the experts

Fig. 2 Model Formulation Process
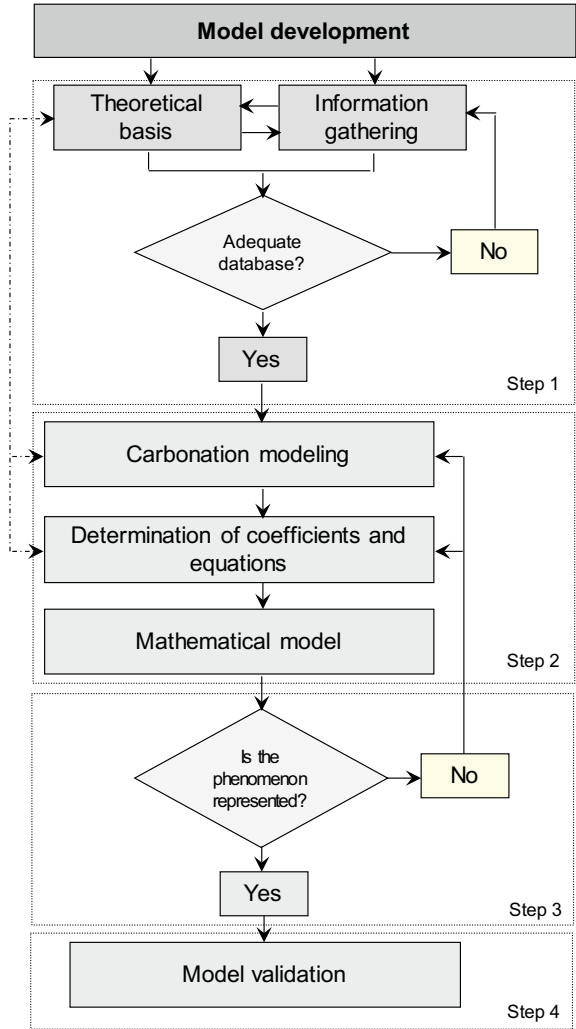
was related to concrete behavior due to degradation by carbonatation according to the area literature (Houst and Wittmann 2002; Neville 2012; Pauletti et al. 2007; Ekolu 2018). Based on the acquired knowledge, the experts provided a numerical value corresponding to the analyzed situation. The average results were used on the concrete carbonatation modeling after adjustments on Excel Software.

3.2 Determination of Model Variables

The factors and the influence variables are shown on Fig. 1 and Table 1 were used to data collection and carbonation mathematical modeling due to its influence on concrete carbonation.

For each influence factor (see Table 1), the adoption of the main variables was based on the acquisition easiness of model input. Those demanding long-term tests, as well as the use of equipment that is difficult to obtain or access (such as the diffusion coefficient, calcium hydroxide crystals size, among others), were excluded. Data that present major influence on carbonatation phenomenon is easy to collect and maybe gathered on field and lab trials were appreciated. Thus, the following input variables were considered in the model:

(a) concrete compressive strength;
(b) cement type;
(c) type and content of mineral admixture;
(d) CO_2 environmental content;
(e) relative humidity;

Table 1 Selected variables to discussion in the focus group

Factors	Variables	Limits/description
Concrete characteristics	Concrete compressive strength (MPa), at 28 days	20–60
	Type of mineral admixture	Silica fume (SF), Metakaolin (MC) Rice husk ash (RHA)
	Mineral admixture content (%)	0–25
	Cement type	CEM I[a], CEM II/A-L[b], CEM II/A-S[c], CEM II/B-S[c], CEM II/A-V[d], CEM III/A[e], CEM IV/A[f], CEM IV/B[f],
Environmental conditions	Relative humidity (%)	50–90
	Temperature (°C)	5–35
	CO_2 environmental content (%)	0.01–3
Exposure conditions	Unprotected from rain	Outdoor
	Protected from rain	Indoor Outdoor
Time	Age (years)	0–60

[a]Ordinary Portland Cement—Equivalent at Brazilian Cement CP I and CP V/ASTM C 150
[b]Portland cement with limestone filler—Equivalent at Brazilian Cement CP II F/ASTM C 150
[c]Portland cement with slag—Equivalent at Brazilian Cement CP II E/ASTM C 595/IP
[d]Portland cement with pozzolan—Equivalent at Brazilian Cement CP II Z/ASTM C 595/IS
[e]Portland cement with slag—Equivalent at Brazilian Cement CP III/ASTM C 595
[f]Portland cement with pozzolan—Equivalent at Brazilian Cement CP IV/ASTM C 595

(f) structure exposure condition (microclimate); and,

(g) time.

Regarding the choice for the compressive strength as a study parameter, there are two basic parameters that can be used to classify concrete according to its durability: the first is based on its compressive strength and the second is based on the water/cement or water/binder ratio. The use of compressive strength in the model is grounded for its easiness to determine it in loco and because it's a parameter of mandatory determination to technological control of concrete. It's known that the compressive strength alone doesn't describe the concrete durability characteristics (Mehta and Monteiro 2014), once other factors, such as cement type and content, mineral admixture type and content, among other factor interfere in the microstructural behavior, most of all in the material porosity, affecting durability properties (Saetta et al. 1993; Neville 2012; Mehta and Monteiro 2014). However, it must be pointed that compressive strength was not considered in an isolated way, depending on other variables (like cement and mineral admixtures) used in the concrete products that have a significant influence in compressive strength values.

3.3 Assumptions and Theoretical Foundation

The proposed model describes the concrete's behavior due to the CO_2 effect at time t, covers in its formulation the main influence variable xi that governs the concrete carbonatation y_i. Its applicability is dependent on many factors related to the degradation process in a way that, to establish adequate limits as well as the space of its coverage, it's assumed the following boundary conditions:

(a) the analysis is one-dimensional;
(b) the carbonatation front is well established, so it's uniform;
(c) the concrete is homogeneous and isotropic;
(d) the concrete doesn't show cracking; and
(e) the concrete structure was executed following good construction practice.

It is assumed in the modeling that the advance of the carbonation front through the concrete is a function, directly or indirectly of:

(a) the cementing matrix's porous structure expressed through:

    i. the strength or w/c ratio associated with binders presence;
    ii. the binder chemical composition, given by the cement and type of mineral admixtures;
    iii. the mineral admixtures, fineness and content;
    iv. the concrete compaction (densification).

(b) the CO_2 availability and diffusibility, which in this case is a function of:

    i. the CO_2 content in the environment;

ii. the cementing matrix's porous structure (see point "a");
iii. the relative humidity.

(c) the calcium hydroxide (($Ca(OH_2)$)) availability which is admitted as the function of:

i. the mineral admixture type and content;
ii. the binder's chemical composition defined by the cement type;
iii. the amount and size of the formed crystals.

(d) the concrete moisture conditions expressed by:

i. the most favorable condition to CO_2 diffusion—relative humidity above 40% and under 85%;
ii. the protection and the rain (protected indoor and outdoor, unprotected).

(e) the concrete's pore-clogging:

i. brings phenomenon attenuation due to carbon precipitation over time.

It was conducted a concrete carbonation modeling based on the premises mentioned above, evaluating the influence variables' contributions to the increase or reduction of the concrete's carbonation front. The data provided by the focus group were decisive to adjust these equations. After that, with these data, the model's parameters were determined and a general equation was developed (carbonation prediction model), representing the CO_2 ingress through the concrete. Finally, the model was tested with another database, from published studies in the literature.

3.4 Proposed Model's Variables Description

The influence variables x_i were analyzed in function of their effects in the concrete's carbonation depth y_i, leading to individual relationships explained by the following equations.

Regarding the concrete's axial compressive strength (f_c): it's assumed that the CO_2 ingress is inversely proportional to the concrete's axial compressive strength follow the Abrams (1927) principle, according to Eq. (2).

$$y_{fc} \cong \left(\frac{a_{fc}}{f_c} \right)^{k_{fc}} \tag{2}$$

where: f_c is the concrete compressive strength at 28 days, in MPa, a_{fc} is the model parameter and k_{fc} is the constant in function of concrete cement type.

Regarding the cement type (c): the cement chemical composition influence in the alkali content during hydration (Mehta and Monteiro 2014). In general, the greater carbonatable products content gets the slower the carbonation speed (Singh and Singh

2016). The cement type effect in the carbonatation depth advance is represented by constant k_c.

Regarding the mineral admixture (ad): it was assumed that for the carbonation phenomenon the presence of mineral admixtures has two effects: alkaline reserve *versus* pore structure changes (Singh and Singh 2016). The main effect is dependent on the level of w/b ratio (Felix and Possan 2018), addressed here through the concrete's compressive strength at 28 days. Must be pointed that for high strength concretes the microstructural changes are predominant, while for concretes with low strength values (usually smaller than 25 MPa), the effect of the alkaline reserve is more significant (Kulakowski et al. 2009). These effects are considered in Eq. (3).

$$y_{ad} \cong \exp\left(\frac{k_{ad}.ad^{b_{ad}}}{f_c + a_{ad}}\right) \tag{3}$$

where: y_{ad} is the mineral admixture content effect in the concrete carbonatation depth; ad is the mineral admixture content to concrete (silica fume, metakaolin and rice husk ash); f_c is the concrete's compressive strength at 28 days; k_{ad} constant for the mineral admixture in function of cement type; and a_{ad} and b_{ad} are the model's parameters.

Regarding the relative humidity (UR): the carbonatation reactions are dependent on concrete pores' moisture content (Neves et al. 2013). The fastest CO_2 diffusion rate occurs when the pores are partially full, neither saturated nor empty of the water (Parrot 1987; Papadakis et al. 1989; Neville 2012; Possan et al. 2017; Ekolu 2018; Chen et al. 2018). The relative humidity's influence in carbonatation is represented in the modeling by Eq. (4).

$$y_{RH} \cong \exp\left(-\frac{(k_{RH}RH + a_{UR1})^{b_{RH}}}{f_c + a_{RH2}}\right) \tag{4}$$

where: y_{RH} is the relative humidity's effect RH in concrete's carbonatation depth; f_c is the compressive strength at 28 days; k_{RH} constant for the mineral admixtures in function of cement type; and a_{RH1}, a_{RH2} and b_{ad} are the model's parameters.

For the carbon dioxide (CO_2): the CO_2 ingress through concrete is represented by Eq. (5) and depends on CO_2 environmental content (Rougeau 1997; Pauletti et al. 2007; Hyvert 2009; Cui et al. 2015) and cementing matrix's porosity (Parrot 1987; Kulakowski et al. 2009; Zhu et al. 2019).

$$y_{CO_2} \cong \exp\left(\frac{k_{CO_2}CO_2^{b_{CO_2}}}{f_c + a_{CO_2}}\right) \tag{5}$$

where: y_{CO_2} is the content of carbon dioxide (CO_2) in the concrete's carbonatation depth; f_c is the compressive strength at 28 days; k_{CO_2} constant of CO_2 in function of cement type; and a_{CO_2} and b_{CO_2} are the model's parameters.

Regarding the exposure conditions (*ce*): this characteristic is related to the watering and drying process (Hamada 1969; Houst and Wittmann 2002), directly related to the concrete's intern moisture equilibrium (Pauletti et al. 2007), and indirectly associated with the exposure environment (Yoon et al. 2007; Possan et al. 2017; Otieno et al. 2020). Concrete carbonation is higher indoors than outdoors environments. In outdoor environment it is higher when it is protected from rain (Possan et al. 2017; Ekolu 2016; Otieno et al. 2020). It's considered in modeling by the coefficient $k_{ce.}$.

Regarding the time (*t*): the formed carbonates in carbonatation reactions lead to concrete pore rectifying, making it difficult for the CO_2 access through concrete to occur, reducing the carbonatation speed (Hamada 1969; Pauletti et al. 2007). This tendency of attenuating carbonatation is expressed by Eq. (6).

$$y_t \cong \left(\frac{t}{a_t} \right)^{b_t} \tag{6}$$

where y_t is the effect of time on the concrete's carbonation depth; t concrete's exposure time to CO_2 or the structure age; a_t and b_t are model's parameters.

3.5   The Model

From the individual equations representing the influence of each variable on the concrete carbonation phenomenon (Eqs. 2–6), adjusted with the data from the focus group, it was possible to determine the fixed parameters by non-linear multiple regression, a_i and b_i and that integrate the formulations, which are presented in Table 2.

Table 2 Parameters ai and bi from individual equations

Interest variables	Parameters	Values
Compressive strength	a_{fc}	20.00
Mineral admixture (type and content)	a_{ad}	40.00
	b_{ad}	1.50
Relative humidity	a_{RH1}	100.00
	a_{RH2}	0.68
	b_{RH}	2.00
CO_2 content	a_{CO_2}	60.00
	b_{CO_2}	0.50
Time	a_t	20.00
	b_t	0.50

From the individual equations representing the influence of each variable on the concrete carbonation phenomenon presented above, adjusted with the data from the focus group.

So, the data collected during the focus group meeting (answers to the asked questions) were scaled from the main average (obtained in the first question) which was taken as one (these same data helped to define the acceleration equations' trend). The other values were referenced from this average, in upper or lower limits. With the spread averages, the behavior graphs were plotted and adjusted by non-linear regression, determining the parameters a_i and b_i for the individual equations of the interest variables.

Inserting the parameters' values from Table 2 in the equivalent formulations, the proportional relationships of each variable are expressed by the Eqs. (7)–(11), are referred to as compressive strength, mineral admixture content and type, relative humidity, CO_2 content and time, respectively.

$$y_{fc} \cong \left(\frac{20}{f_c}\right)^{k_{fc}} \tag{7}$$

$$y_{ad} \cong \exp\left(\frac{k_{ad}.ad^{\frac{3}{2}}}{f_c + 40}\right) \tag{8}$$

$$y_{RH} \cong \exp\left(-\frac{(k_{RH}.RH - 0.58)^2}{f_c + 100}\right) \tag{9}$$

$$y_{CO_2} \cong \exp\left(\frac{k_{CO_2}CO_2^{\frac{1}{2}}}{f_c + 60}\right) \tag{10}$$

$$y_t \cong \left(\frac{t}{20}\right)^{\frac{1}{2}} \tag{11}$$

The concrete's carbonatation depth y_i over time t may be described, in a generic way, through Eq. (12).

$$y_i = f(x_i, a) + \varepsilon_i \tag{12}$$

where $f(x_i, a)$ is the expected function to the i-ith case, to $x \geq 1$; y_i is the concrete's carbonatation depth, in function of variables x_i, to $i = 1, 2, 3\ldots$; x_i is the variables that influence the carbonatation phenomenon (Table 1); a is the model's fixed parameters, obtained by the focus group's data adjustment (Table 2) and ε_i is the associated error, with zero average.

Finally, all regression models obtained separately were grouped. Thus, the final model that describes the action of CO_2 through concrete, for the corrosion's beginning time due to carbonation is shown by Eq. (13).

$$y = k_c \times \left(\frac{20}{f_c}\right)^{k_{fc}} \times \left(\frac{t}{20}\right)^{\frac{1}{2}}$$

$$\times \exp\left[\left(\frac{k_{ad} \times ad^{\frac{3}{2}}}{40 + f_c}\right) + \left(\frac{k_{co_2} \times CO_2^{\frac{1}{2}}}{60 + f_c}\right) - \left(\frac{k_{RH} \times (RH - 0,68)^2}{100 + f_c}\right)\right] \times k_{ce}$$

(13)

where y is the average concrete carbonation depth, in mm; f_c is the concrete compressive strength, in MPa; k_c is the the variable factor regarding the cement type used (Table 3a); k_{fc} is the variable factor regarding concretes compressive strength, in function of used cement type (Table 3a); t is the concrete age, in years; ad is the pozzolanic addition content in concrete, in % related to cement mass; k_{ad} is the the variable factor regarding pozzolanic addition in concrete—silica fume, metakaolin and rice husk ash—in function of used cement type (Table 3a); RH is the relative humidity, in %*0,01; k_{rh} is the variable factor regarding relative humidity, in function of used cement type (Table 3a); CO_2 is the CO_2 content in the atmosphere, in %; k_{CO_2} is the variable factor regarding environment's CO_2, in function of used cement

Table 3 Model coefficients as a function (a) concrete characteristics and environmental conditions and, (b) exposure conditions

(a)

Cement type	Concrete characteristics			Environmental conditions	
	Cement	f_c	Addition	CO_2	RH
	k_c	k_{fc}	k_{ad}	k_{CO_2}	k_{UR}
CEM II/A-L[b]	22.48	1.50	0.32	15.50	1300
CEM II/A-S[c] CEM II/B-S[c]	21.68	1.50	0.24	18.00	1100
CEM II/A-V[d]	23.66	1.50	0.32	15.50	1300
CEM III/A[e]	30.50	1.70	0.32	15.50	1300
CEM I[1]	33.27	1.70	0.32	15.50	1000
CEM IV/A[f], CEM IV/B[f]	19.80	1.70	0.24	18.00	1300

(b)

Structure exposure conditions	Coefficient (k_{ce})
Indoor, sheltered from rain	1.30
Outdoor, sheltered from rain	1.00
Outdoor, exposed to rain	0.65

[a]Ordinary Portland Cement—Equivalent at Brazilian Cement CP I and CP V/ASTM C 150
[b]Portland cement with limestone filler—Equivalent at Brazilian Cement CP II F/ASTM C 150
[c]Portland cement with slag—Equivalent at Brazilian Cement CP II E/ASTM C 595/IP
[d]Portland cement with pozzolan—Equivalent at Brazilian Cement CP II Z/ASTM C 595/IS
[e]Portland cement with slag—Equivalent at Brazilian Cement CP III/ASTM C 595
[f]Portland cement with pozzolan—Equivalent at Brazilian Cement CP IV/ASTM C 595

type (Table 3a) and k_{ce} is the variable factor regarding the rain protection, in function of structures exposure conditions (Table 3b).

4 Parametric Analysis

The model for an estimate of the concrete carbonation depth proposed will be analyzed regarding the variables that influence in CO_2 ingress, verifying their behavior. In this way, the effect of compressive strength, cement type, type and content of mineral admixtures, relative humidity, CO_2 content and exposure condition were evaluated separately.

4.1 Effect of Variables in Model Behavior

For the analysis of each variable, their levels were changed separately, considering the limits established in Table 4, and the analysis were conducted comparing the results with the low level presented.

Table 4 Values adopted for the verification of the model—application example

Variable	Level		
	Low	Medium	High
Cement type	CEM I[a]	CEM I	CEM I
Concrete compressive strength (MPa)	20.0	30.0	50.0
Amount of mineral admixture (%)	0.0	5.0	10.0
Type of mineral admixture	SF[b]	SF	SF
Temperature (°C)	18.0	20.0	22.0
Relative humidity (%)	60.0	70.0	80.0
Environmental CO_2 concentration (%)	0.05	00.5	01.0
Time (years)	30.0	40.0	50.0
Concrete cover (mm)	20.0	25.0	30.0

[a]Ordinary Portland Cement—Equivalent at Brazilian Cement CP I and CP V/ASTM C 150
[b]SF—Silica fume

4.1.1 Effect of Parameters Related to Compressive Strength of Concrete

The effect of compressive strength in carbonation depth is presented in Fig. 3, while Fig. 4 shows the evolution of carbonation depth in time for the three levels of compressive strength under analysis (see Table 4).

The literature describes that the carbonation depth decreases with the increase of concrete compressive strength (Ekolu 2016; Chen et al. 2018; Sun et al. 2020). Kulakowski et al. (2009) investigated the effect of SF in compressive strength and found that, for w/b ratios higher than 0.50 and the same silica content, the compressive strength is inversely proportional to the carbonation depth.

It can be observed in Fig. 3 that the proposed model represents the tendency to decrease the carbonation depth in 30 years to values less than 10 mm when the compressive strength is greater than 40 MPa. When the resistance is lower than

Fig. 3 Effect of compressive strength on the carbonation depth
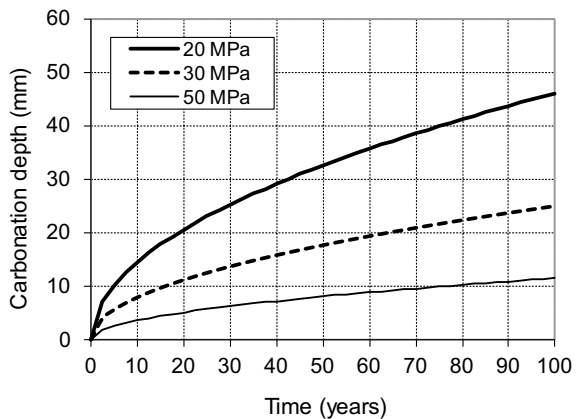
Fig. 4 Carbonation depth over time, depending on the compressive strength
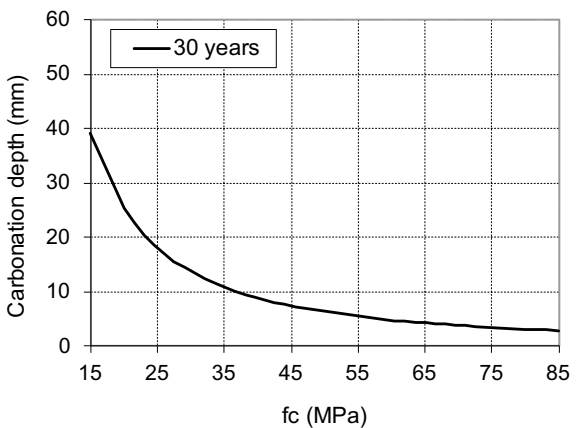
this value, the carbonation depth presents the highest values, being significantly influenced by this variable. That behavior is attributed to the porous structure of the cement matrix, which changes according to the increase of water content in concrete. In concretes with low resistance—with higher w/b—the amount and connectivity of the pores are greater, increasing the CO_2 ingress, consequently, the carbonation is also higher.

For concretes with 20 MPa, the effect of cement type on the carbonation depth (Fig. 5) is 30% greater for those produced with cement with a high content of pozzolanic material and slag (CEM III/A, CEM IV/A, CEM IV/B) and lower for other cement types (Table 1). The cement type, the compressive strength and the interaction between these two variables have a significant influence in carbonation depth. It was verified that the cement type has no significant influence on the carbonation depth, indicating that it depends mainly on compressive strength. The comparisons of means (considering a decision limit equal to twice the standard deviation) do not present significant differences between the cement evaluated for concretes with compressive strength of 40 MPa. For concretes with 20 MPa, the differences observed are significant for cement with pozzolanic or slag, concerning the other cement types.

Figure 6 shows the influence of the cement type in carbonation depth over time. It can be observed that concrete produced with ordinary cement Portland and early-age cement have small variations in carbonated depth. However, this difference becomes significant when comparing these cement types with pozzolanic (GGBFS and fly ash) ones.

The negative influence of mineral admixtures in carbonation depth was discussed by many researchers (Jiang et al. 2000; Pauletti et al. 2007; Kulakowski et al. 2009; Zhao et al. 2018; Ekolu 2018; Otieno et al. 2020, among others) and was considered in model (Figs. 7 and 8). It is observed that for concrete with lower strength, the carbonation depth increases with the silica fume content. However, for high performance concretes (HPC) small levels (from 0 to 5%) of silica fume are not significant

Fig. 5 Effect of cement type and compressive strength on carbonation depth
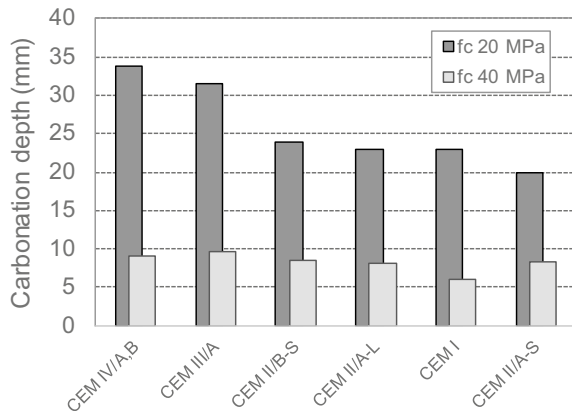
Fig. 6 Evolution of the carbonation depth over time depending on the cement type
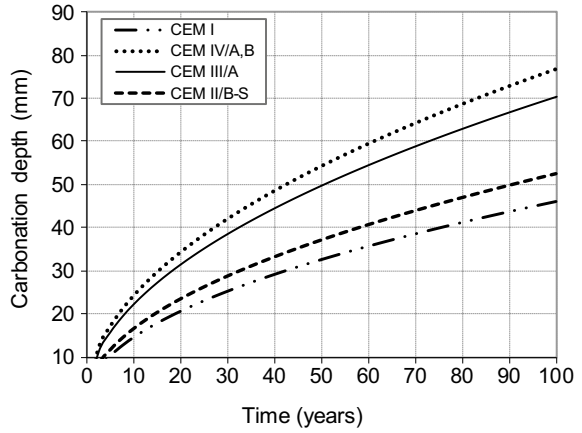
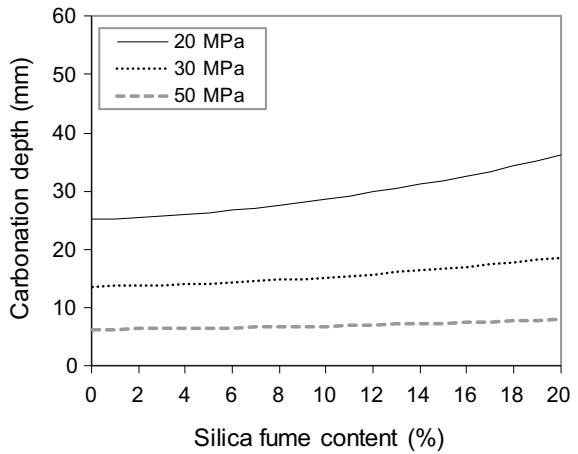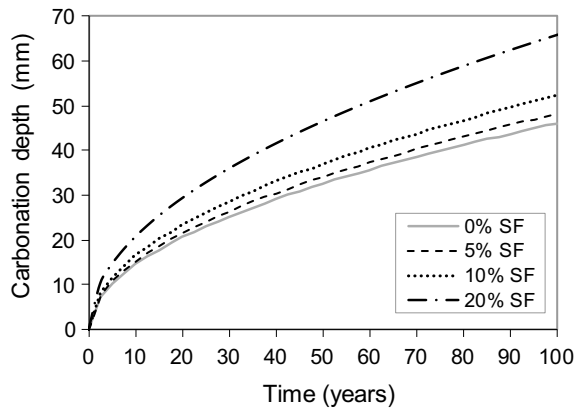**Fig. 7** Effect of addition content and compressive strength on the carbonation depth

Fig. 8 Carbonation depth over time x addition content

in the carbonation depth. In these concretes, the effect of porosity is predominant in relation to the alkaline reserve, as reported by Kulakowski et al. (2009).

It must be pointed that concretes with a compressive strength lower than 30 MPa or high w/b ratio (>0.50) presents higher porosity, increasing the carbonation rate. When this concrete is produced with cement with mineral admixtures their effect is not enough to prevent the ingress of CO_2. Therefore, in this case, the reduction of the alkaline reserve is more relevant to the pore-refining effect (Ceukelaire and Nieuwenburg 1993). In concrete with compressive strength over 30 MPa the porosity is lower, decreasing the carbonation depth, even for concrete with low alkaline reserve (Kulakowski et al. 2009).

In this way, for compressive strength higher than 40 MPa (lower w/b ratio), the CO_2 ingress is independent of the mineral admixtures and the cement type. For lower strength concretes (higher w/b ratio), the mineral admixtures increase the carbonation depth, and the alkaline reserve effect predominates (Kulakowski et al. 2009). Therefore, for this resistance level, the selection of the cement type and the mineral admixtures to be used in the concrete mix proportioning is very important considering the carbonation depth.

4.1.2 Effect of Parameters Related to Environmental Conditions

Several works (Parrot 1987; Papadakis et al. 1989; Neville 2012; Possan et al. 2017; Ekolu 2018; Chen et al. 2018) have shown that relative humidity (RH) levels between 50 and 80% are more appropriate to begin the carbonation process.

As RH is one of the most influential variables in carbonation depth, the Papadakis et al. (1989) experiment was used to compare the model's behavior with real carbonation data under RH variations (Fig. 9), whose model developed present a good agreement with the data.

Fig. 9 Behavior of the proposed model" x experimental
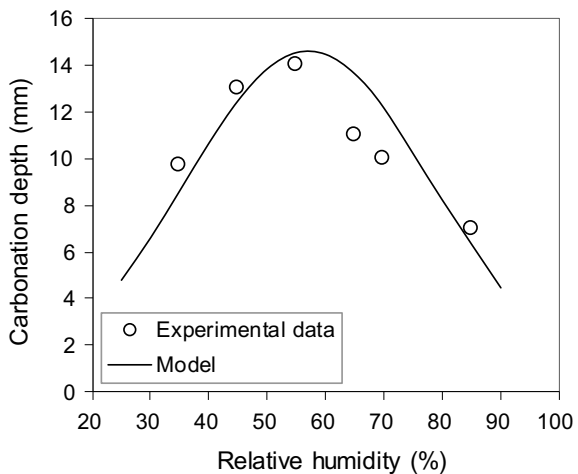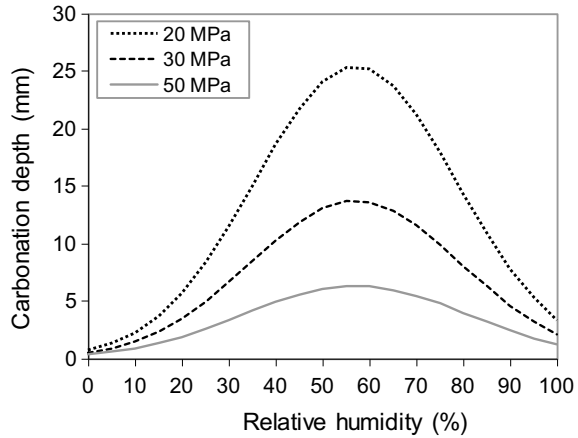
Fig. 10 Effect of relative humidity and compressive strength on carbonation depth

It can be seen in Fig. 10 that the model developed indicates an area in which the carbonation depth tends to be maximum (RH around 60%) and very high (90%) or very low (30%) levels result in small carbonated depths.

The influence of RH varies according to the concrete compressive strength, i.e., it is directly related to their porosity. Possan et al. (2017) showed the effect of concrete internal moisture on carbonation depth in a real structure (Fig. 11), whose authors verified that the carbonation depth was zero for RH close to 100% and maximum for internal moisture around 70%.

The model developed considers the increase of carbonation depth with the concentration of CO_2 in the environment (Figs. 12 and 13. However, in concretes with a compressive strength lower than 30 MPa, the influence of CO_2 concentration in concrete carbonation is more noticeable, decreasing with the increase of compressive strength.

It can be observed in Fig. 12 that the CO_2 concentrations commonly found in the atmosphere (between 0.03 and 0.1%) do not result in high variations in carbonation depth. The world average in 2020 being 414.11 ppm, as measured by NOAA (2020).

Fig. 11 effect of an internal moisture of concrete at carbonation depth (Possan et al. 2017)
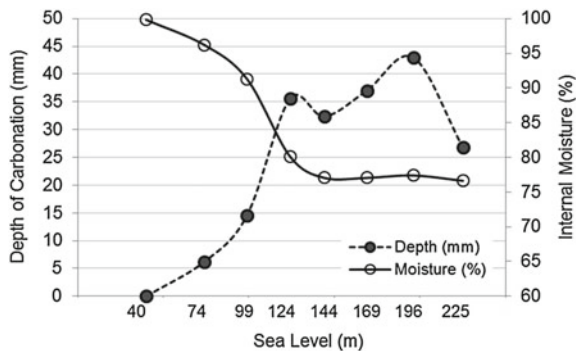
Fig. 12 Effect of CO_2 content and compressive strength on carbonation depth
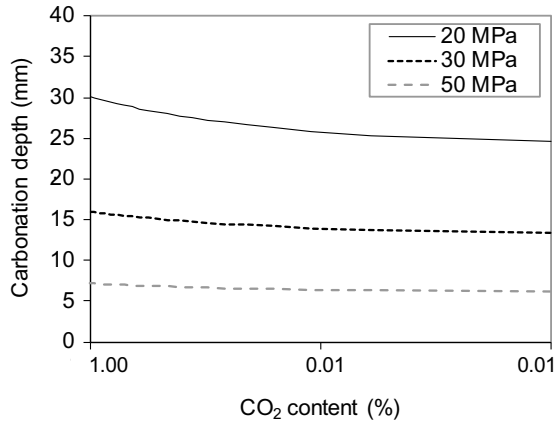
**Fig. 13** Depth of carbonation over time x CO_2 content
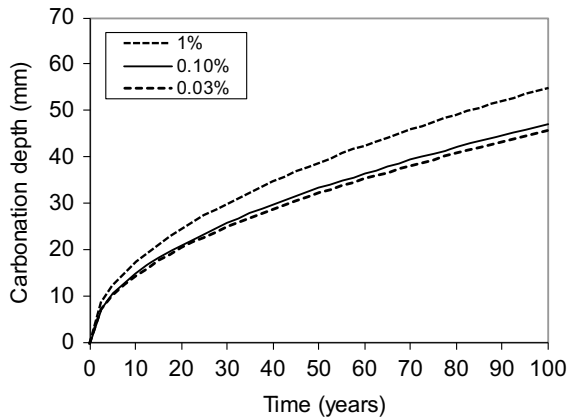
However, when this content is increased to 1 and 5%, normally used in accelerated tests, the carbonation depth is significantly increased, as presented by Yoon et al. (2007). For studies where the carbonation process is accelerated, the results showed that the increase in CO_2 concentration is not directly related to the increase in carbonation depth values (Rougeau 1997; Hyvert 2009; Cui et al. 2015).

4.1.3 Effect of Parameters Related to Exposure Condition

Figure 14 shows that the carbonation depth is greater for concrete exposed in indoor environments protected from rain, followed by the protected and unprotected outdoor environment from rain.

Fig. 14 Depth of
carbonation over time x rain
protection
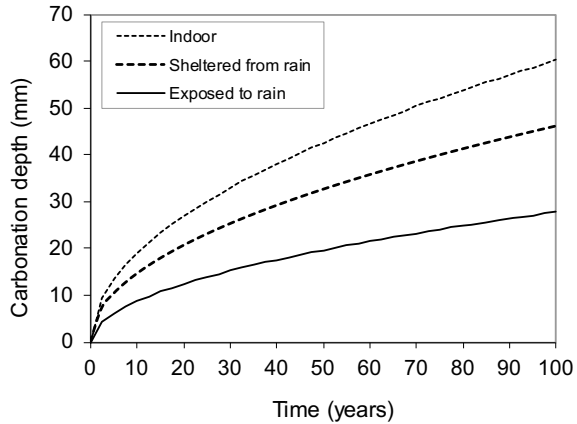
The CO_2 ingress through the concrete occurs by a diffusion mechanism and depends on the RH levels to occur, whose is directly associated with the conditions of exposure to rain, the wetting and drying of the structure and the dimensions of the structural elements of the structure. The longer the exposure time of the structure, i.e., its age, the higher is the carbonation depth of the concrete. It should be noted that several researchers (Neville 2012; Bakker 1988; Dyer 2014) describe that, for more advanced ages, this phenomenon tends to stabilize.

So, it should be noted that the model results represent the carbonation behavior of concrete concerning CO_2 for typical concentrations in natural environments.

5 Validation and Discussion

5.1 Sensitivity Analysis of Proposed Model

The sensitivity analysis seeks to determine the variation degree effect of model parameters in the result (in this case, on the carbonation depth). It is used to determine a study's results sensitivity when its premises are changed, and it is possible to assess the result's confidence degree in situations of uncertain decisions or assumptions about the data and results used. It allows evaluating the impacts associated with changes in input variables values, system parameters and structural changes in a model. These impacts are determined by analyzing the output variables.

The sensitivity analysis is used to verify the influence of variables x_i that compound the proposed model. For this, each of the variables had their levels changed around the average to more (maximum level) and less (minimum level), as shown in Fig. 15.

The sensitivity analysis shows that compressive strength has the greatest influence on the carbonated depth. The increase in concrete strength from 20 to 60 MPa reduces

Fig. 15 Sensitivity analysis of the proposed model variables
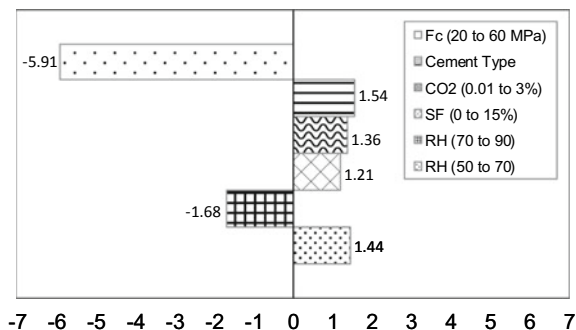
approximately six times the concrete carbonation depth, as reported by Ho and Lewis (1987). When the content of silica fume is increased from 0 to 15%, and there is variation in the cement type (see Table 1), the carbonated depth is increased by 1.2 times. The negative effect of mineral admixture on concrete carbonation, especially in concretes with a w/b ratio higher than 0.50 is reported in the literature (Kulakowski et al. 2009; Felix and Possan 2018).

It is observed that the increase in relative humidity from 50 to 70% raises the carbonation depth in one and a half times. The increase in humidity from 70 to 90% reduces the carbonated depth, indicating that carbonation is greater for humidity around 70%, as described in literature (Tuutti 1982; Parrot 1987; Papadakis et al. 1989; Neville 2012) and proved in real structures evaluations (Possan et al. 2017).

5.2 Residual Analysis

The results collected in the focus group (see Appendix B), which provided the database for model development, were compared with the predicted values (also presented in Appendix B) by the proposed model.

It is noted that the data obtained in the focus group interview showed excellent statistical adjustments for determining partial equations, with determination coefficients (r^2) higher than 0.90. The data were also analyzed based on residues generated (the difference between the values observed in the focus group and those predicted by the adjustment model). The regression models are considered adequate when residues are randomly distributed around the zero average.

In Figs. 16 and 17 are presented, respectively, the observed values (collected in the focus group) *versus* values predicted by the model and the residual. Considering a 95% confidence interval, Table 5 shows the residual analysis results, as well as the model determination coefficient (r^2).

It is observed that, for the response variable of interest (in this case, concrete carbonation depth), the residues are randomly distributed around the zero average, indicating that the adopted regression model is satisfactory. For carbonated depth,

Fig. 16 Values reported by
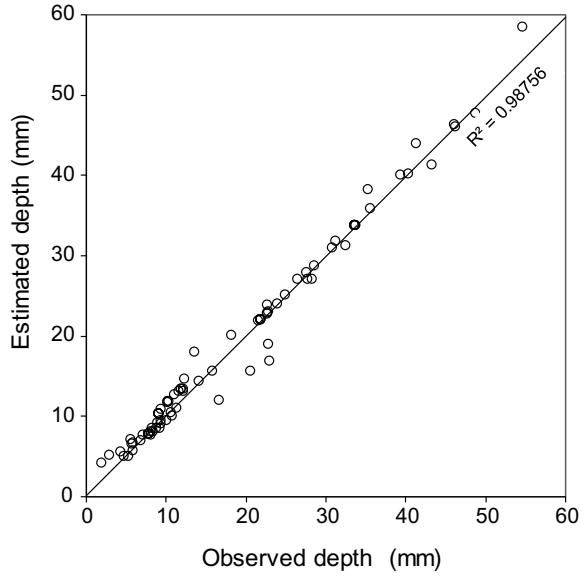experts x values predicted by
the model

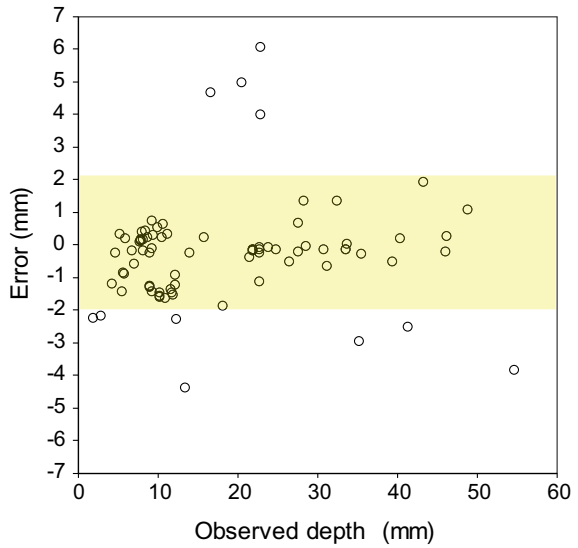**Fig. 17** Distributions of
model errors

Table 5 Residual analysis of the proposed model

Parameter	Minimum	Maximum	Deviation	Average	r^2
Result	0.00	6.00	1.50	0.30	0.9860

residues average values are around 0.3 mm, a value compatible with specified by RILEM CPC 18 (1988), which errors associated with tolerated measurement are approximately 0.5 mm.

It is noted that the prediction model developed showed excellent adherence to experts' data, obtained during a focus group. However, for its validation, it is necessary to insert degradation data from real works or natural carbonation tests. For this, the technical-scientific community collaboration is fundamentally important, especially for a database arrangement with concrete degradation by carbonation.

5.3   Comparison with Literature Data

Over the years, several models for estimating the carbonation depth of concrete have been proposed by the literature (Possan 2010a; Rigo et al. 2018). It is noteworthy that carbonation depth estimation models can be useful tools for technological control of concrete structures. Its use is essential in structural projects where economic, social and/or environmental importance is high. Rigo et al. (2018) highlight that it is necessary to evaluate the adequacy of these models to reality, comparing the predictions with real gradation data, to identify the best model that represents adequately the carbonation phenomenon.

Thus, to verify the general applicability of the proposed model and its generalization potential, the same test was done with literature data. The database used was formed by data from natural carbonation tests of long-term concrete from Possan (2004), Figueiredo (2004), Meira (2004), Isaia (2007), Ferreira (2013) and Dal Molin (2018).

Each database was included individually in the Excel spreadsheet for model programming, considering the test exposure conditions, as well as the concrete characteristics. Figure 18 shows the correlation of 298 natural carbonation depth data for different concretes. Note that the errors are well distributed around zero (see Fig. 19), concentrated between +2 and −2 mm.

The largest error variation was observed in concretes with a low w/c ratio (Fig. 20). The average error for Ferreira's data (2013) was 2.41 mm for concrete with a/c 0.40. For these data, the model estimated depths greater than those observed experimentally, which is favorable to safety. For concretes with a/c 0.55 and 0.70 the average error observed was around 1.71 mm and 0.41 mm. Considering the large number of variables that influence concrete carbonation, these errors can be considered acceptable in the modeling process.

Considering that RILEM-CPC-18 (RILEM 1988) indicates that carbonation depths below 0.5 mm are not differentiated in the measurements; the errors found in the simulations performed in the present study can be considered satisfactory. This indicates that the proposed model represents the carbonation depth of different concretes, respecting the limits established in the modeling process.

It is important to note that most of the carbonation data available in the literature are the short periods of natural exposure, which are important for analyzing the

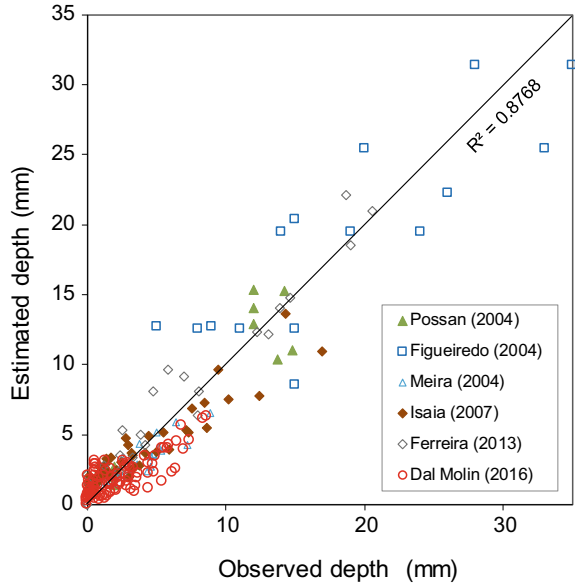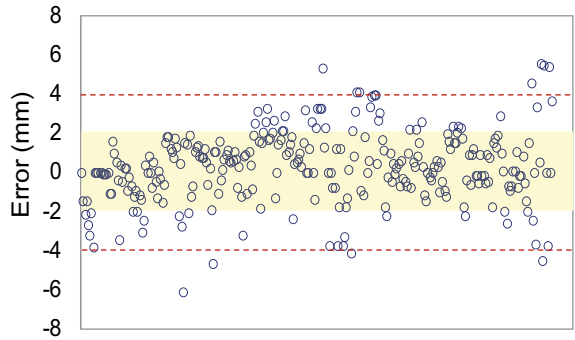**Fig. 18** Carbonation depth observed experimentally x estimated by the proposed model

**Fig. 19** Error in estimates of carbonation depth over time

beginning of CO_2 diffusion through concrete. The limited availability of long-term natural degradation data (over 5 years), unfortunately, is a challenge in the modeling processes.

6 Final Remarks and Conclusions

The average error obtained by the proposed model was 0.3 mm, with a determination coefficient of 0.9860, indicating that the developed model has the potential to

Fig. 20 Modeling
carbonation depth over time
x Experimental data
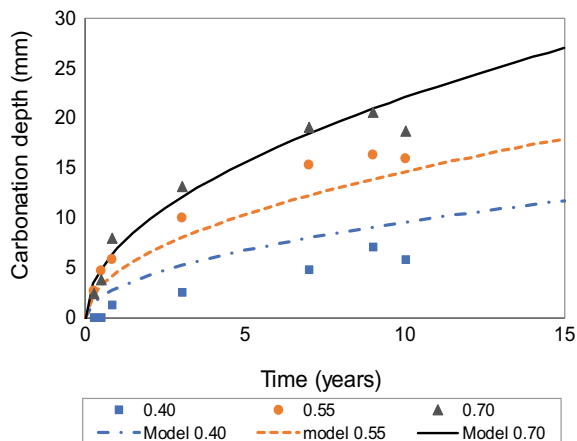
predict concrete carbonation depth for the boundary conditions that guided its development/design. In comparison with studies in literature, the model has a prediction potential in 85% of evaluated cases.

The proposed model is simple to apply because it uses easily obtained input variables (such as compressive strength, type of cement, etc.). It can be used in studies and design definitions for new structures and existing structures studies, acting as a helpful potential tool to determine concrete cover thickness for the desired service life. Likewise, it can be used for purposes of estimating desired service life, given the structure design and exposure conditions (example Andrade et al. 2017). It can still be used in studies whose purpose is to calculate the CO_2 capture due to concrete carbonation (this subject is detailed in Possan et al. 2017).

The main advantage of the model concerning others in literature is that input data to carrying out simulations are easy to obtain, not requiring complex laboratory tests for this. Simulation can also be conducted easily with deterministic or more sophisticated processes, with greater proximity to reality, through probabilistic simulations.

The model can be used as a function of durability limit state (DLS) in probabilistic studies and can be used for service life predictions of concrete structures subjected to carbonation action, as presented by Andrade et al. (2017), serving as a tool for approximation of reality, since it contains uncertainties.

The proposed model, by the way of conception, has applicability for concretes with environmental and exposure characteristics and conditions described in this study, if limits established in the mathematical modeling for each input variable are met. Extrapolation to different conditions or beyond the limits established in the model may require further studies and should be taken with caution.

References

Abrams DA (1927) Water-cement ratio as a basis of concrete quality. J Am Concr Inst 452–457

Andrade, C (2016) Future trends in research on reinforcement corrosion. In: Corrosion of Steel in Concrete Structures, pp 269–288. https://doi.org/10.1016/b978-1-78242-381-2.00014-6

Andrade JJO, Possan E, Dal Molin DCC (2017) Considerations about the service life prediction of reinforced concrete structures inserted in chloride environments. J Building Pathol Rehabil 2:1–8. https://doi.org/10.1007/s41024-017-0025-x

Bakker RFM (1988) Initiation period. In: Corrosion of steel in concrete. London: Chapman & Hall

Bust AG, Gibb F, Haslam RA (2005) Manual handling of highway kerbs: focus group findings. Appl Ergonom 36:417–425. https://doi.org/10.1016/j.apergo.2004.05.005

Ceukelaire L, Nieuwenburg V (1993) Accelerated carbonation of a blast-furnace cement concrete. Cement Concr Res 442–452

Chen Y, Liu P, Yu Z (2018) Effects of environmental factors on concrete carbonation depth and compressive strength. Materials 11:2167. https://doi.org/10.3390/ma11112167

Cui H, Tang W, Liu W, Dong Z, Feng X (2015) Experimental study on effects of CO_2 concentrations on concrete carbonation and diffusion mechanisms. Constr Build Mater 522–527. https://doi.org/10.1016/j.conbuildmat.2015.06.007

Dal Molin DCC (2018) Contributions for the improvement of the technical standard for performance evaluation of residential building NBR 15575. Research Report. Research Report. INOVATEC—FINEP Network. Public Call MCT/MCidades/FINEP/transversal action environmental sanitation and housing—07/2009. Agreement 01.11.0142.00 (Portuguese)

Dyer T (2014) Concrete durability. CRC Press, Taylor & Francis Group

Ekolu SO (2016) A review on effects of curing, sheltering, and CO_2 concentration upon natural carbonation of concrete. Constr Build Mater 127:306–320. https://doi.org/10.1016/j.conbuildmat.2016.09.056

Ekolu SO (2018) Model for practical prediction of natural carbonation in reinforced concrete: Part 1-formulation. Cement Concr Compos 86:40–56

Felix EF, Possan E (2018) Balance emissions and CO_2 uptake in concrete structures: simulation based on the cement content and type. Revista ibracon de estruturas e materiais. 11:135–162. http://dx.doi.org/10.1590/S1983-41952018000100008

Ferreira MB (2013) Study of natural carbonation of concrete with different mineral admixture after 10 years of exposure. Dissertação, Pós-Graduação em Geotecnia, Estruturas e Construção Civil, Universidade Federal de Goiás, Goiânia, Goiás, 197p (in Portuguese)

Fib Bulletin 34. Model Code for Service Life Design. Lausanne: Fédération Internationale du Béton, 2006

Fib Bulletin 53 (2010) Model code for structural concrete textbook on behavior, design and performance, 2, vol 3, Design of durable concrete structures. Fédération Internationale du Béton

Figueiredo CR (2004) Study of carbonation in reinforced concrete structures in Brasília: evaluation of pillars. Tese (Doutorado em Engenharia)—Departamento de Engenharia Civil, Universidade de Brasília, Brasília, DF, p. 222f (in Portuguese)

François R, Laurens S, Deby F (2018) Predicting the service life of structures. In: Corrosion and its consequences for reinforced concrete structures, pp 175–191. https://doi.org/10.1016/b978-1-78548-234-2.50007-x

García-Alonso MC et al (2007) Corrosion behavior of new stainless steels reinforcing bars embedded in concrete. Cement Concr Res 1463–147. https://doi.org/10.1016/j.cemconres.2007.06.003

Hamada M (1969) Neutralization (carbonation) of concrete and corrosion of reinforcing steel. In: 5th International symposium on the chemistry of cement, Tokyo, pp 343–369

Hills TP, Gordon F, Florin NH, Fennell PS (2015) Statistical analysis of the carbonation rate of concrete. Cement Concr Res 98–107. http://dx.doi.org/10.1016/j.cemconres.2015.02.007

Ho DWS, Lewis RK (1987) Carbonation of concrete and its prediction. Cement Concr Res 489–504. https://doi.org/10.1016/0008-8846(87)90012-3

Houst YF, Wittmann FH (2002) Depth profiles of carbonates formed during natural carbonation. Cement Concr Res 12:1923–1930. https://doi.org/10.1016/s0008-8846(02)00908-0

Hyvert N (2009) Application de l'approche probabiliste à la durabilité des produits préfabriqués en béton. Université Paul Sabatier, Toulouse. Thèse de doctorat

Idorn GM (2005) Innovation in concrete research: review and perspective. Cement Concr Res 3–10. https://doi.org/10.1016/j.cemconres.2004.09.006

IPCC (2006) Guidelines for National Greenhouse Gas Inventories. Intergovernmental Panel on Climate Change. http://www.ipcc.ch

Isaia GS (2007) Accelerated and natural carbonation of concrete with a high content of pozzolans. Res Rep (in Portuguese)

Ishida T, Maekawa K (2001) Modeling of pH profile in pore water based on mass transport and chemical equilibrium theory. JSCE 131–146

ISO 13823 (2008) General principles on the design of structures for durability. International Organization for Standardization, Geneva. ISO/TC

ISO 16204 (2012) Durability—service life design of concrete structures. International Organization for Standardization, Geneva

Jiang JL, Lin B, Cai Y (2000) A model for predicting carbonation of high-volume fly ash concrete. Cement Concr Res 699–702. http://dx.doi.org/10.1016/S0008-8846(00)00227-1

Kulakowski MP, Pereira FM, Dal Molin DCC (2009) Carbonation-induced reinforcement corrosion in silica fume concrete. Constr Build Mater 1189–1195. http://dx.doi.org/10.1016/j.conbuildmat.2008.08.005

Kwon SJ, Song HW (2010) Analysis of carbonation behavior in concrete using neural network algorithm and carbonation modeling. Cement Concr Res 119–127. https://doi.org/10.1016/j.cemconres.2009.08.022

Marchand J, Samsonb E (2009) Predicting the service-life of concrete structures: limitations of simplified models. Cement Concr Compos 8:515–521. https://doi.org/10.1016/j.cemconcomp.2009.01.007

Mehta PK (1994) Concrete technology at the crossroads: problems and opportunities. In: Concrete technology: past, present and future, São Paulo

Mehta PK, Monteiro PJM (2014) Concrete: microstructure, properties, and materials, Fourth edn. McGraw-Hill

Meira GR (2004) Agressividade por cloretos em zona de atmosfera marinha frente ao problema da corrosão em estruturas de concreto armado. tese (doutorado em Engenharia Civil) Universidade Federal de Santa Catarina, Florianópolis, 2004, 346p

Monteiro IF, Branco A, Brito JR, Neves R (2012) Statistical analysis of the carbonation coefficient in open air concrete structures. Constr Build Mater 263–269. http://dx.doi.org/10.1016/j.conbuildmat.2011.10.028

Morgan DL (1997) Focus groups as qualitative research. Qualitative Research Methods Series, 2, vol 16. Sage Publications, London

Neves R, Branco F, Brito J (2013) Field assessment of the relationship between natural and accelerated concrete carbonation resistance. Cement Concr Compos 9–15. http://dx.doi.org/10.1016/j.cemconcomp.2013.04.006

Neville AM (2012) Properties of concrete, 5. Prentice Hall

NOAA (2020) National Oceanic and Atmospheric Administration. Earth System Research Laboratory. Global Monitoring Division. Trends in Atmospheric Carbon Dioxide. https://www.esrl.noaa.gov/gmd/ccgg/trends/index.html. Accessed March 2020

Otieno M, Ikotun J, Ballim Y (2020) Experimental investigations on the effect of concrete quality, exposure conditions and duration of initial moist curing on carbonation rate in concretes exposed to urban, inland environment. Constr Build Mater 246:118443. https://doi.org/10.1016/j.conbuildmat.2020.118443

Papadakis VG, Vayenas CG, Fardis MN (1991) Fundamental modeling and experimental investigation of concrete carbonation. ACI Mater J 363–373

Papadakis VG, Vayenas CG, Fardis MN (1989) Reaction engineering approach to the problem of concrete carbonation. AIChE J, 35(10):1639–1650

Parrot LJ (1987) A review of carbonation in reinforced concrete. Cement and Concrete Association Report

Pasupathy K, Berndt M, Castel A, Sanjayan J, Pathmanathan R (2016) Carbonation of a blended slag-fly ash geopolymer concrete in field conditions after 8 years. Constr Build Mater 661–669.. https://doi.org/10.1016/j.conbuildmat.2016.08.078

Pauletti C, Possan E, Dal Molin DCC (2007) Accelerated carbonation: state of the art of research in Brazil. Ambiente Construído 4:7–20 (in Portuguese)

Possan E, Andrade JJO (2014) Markov chains and reliability analysis for reinforced concrete structure service life. Mater Res 593–602. http://dx.doi.org/10.1590/S1516-14392014005000074

Possan E (2010) Carbonation Modeling and service life prediction of concrete structures in urban environment. Engineering School, Federal University of Rio Grande do Sul, Porto Alegre. PhD Thesis in Engineering (in Portuguese)

Possan E (2004) Contribution to the study of concrete carbonation with silica fume addition in a natural and accelerated environment. Engineering School, Federal University of Rio Grande do Sul, Porto Alegre. Dissertation in Engineering (in Portuguese)

Possan E, Thomaz WA, Aleandri GA, Felix EF, e Dos Santos ACP (2017) CO_2 uptake potential due to concrete carbonation: a case study. Case Stud Constr Mater. http://dx.doi.org/10.1016/j.cscm.2017.01.007

Possan E, Andrade JJO, Dal Molin DCC (2018) A conceptual framework for service life prediction of reinforced concrete structures. J Build Pathol Rehabil 3:1–11. https://doi.org/10.1007/s41024-018-0031-7

Rigo E, Oliveira CE, Possan E (2018) The reinforced concrete structures service life predictability: an analysis from the perspective of depth of carbonation. Revista técnico científica do CREA-PR, pp 1–18 (Portuguese)

Rilem - Reunion Internationale de Laboratoires D'essais et Materiaux (1988) CPC-18: Measurement of hardened concrete carbonation depth. Materials and Structures, RILEM Recommendations CPC-18

Rilem TC (2015) 230-PSC. Performance-Based Specifications and Control of Concrete Durability. State-of-the-Art Report. Hans, Fernandez Luco, Luis Beushausen, Edição, vol 18. Springer

Rougeau P (1997) Les résultats d'essais croises AFREM: Essai de carbonatation accélere. Etat des lieux et reflexions sur la carbonatation du béton armé. Laboratoire Central Des Ponts et Chaussées, Paris, pp 87–103. (in French)

Saetta AV, Vitaliani RV (2004) Experimental investigation and numerical modeling of carbonation process in reinforced concrete structures. Part I: theoretical formulation. Cement Concr Res 571–579. http://dx.doi.org/10.1016/j.cemconres.2003.09.009

Saetta AV, Schrefler BA, Vitaliani RV (1993) The carbonation of concrete and the mechanism of moisture, heat and carbon-dioxide flow-through porous materials. Cement Concr Res 761–772. https://doi.org/10.1016/0008-8846(93)90030-d

Silva A, Neves R, Brito J (2014) Statistical modeling of carbonation in reinforced concrete. Cement Concr Compos 73–81. http://dx.doi.org/10.1016/j.cemconcomp.2013.12.001

Singh N, Singh SP (2016) Carbonation resistance and microstructural analysis of low and high-volume fly ash self-compacting concrete containing Recycled Concrete Aggregates. Constr Build. https://doi.org/10.1016/j.conbuildmat.2016.10.067

Steffens A, Dinkler D, Ahrens H (2002) Modeling carbonation for corrosion risk prediction of concrete structures. Cement and Concrete Research. 32:935–941. https://doi.org/10.1016/S0008-8846(02)00728-7

Sun B, Xiao R, Ruan W, Wang P (2020) Corrosion-induced cracking fragility of RC bridge with improved concrete carbonation and steel reinforcement corrosion models. Eng Struct 208:110313. https://doi.org/10.1016/j.engstruct.2020.110313

Ta VL, Bonnet S, Kiesse TS, Ventura A (2016) A new meta-model to calculate carbonation front depth within concrete structures. Constr Build Mater 172–181. http://dx.doi.org/10.1016/j.conbuildmat.2016.10.103

Thiéry M (2005) Modélisation de la carbonatation atmosphérique des bétons: Prise en compte des effets cinétiques et de l'état hydrique. Ecole Nationale des Ponts et Chaussées. Thèse de doctorat, Paris

Tuutti K (1982) Corrosion of Steel in Concrete. Swedish Cement and Concrete Research Institute. Stockholm, Suecis

Yoon I-S, Çopuroğlu O, Park K-B (2007) Effect of global climatic change on carbonation progress of concrete. Atmos Environ 34:7274–7285

Zhao H, Sun W, Wu X et al (2018) The effect of the material factors on the concrete resistance against carbonation. KSCE J Civ Eng 22:1265–1274. https://doi.org/10.1007/s12205-017-0988-9

Zhu J, Zhang R, Zhang Y, He F (2019) The fractal characteristics of pore size distribution in cement-based materials and its effect on gas permeability. Sci Rep 9:17191. https://doi.org/10.1038/s41598-019-53828-5

Artificial Intelligence Applied in the Concrete Durability Study

E. F. Felix, E. Possan, and R. Carrazedo

Abstract Interest in artificial intelligence (AI) in engineering research and practice has increased in recent years, especially the use of artificial neural network (ANN). The ANN has similar characteristics to biological neural networks, efficiently recognizing patterns and behaviors, suited to provide an accurate tool to map and understand the concrete degradation. This chapter presents the positive aspects of artificial neural network to model different concrete degradation mechanisms and provides a detailed procedure for ANN design. As example, the concrete carbonation depth is modeled by an ANN and the results show the its ability to map the carbonation phenomenon.

Keywords Concrete structures · Computer science · Machine learning · Complex systems modeling

1 Introduction

In computer science, Artificial Intelligence (AI) or Machine Intelligence is a branch of computational systems based on human behavior, with the ability to learn and solve problems (Aggarwal et al. 2018). Learning is the link of human behavior and computational tools from AI, for it is this capability that make mankind what it is.

Hertzmann and Fleet (2012) define machine learning as a set of computational tools that provides a way to instruct computer to perform task through examples.

E. F. Felix (✉) · R. Carrazedo
University of São Paulo, São Paulo, Brazil
e-mail: emerson.felipe.felix@gmail.com

R. Carrazedo
e-mail: rogcarrazedo@sc.usp.br

E. Possan
University of Latin American Integration, Foz Do Iguaçu, Brazil
e-mail: edna.possan@unila.edu.br

Fig. 1 Representation of **a** biological and **b** artificial neural network
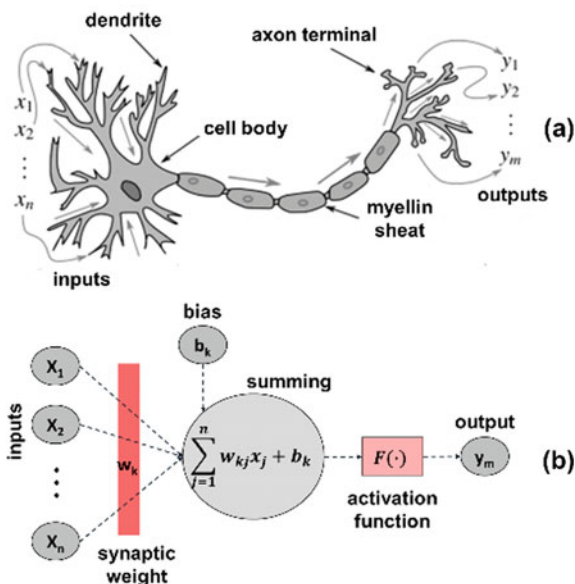
Thus, allowing machines to learn through experience, to adjust to new situations and to perform tasks like human beings.

Over the past few years, the evolution of AI led to the development of several machine learning techniques and methods. We highlight the artificial neural networks (ANN), which have relatively low computational cost and provide simple and efficient solutions.

ANN are systems composed by processing units, called neurons, whose function is based on the human nervous system (Fig. 1) and have the property of mapping complex functions with high generality (Haykin 2008).

Furthermore, ANN go beyond mapping inputs and outputs, and it is able to pick out correlations that are not easily found (Braga et al. 2000), which is the main reason for its increasing exploit in engineering.

1.1 Application of ANN in Civil Engineering

An ANN is a numerical model based on connected units inspired by neural networks, which can transmit information and process it, simulate learning, pattern classification and data processing.

One of the reasons that ANN widely spread is the backpropagation training algorithm (Rumelhart et al. 1986). This technique is easily implemented based on downward Gradient Descent optimization algorithm, and most of the works developed with ANN in civil engineering uses the backpropagation algorithm to train its

network (Adeli 2001; Lazarevska et al. 2014; Shafabakhsh et al. 2015; Abambres and Lantsoght 2019).

The first publication about machine learning in civil engineering was made by Adeli and Yeh (1989). They presented a perceptron ANN to design steel beams. After that, some research using machine learning in civil engineering were developed and, most of them, focused in pattern recognition and data mapping and classification.

As example, Moselhi et al. (1991) applied an ANN to evaluate different scenarios of sale and purchase for real estate market. In the same trend, Chao and Skibniewski (1994), Sonmez and Rowings (1998), Li et al. (1999), Muqeem et al. (2011), Dayanand and Shanmugapriya (2016) published papers that show ANN capable to estimate construction workforce productivity.

Artificial neural networks have also been applied in geotechnics. Williams and Gucunski (1995) used backpropagation neural networks to uncover the average soil thickness and elastic properties, while Goh (1995) shown that an ANN is able to associate soil parameters obtained from laboratory. Other studies proved that ANN are capable to define soil constitutive models and the mechanical behavior of geomaterials (Basheer 2000; Javadi et al. 2003, 2005; Nassr and Javadi 2018).

Nevertheless, ever since the publication of Adeli and Yeh (1989), ANN have been mostly applied to structures and materials studies in civil engineering. In the area of structures, ANN were used for the design and analysis of structural components (Kang and Yoon 1994; Kushida et al. 1997; Gu et al. 2010), structural optimization (Hajela and Berke 1991; Rogers 1994, Jenkins 1999; Babiker et al. 2012), structural dynamics, impact and earthquakes (Adeli 1994; Chen et al. 1995; Stavroulakis and Antes 1998; Vafaei et al. 2013; Al-Suhaili et al. 2014) and also damage assessment and risk management (Wu et al. 1992; Papadrakakis et al. 1996; Masri et al. 2000; Abbas and Khan 2016).

In the area of materials, ANN were used to estimate mechanical properties for concrete, such as compressive strength (Ni and Wang 2000; Kim 2009; Oztas et al. 2006; Alshihri et al. 2009; Diab et al. 2014) and Young modulus (Topçu and Saridemir 2007; Gholampour et al. 2017; Duan et al. 2013, 2017). ANN were also able to evaluate the workability of concrete (Jain 2006; Deepak et al. 2019), consistency of fresh concrete mixture (Poon et al. 2007) and even concrete mix constituents and proportions (Ji et al. 2006).

Works that relate in a multidisciplinary way the areas of materials and structures, such as the durability study, have been developed over the last years (Smets and Bogaerts 1992; Trasatti and Mazza 1996; Cai et al. 1999; Topçu et al. 2009; Karakoç et al. 2011; Felix et al. 2019). Parthiban et al. (2005) verified the efficiency of the ANN applying to create a predictive model for the corrosion potential of steel bars in reinforced concrete structures. It was found that the model was able to estimate the potential under 5% of error. Ukrainczyk and Ukrainczyk (2008) demonstrated the possibility use of ANN to analyze the sensitivity and influence of various parameters related to corrosion (environmental conditions, structure geometry and boundary conditions or material properties) to determine the damage in concrete bridges.

1.2 Predicting Concrete Durability

The concrete structure's durability depends on several parameters such as the characteristics of building construction stages (concept design, construction plans and materials specifications, construction and operation and maintenance), aggressiveness of the environment, use in service life and expected service life of structures (Mehta and Monteiro 2013).

Possan and Andrade (2014) highlight that the degradation of concrete is related to the building's exposure environment (marine, urban, industrial) and its aggressiveness, which is expressed by the aggressive agents present in the atmosphere (CO_2, chloride ions, sulfates, alkalis, among others).

The exposure environment influences the speed and intensity of a structure degradation, and the aggressive agents enables both a durability analysis and evaluation of useful life (Dal Molin et al. 2016).

Considering users safety, the service life of a reinforced concrete structure is about 120 years, if repair and regular maintenance is carried out (ISO 2004). The decrease of the expected service life and the demand for repairs and maintenance follows from design and execution errors as well as pathological manifestations.

Corrosion of reinforcing steel is the leading cause of deterioration in concrete and the most important pathological manifestation of reinforced concrete structures (Taffese and Sistonen 2013; Possan and Andrade 2014).

In concrete structures by the shore, rebar corrosion is mainly function of the chloride ions due to the sea salt spray. In urban regions, corrosion is mainly induced by the ingress of atmospheric carbon dioxide into concrete, commonly referred to as 'carbonation induced corrosion' (Mehta and Monteiro 2013).

Until the mid-1980s, CO_2 or Cl- diffusion models were obtained by linear and non-linear regression, considering, for example, the water/cement ratio (w/c), type of binder and exposure conditions (Kobayashi and Uno 1990). In the following years, physical-chemical mechanisms involved in the hydration reactions of the cement paste and dissolution of CO_2 in the concrete pore fluid were included, providing accuracy to evaluate the carbonation front (Papadakis et al. 1991; Ishida and Maekawa 2001; Maekawa et al. 2003). However, these models are awfully complex, requiring parameters that are not easily measured, such as diffusion coefficient of carbon dioxide in concrete, and laborious equations to be solved.

With the advance of software and hardware, and development of machine learning technique, new formulations were proposed, reducing inherent uncertainties of the prediction models. The use of ANN stood out, especially in modeling concrete carbonation. Depending on the training algorithm, the number of iterations for training could be reduced, also reducing the time spent for the simulation when compared to other techniques (Lu and Liu 2009; Know and Song 2010; Hamzehie et al. 2014; Akpinar and Uwanuakwa 2016).

Thus, in the next chapter we show general aspects regarding the characteristics and functionalities of an ANN employed to model a deterioration mechanism of concrete. It is also introduced an application example of the prediction of the concrete carbonation depth of structures by the shore, using a Multilayer Perceptron Neural Network.

2 Artificial Neural Network: Basic Concepts

McCulloch and Pitts (1943) is the first work to introduce a mathematical model for the representation of an artificial neural system. Fifteen years later, Rosenblatt (1958) brought in the concepts of the perceptron network, which is a network with only one processing layers. This network stood out because it could perform pattern recognition using a supervised learning method.

Although ANN were introduced in the 60 s, they only spread out in the 80 s, after the work of Hopfield (1982). He shown that ANN could solve many different problems in many subjects and was able to publish several works sequentially. Different models and training techniques were proposed, that could fit in each area of knowledge.

2.1 Neuron Model

Neural networks are models based on connected units called "artificial neurons" that resemble neuron in a human brain. These neurons are disposed in layers, interconnected though connections associated with synaptic weights. These weights are adjusted as learning proceeds, resembling the property of storing knowledge.

Haykin (2008) states that an ANN have five basic elements:

(a) A set of input x_k carrying its own synaptic weight w_k;
(b) An adder to the input, weighted by the respective neuron weights;
(c) An activation function $F(\cdot)$, restricting the output range;
(d) A bias b_k, responsible to increase or decrease net input of the activation function;
(e) An output y_k, as indicated in Fig. 1b.

Thereby, the output of neuron k of a Perceptron network is given by:

$$y_k = F(z_k) = F\left(\sum_{j=1}^{n} w_{kj}x_j + b_k\right) \tag{1}$$

Each entry $x_k \in \mathbb{R}$ is weighted by a $w_{kj} \in \mathbb{R}$, which forms the current neuron weight vector $w_k = (w_{k1}, w_{k2}, \ldots, w_{kn})^T$. Each neuron has a bias $b_k \in \mathbb{R}$ which is a

fixed addition, evolving into the parameter z_k. $F: \mathbb{R} \to \mathbb{R}$ is an activation function that process the net input parameter z_k and yields the neuron output $y_k \in \mathbb{R}$.

2.2 Activation Function

The activation function converts the net input parameter into the net output, and evaluate the neural decision considering the neuron internal state (Haykin 2008).

ANNs have processing units (neurons) that are associated with an activation state. This state is characterized by the activation functions, which can be discrete or continuous, chosen according to the problem to be modeled. Activation functions are also known to be logical thresholds.

In general, there are several activation functions that can be used. Silva et al. (2004) states that the linear, stepped, logistical sigmoid and hyperbolic tangent are the most used functions to solve problems associated to mapping and pattern recognition (Fig. 2).

According to Haykin (2008) the sigmoid functions are the most frequently used function in the construction of an ANN, as these increasing functions are homogeneous and asymptotic. Besides, these functions are continuous, symmetric, monotonic increasing, limited and with derivatives that can easily be obtained.

2.3 Topology of an Artificial Neural Network

The topology of an ANN limits the type of problem that can be solved by the neural system. Networks with only one processing layer can solve only linearly separable problems, and recurring networks can solve even dynamics (Braga et al. 2000).

The topology is distinguished by the number of processing layers and how one layer interacts with each other. There are several studies that describes how neurons should be arranged according to the type of problem to be modeled (Berthold et al. 2010; Zhang 2017; Felix et al. 2019). However, there is no specific rule to stablish the best structure for each problem.

Some rules from practice may serve as guideline, but no predetermined rule exist for stablishing the training algorithm, the number of processing layers, the number of hidden layers and the type of connection. Thus, the topology must be adjusted to each problem (Fausett 1993).

Pruning a network is made by successive refinements, reducing the size of the neural network, checking the importance of each connection, until the number of neurons be within an acceptable range. Overfitting is expected when the number of neurons is in excess, and the networks might lose its ability to recognize patterns or even memorizing data (Haykin 2008).

Fig. 2 Representation of a function: **a** linear; **b** Heaviside; **c** hyperbolic tangent; and **d** sigmoid
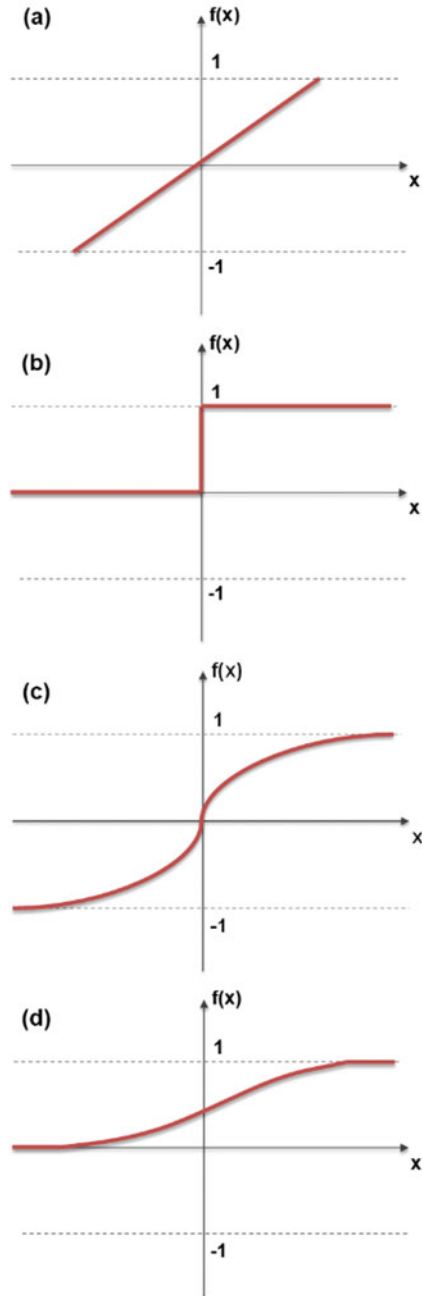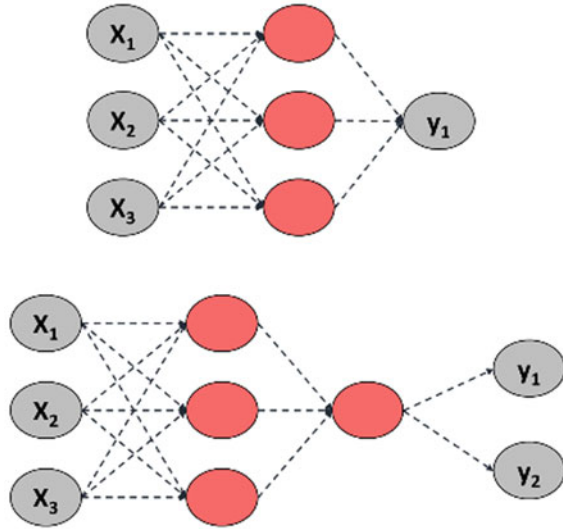
Figure 3 presents two topologies, where variables x_1, x_2, ..., x_n are the inputs, and y_1, y_2, ..., y_n, are the outputs. Dotted lines are links between neurons, from one layer to another, and it is through these connections that information is processed.

There are several ways to link neurons, such as feedforward and feedback. In the former, connections are sequential, that is, the output of a neuron in a layer is the input of a neuron in the next one, as seen in Fig. 4a. In the latter, connections can be made in either way (Fig. 4b).

2.4 Learning Method

One of the most important characteristics of an ANN is the ability to learn. Learning is associated to adapting the weights of the network, following a pre-stablished rule, improving the results. Learning is defined as the process that changes the free parameters by a stimulation from the environment which the network is inserted (Fausett 1993). Thus, the objective of a network is stablishing an implicit model by adjusting its parameters.

The method responsible for adjusting the network parameters and consequently how the synaptic weights are adjusted defines the type of learning. According to Martins et al. (2001), the supervised learning is the most used training method, in which the network is initially controlled by a supervisor that provides both input and output as pairs with the objective to map a relationship between them (see Fig. 5). Once such map is found, new outputs are provided and compared with the expected target values. If output and target values diverge, the connection weights are adjusted.

Fig. 4 Representation of
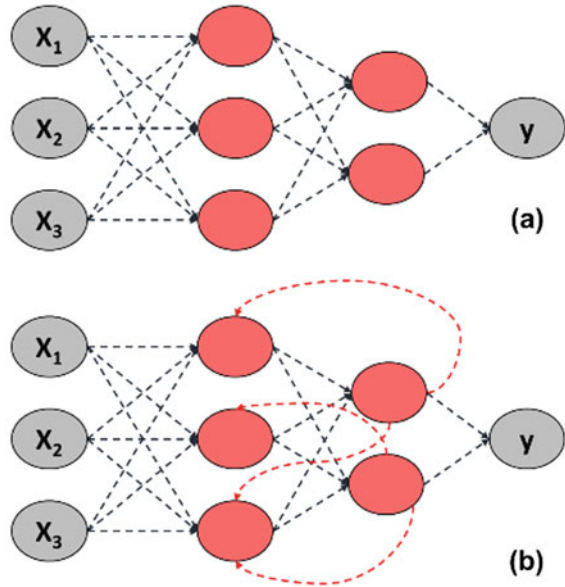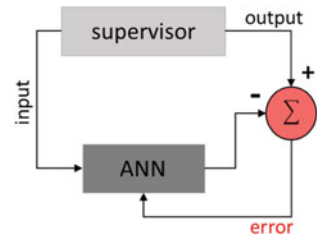**a** feedforward ANN and
b feedback ANN

Fig. 5 Representation of
supervised learning

Error minimization is incremental, since small adjustments are made at each stage of the training process. Training process is concluded when a tolerance for the error is reached, or a threshold is achieved, such as a certain number of iterations. Synaptic weights are no longer modified.

2.5 Training Algorithm

Perceptron is the simplest form of an ANN and is used for binary classification separated by hyperplanes (Haykin 2008). Thus, perceptron networks can only solve linearly separable problems, and is able to solve logical problems with binary response.

Rosenblatt (1958) proposed the perceptron network, using only a single neuron, being able to pattern recognition and classification in two classes. The number of
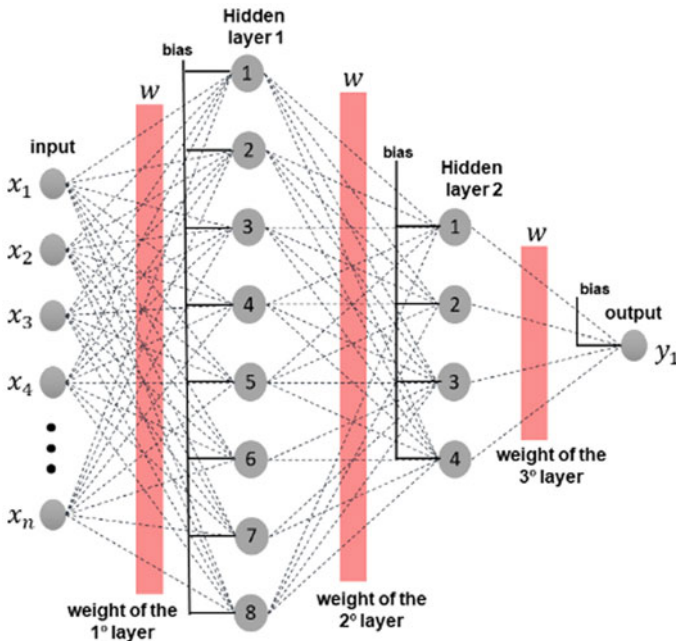
Fig. 6 Representation of a multilayer perceptron ANN

neurons must be increased in order to classify multi-pattern classes. The training algorithm used in the perceptron network is known as backpropagation algorithm or only backpropagation.

The multilayer perceptron (MLP) is a class of feedforward network composed of more than one processing layer (Fig. 6). This enables the network to solve non-linear problems.

According to Fausett (1993), MLPs have three fundamental layers: input; hidden layer; and output. The first and the last layer do not have computational potential, they only store values and build patterns. The hidden layers, on the other hand, are the computational layers, since process takes places in these layers to generate the implicit model.

The same training algorithm of perceptron is used on MLP networks, the backpropagation. This algorithm was developed based on learning by error correction. In Fig. 7, a simplified representation of the backpropagation process is presented.

3 Application of ANN to Model the Concrete Carbonation

Carbonation study and their influence factors have been reported for over half of a century and a large theoretical background on the topic is available (Meira et al. 2003;

Fig. 7 Flowchart of backpropagation algorithm
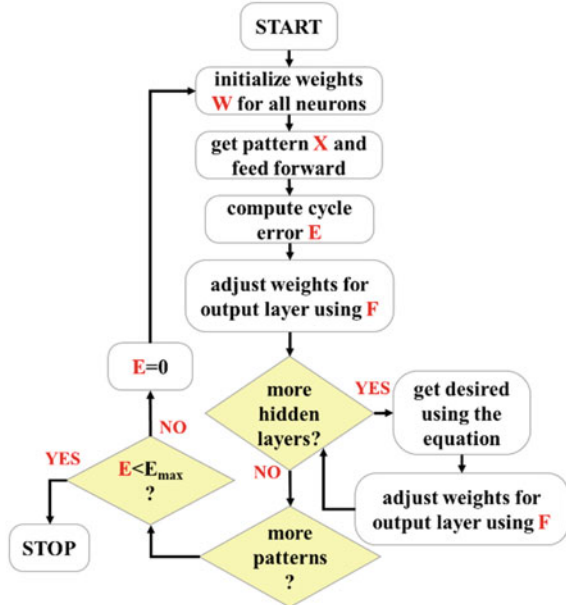
Kwon and Song 2010; Izumi et al. 1986; Kari et al. 2014; Felix and Possan 2018). Interest in the area has led several researchers to develop models of concrete carbonation evolution and/or prediction over time.

Until the mid-1980s, models for carbonation depth prediction were obtained through linear and non-linear regression, considering different factors, such as the water/cement ratio, the binder type and the exposure conditions (Izumi et al. 1986).

Because of increasing computing technologies and improvement of machine learning techniques, new formulations for carbonation depth prediction were developed aiming to reduce uncertainties associated to modeling. Among these techniques, ANN has been becoming commonplace regarding the carbonation phenomenon modeling. Whereas 492 articles were published in Science Direct database related to concrete carbonation modeling in the last decade reached, 27.6% employed a machine learning technique (Support Vector Machine, ANN, generic algorithms and others).

Within the 492 articles related to concrete carbonation modeling, only 8.2% are related to structures by the shore, due to difficulties to associate the carbonation depth with both CO_2 content and Cl^- concentration because most models are either deterministic or based on nonlinear regressions that involve only one of the agents (Liu et al. 2016; Zhu et al. 2016).

Thus, there are only a few models capable to estimate the concrete carbonation depth with the combined effect of chloride ions and CO_2. In this sense, authors present a Multilayer Perceptron ANN to predict the concrete carbonation depth in structures by shore. The following parameters are considered: water/cement ratio, exposure

time, and distance of the structure to the shore, the latter being the representative parameter of the combined action of CO_2 and Cl^-.

3.1 General Aspects of the ANN Modeling Process

Figure 8 shows the steps to obtain a prediction model of carbonation depth by an MLP neural network, using backpropagation training algorithm, with the following requirements: minimum error, the average error, the correlation coefficient, among others.

The first step is to define a database, divided in three sets: training, validation and performance. After some topologies are defined, a convergence analysis is performed to determine the best learning rate of the training algorithm and the activation function that better fits the problem. The third step is the networks training and validation, reducing chances of over-training the networks (overfitting). At last, at the fourth step, a performance analysis is carried out, selecting the network that better fits the problem.

These steps were applied to model the concrete carbonation depth, and all procedures and results are presented in sequence.
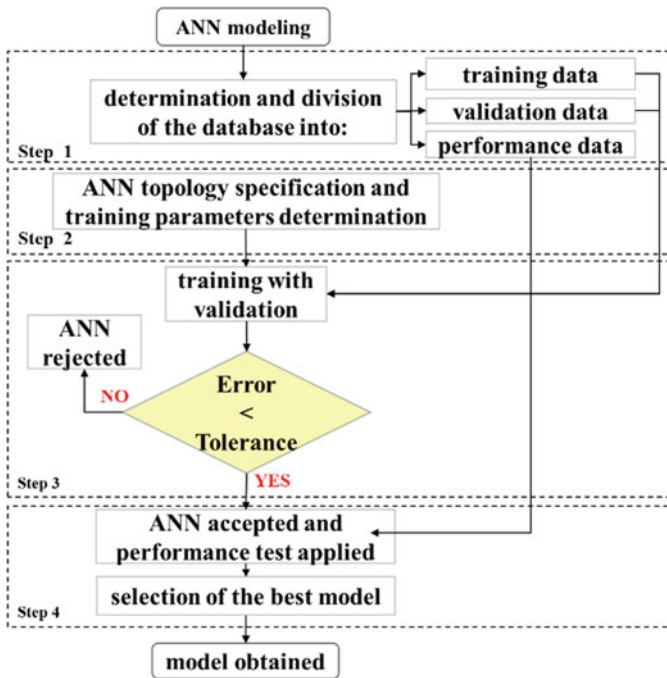

Fig. 8 ANN modeling process

3.2 Database Assembly

The database is provided by Meira et al. (2006), which presents the carbonation depth of concrete structures located close to marine environment, in João Pessoa, Brazil. They provided the carbonation depth of specimens of $15 \times 15 \times 140$ cm made of CP-II E Portland cement (equivalent to the ASTM C 595/IP and/or CEM II/B-S), with cement/water ratio of 0.5, 0.57 and 0.60, with distances of 10, 100, 200 and 500 m from the sea, and carbonation depths collected at 6, 10, 14, 18 and 46 months after exposure.

The database was divided into three sets, one for training, other for validation and the last for the testing. Figure 9 shows how data was distributed in each set, as follows: 60% for the training, 20% for the validation and 20% for the performance analysis.

Selecting the input variables may hinder mapping between input and output. In this sense, the following input variables were employed: w/c ratio, exposure tine to the aggressive atmosphere, distance from the shore. The w/c ration is related to the compressive strength and concrete compactness, as wells to the void ratio of the cement matrix. The distance from the shore is related to the exposure to the aggressive

Fig. 9 Database division
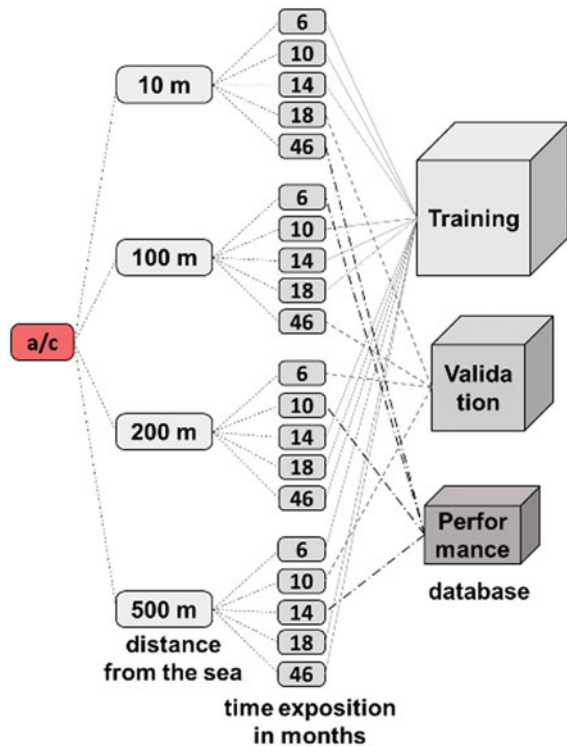
agents – the combined diffusion of CO_2 and Cl^-. Meira et al. (2003) describe that low carbonation depth is found closer to the coast, as diffusion of chlorides increases.

3.3 Training Parameters and ANN Topology

The topology of an ANN is defined by the number of input and output neurons, by the number of hidden layers and the number of neurons in each hidden layer. In this work, 90 topologies were created, employing one or two hidden layers, with one to nine neurons (see Fig. 10).

As the network learning is supervised through backpropagation training algorithm, it must be stablished the value of the learning rate, which is related to the network convergence. Therefore, twelve networks were simulated varying the learning rate from 0.05 to 0.6 (increments of 0.05). A network with topology [3-4-1] was adopted, which represents a network with "3" neurons in the input layer, "4" neurons in the processing layer and "1" neuron in the output layer. The former are the selected input variables and the latter is the concrete carbonation depth.

Figure 11 presents the required number of iterations to train the selected topology network, as well the root mean squared error (RMSE) for training and validation. It
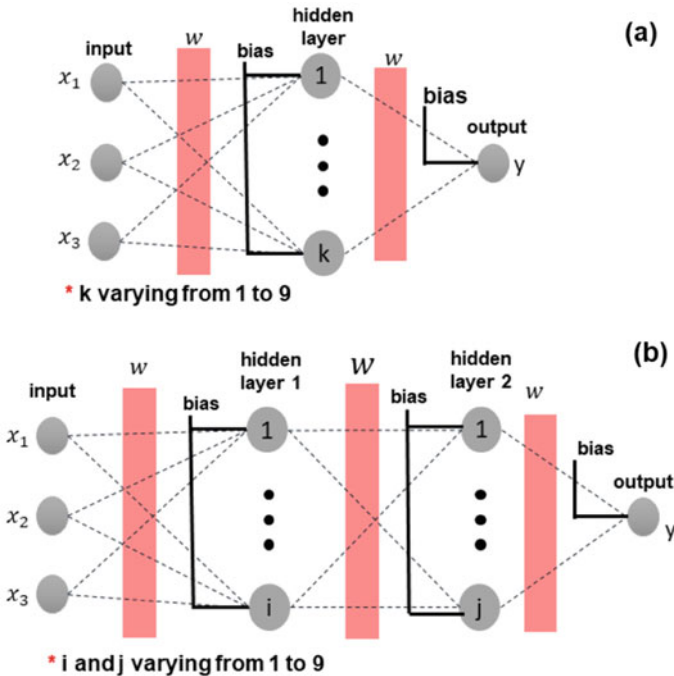

Fig. 10 The basic topology selected to train with **a** one hidden layer and **b** two hidden layers
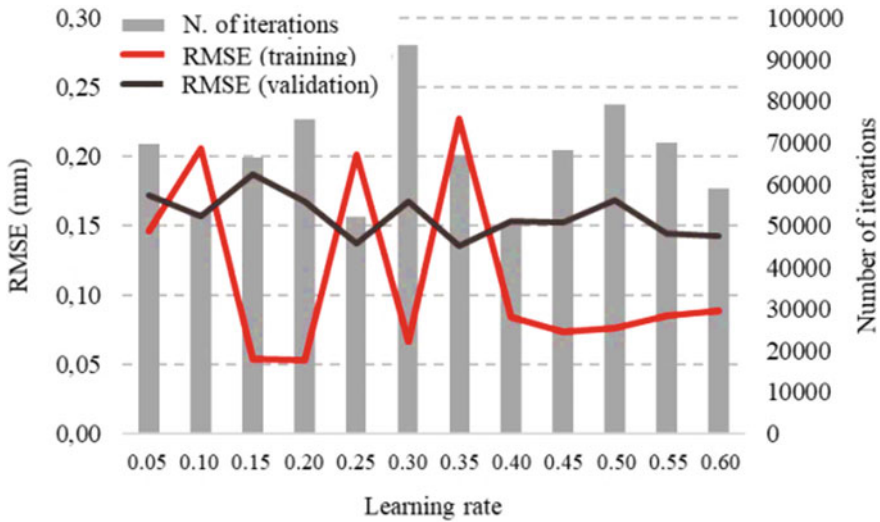
Fig. 11 Influence of the learning rate on training and validation

can be observed that the learning rate $\alpha = 0.4$ resulted in the best mapping for the concrete carbonation phenomenon, considering RMSE (of training and validation) and number of required iterations for network learning.

Figure 11 express the importance of choosing a learning rate that provides efficient and optimized training. Adoption of inadequate rate could result in slow (in terms of processing) and inefficient (in terms of accuracy) training.

3.4 ANN Training and Validation

After choosing an adequate learning rate, ANN training was initiated. The maximum number of interactions $(10E + 5)$ and the root mean squared error (RMSE), according to Eq. (2), were used as convergence criteria.

$$\text{RMSE} = \sqrt{\frac{1}{n} \sum_{i=1}^{n} (y_i - \bar{y})} \tag{2}$$

where RMSE is the root mean squared error of the network, n is the output number, y_i is the output of the network and $\bar{y}$ is the average of the outputs.

The ANN were created with a computational package called project-yapy, proposed by Konzen and Felix (2011) in C++ object-oriented language. The code was employed and validated in Felix et al. (2018) and Felix et al. (2019). Nevertheless, there are several software's that provide packages and libraries with ANN,

Table 1 ANN with the best RMSE

Topology	Training		Validation	
	RMSE	R[b]	RMSE	R[b]
[3-7-1][a]	0.2852	0.9882	0.1963	0.9619
[3-1-3-1][b]	0.4124	0.9794	0.2423	0.9650
[3-1-7-1][b]	0.2294	0.9947	0.2307	0.9748
[3-2-3-1][b]	0.2593	0.9931	0.2692	0.9294
[3-2-7-1][b]	0.1790	0.9957	0.2995	0.9138
[3-4-5-1][b]	0.0885	0.9990	0.2836	0.9593
[3-5-1-1][b]	0.4399	0.9723	0.2658	0.9492
[3-6-3-1][b]	0.2229	0.9936	0.2765	0.9660
[3-7-8-1][b]	0.2994	0.9883	0.2632	0.9758
[3-8-5-1][b]	0.4506	0.9708	0.2705	0.9603
[3-9-5-1][b]	0.1036	0.9990	0.2312	0.9676
[3-9-8-1][b]	0.2677	0.9912	0.3627	0.9443
[3-9-9-1][b]	0.0565	0.9996	0.2969	0.9798

[a][x-y-z] topology, where x indicates the input number, y the neuron number in the hidden layer and z the output number
[b][x-y-w-z] topology, where x indicates the input number, y the neuron number in the first hidden layer, w the neuron number in the second hidden layer, and z the output number

where users can assemble the network architecture, calibrate the training parameters, and more, making modeling quite simple.

Table 1 presents the ANN results for network with RMSE below 0.3. The following three ANN were selected, considering both coefficient of determination (R^2) and the root mean squared error (RMSE): [3-7-1], [3-1-7-1] e [3-9-5-1]. Figures 12, 13 and 14 present comparative graphs between carbonation depth provided by reference and calculated by the selected networks, as well their respective coefficient of determination.

Table 2 presents the overall performance of the selected networks.

The RMSE from training and validation data observed in Table 1 and the performance analysis from Table 2 show that the network [3-9-5-1] is the network that best describes the carbonation evolution in reinforced concrete structures by the shore. This network presented a coefficient of determination of 0.974 and a maximum error of only 0.54 mm for the carbonation depth. This difference is twice smaller than the accuracy of the equipment used to examine the carbonation depth in concrete structures.

After selecting the network, the network was once again required to calculate the carbonation depths for all initial database, and results are compared with the observed in situ depths. Residues are presented in Fig. 15.

The difference between measured and calculated results muster around zero, which indicates that the network adequately describes the carbonation phenomenon.

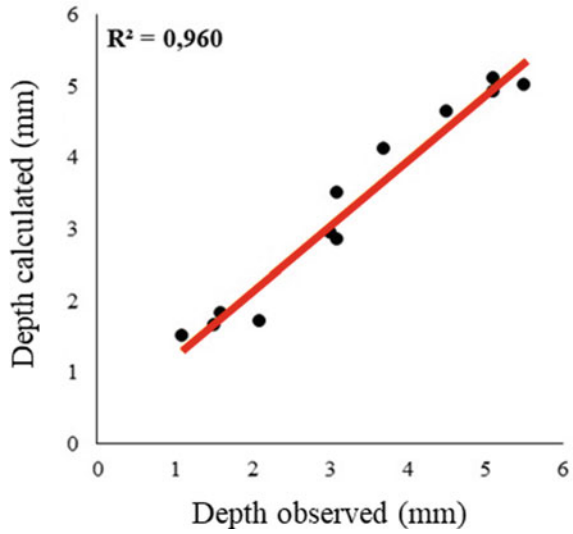**Fig. 12** Coefficient of determination obtained in the performance analysis with the ANN [3-7-1]

R² = 0,960

Depth calculated (mm)

Depth observed (mm)

Fig. 13 Coefficient of determination obtained in the performance analysis with the ANN [3-1-7-1]
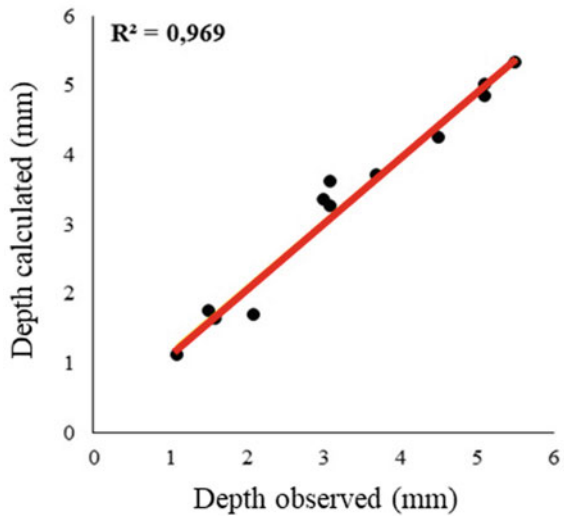
R² = 0,969

Depth calculated (mm)

Depth observed (mm)

Figure 16 maps the carbonation depth of a concrete structure with w/c ratio of 0.5 yet varying distance from the shore and exposure time to atmosphere. As expected, the carbonation depth decreases as the structure is closer to the shore.

At last, the use of an ANN for modeling engineering problems may be summarized as follows:

1. Implement a training program of neural networks with supervised learning, or define a commercial software that provides libraries with ANN;

Fig. 14 Coefficient of
determination obtained in the
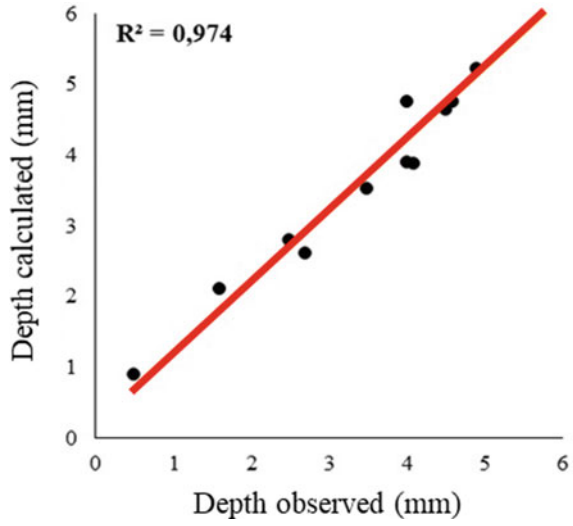performance analysis with
the ANN [3-9-5-1]

Table 2 Performance
Analysis of the 3 best ANN

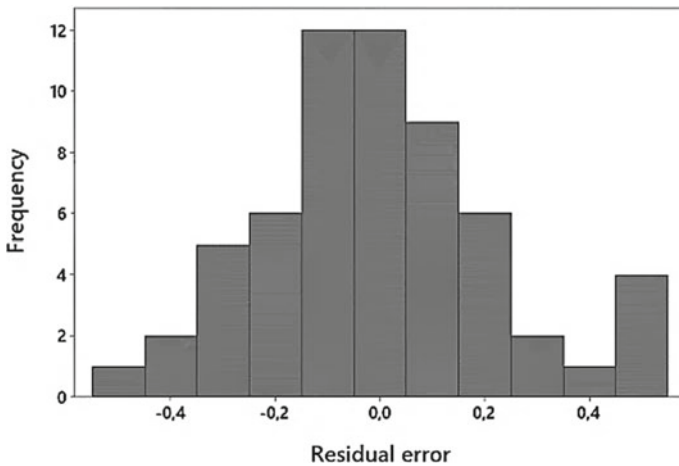| Topology	RMSE	R^2	E_{max}
[3-7-1]	0.181	0.942	0.613
[3-1-7-1]^2	0.500	0.951	0.597
[3-9-5-1]^2	0.130	0.974	0.542

Fig. 15 Histogram of the obtained residues with the compared carbonation depths
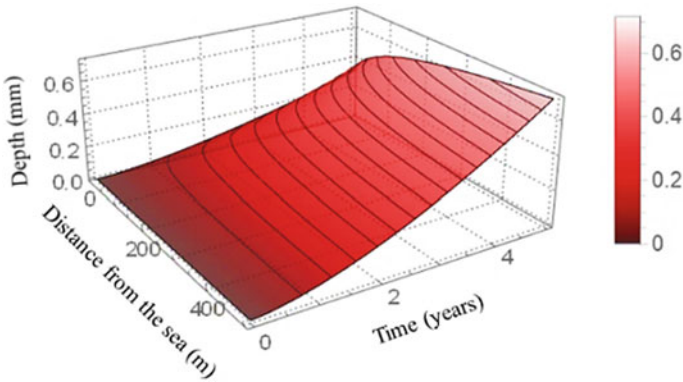
Fig. 16 Carbonation depth in function of the exposure time and distance from the shore

2. Define the database;
3. Split the database in three set: training, validation and network testing;
4. Select input variables and network topologies for training;
5. Specify training parameters, such as activation function, training algorithm, algorithm learning rate, stop conditions of training;
6. Train with simultaneous validation;
7. Select some networks with best fitting;
8. Select of best model through performance tests.

4 Final Remarks and Conclusions

Neural networks are under development ever since 1940, however only recently it evolved for most diverse areas. Nowadays the numbers of studies and development of new technologies and tools associated to Artificial Intelligence is expanding, mainly within engineering.

In this work, we presented a Multilayer Perceptron Neural Network capable to predict the carbonation depth of concrete structures located by shore. The model adequately represented the influence of CO_2 in concrete structures, considering the distance of concrete element from shore. It was able to represent the inverse effect of the combined action of CO_2 and Cl^-, where chloride ions ingress is preponderant comparing to CO_2 action.

The developed model supports the concept that artificial intelligence can be applied to solve several problems related to civil and materials engineering. ANN may improve researches regarding life cycle, sustainability and durability of concrete structures. Yet we miss one thing for the dissemination in technical environment, a software with a friendly interface.

References

Abambres M, Lantosoght EOL (2019) ANN-based fatigue strength of concrete under compression. Materials 12(22):1–21

Abbas YM, Khan MI (2016) Influence of fiber properties on shear failure of steel fiber reinforced beams without web reinforcement: ANN modeling. Latin Am J Solids Struct 13(8):1483–1498

Adeli H (1994) Advances in design optimization. E. & F. N. Spon, London

Adeli H (2001) Neural networks in civil engineering: 1989-2000. Comput-Aided Civil Infrastruct 16(2):126–142

Adeli H, Yeh C (1989) Perceptron learning in engineering design. Microcomput Civil Eng 4(4):247–256

Aggarwal CC (2018) Neural networks and deep learning: a textbook, 1th ed. Springer, New York

Akpinar P, Uwanuakwa ID (2016) Intelligent prediction of concrete carbonation depth using neural networks. Bull Transylv Univ Brasov 9(2):99–108

Al-Suhaili RHS, Ali AAM, Behaya SAK (2014) Artificial neural network modeling for dynamic analysis of a DamReservoir-Foundation system. Int J Eng Res Appl 4(1):121–143

Alshihri MM, Azmy MA, El-Bisy SM (2009) Neural networks for predicting compressive strength of structural light weight concrete. Constr Build Mater 23(6):2214–2219

Babiker AA, Adam FM, Mohamed AE (2012) Design optimization of reinforced concrete beams using artificial neural network. Int J Eng Invent 1(8):7–13

Basheer IA (2000) Selection of methodology for neural network modeling of constitutive hysteresis behavior of soil. Comput-Aided Civil Infrastruct Eng 15(6):445–63

Berthold T, Milbradt P, Berkhahn V (2010) Determination of network topology for ANN-bathymetric models. In: Proceedings of ninth international conference on hydro-science and engineering (ICHE 2010), IIT Madras, Chennai, India, pp 1–12

Braga AP, Ludermir TB, Carvalho AC (2000) Redes Neurais Artificiais: Teoria e Aplicações. LTC—Livros Técnicos e científicos Editora, Rio de Janeiro

Cai J, Cottis RA, Lyon SB (1999) Phenomenological modelling of atmospheric corrosion using an artificial neural network. Corros Sci 41(10):2001–2030

Chao L, Skibniewski MJ (1994) Estimating Construction productivity: neural network-based approach. J Comput Civil Eng 8(2):234–251

Chen HM, Qi GZ, Yang JCS, Amini F (1995) Neural network for structural dynamic model identification. J Eng Mech 121(12):1377–1381

Dal Molin DCC, Masuero AB, Andrade JJO, Possan E, Masuero JR, Mennucci MM (2016) Contribuição à previsão da vida útil de estruturas de concreto. In: de Souza Kazmierczak C, Minto Fabrício M (eds) Avaliação De Desempenho De Tecnologias Construtivas Inovadoras: Materiais e Sustentabilidade, Editora Scienza, pp 223–270

Dayanand TA, Shanmugaoriya S (2016) ANN model for estimation of construction labour productivity. Int J Modern Trends Eng Sci 3(8):231–238

Deepak M, Gopalan R, Akshay Raj R, Shanmugi S, Usha P (2019) Modeling of concrete slump and compressive strength using ANN. Int J Innov Technol Explor Eng 8(5)

Diab AM, Elyamany HE, Abd Elmoaty AEM, Shalan AH (2014) Prediction of concrete compressive strength due to long term sulfate attack using neural network. Alex Eng J 53(3):627–642

Duan ZH, Kou SC, Poon CS (2013) Using artificial neural networks for predicting the elastic modulus of recycled aggregate concrete. Constr Build Mater 44:524–532

Duan Z, Poon CS, Xiao J (2017) Using artificial neural networks to assess the applicability of recycled aggregate classification by different specifications. Mater Struct 50:1–14

Fausett L (1993) Fundamentals of neural networks: architectures, algorithms and applications. Pearson

Felix EF, Possan E (2018) Modeling the carbonation front of concrete structures in the marine environment through ANN. IEEE Latin Am Trans 16(6):1772–1779

Felix EF, Possan E, Carrazedo R (2019) Analysis of training parameters in the ANN learning process to mapping the concrete carbonation depth. J Build Pathol Rehabil 4(16):1–13

Gholampour A, Gandomi AH, Ozbakkaloglu T (2017) New formulations for mechanical properties of recycled aggregate concrete using gene expression programming. Constr Build Mater 130:122–145

Goh ATC (1995) Neural networks for evaluating CPT calibration chamber test data. Microcomput Civil Eng 10(2):147–51

Gu XL, Zhang WP, Shang DF (2010) Flexural behavior of corroded reinforced concrete beams. In: Song GB, Malla RB (eds) Earth and space, 2010: engineering, science, construction and operations in challenging environments, pp 3545–3552

Hajela P, Berke L (1991) Neurobiological computational models in structural analysis and design. Comput Struct 41(4):657–67

Haykin S (2008) Neural networks: a comprehensive foundation, 2th ed. Practice-Hall, New Delhi

Hamzehie ME, Mazinani S, Davardoost F, Mokhtare A, Najibi H, Van der Bruggen B, Darvish-manesh S (2014) Developing a feed forward multilayer neural network model for prediction of CO2 solubility in blended aqueous amine solutions. J Nat Gas Sci Eng 21:19–25

Hertzmann A, Fleet D (2012) Machine learning and data, Lecture Notes CSC 411/D11, Computer Science Department, University of Toronto, Canada

Hopfield JJ (1982) Neural networks and physical systems with emergent collective computational abilities. Proc Natl Acad Sci USA 79(8):2554–2558

International Organization for Standardization (2004) Buildings and constructed assets. ISO15686-6: Service Life Planning. Procedures for considering environmental impacts. ISO, Geneva

Ishida T, Maekawa K (2001) Modeling of pH profile in pore water based on mass transport and chemical equilibrium theory. Concr Libr JSCE 37:151–166

Izumi I, Kita D, Maeda H (1986) Carbonation, kibodang publication, p 35–88

Jain A, Jha SK, Misra S (2006) Modeling the compressive strength of concrete using Artificial Neural Networks. Cem Concr Res 36(7):1399–1408

Javadi AA, Tan TP, Zhang M (2003) Neural network for constitutive modelling in finite element analysis. Compu Assist Mech Eng Sci 10(4):375–381

Javadi AA, Tan TP, Elkassas ASI (2005) Intelligent finite element method. Proceeding of the 3rd MIT conference on computational fluid and solid mechanics, Cambridge, Massachusetts, USA, pp 347–350

Jenkins WM (1999) A neural network for structural re-analysis. Comput Struct 72:687–98

Ji T, Lin T, Lin X (2006) A concrete mix proportion design algorithm based on artificial neural networks. Cem Concr Res 36(7):1399–1408

Kang HT, Yoon CJ (1994) Neural network approaches to aid simple truss design problems. Microcomput Civil Eng 9(3):211–18

Karakoç MB, Demirboga R, Türkmen I, Can I (2011) Modeling with ANN and effect of pumice aggregate and air entrainment on the freeze–thaw durabilities of HSC. Constr Build Mater 25(11):4241–4249

Kari OP, Puttonen J, Skantz E (2014) Reactive transport modelling of long-term carbonation. Cem Concr Compos. 52:42–53

Kim DK (2009) Neuro-control of fixed offshore structures under earthquake. Eng Struct 31:517–522

Kobayashi K, Uno Y (1990) Mechanism of carbonation of concrete. Concr Libr JSCE 16:139–151

Konzen PHA, Felix EFF (2011) Project-yapy—Pacote computacional de RNA's orientado-a-objetos C++. Disponível em: https://code.google.com/archive/p/project-yapy

Kushida M, Miyamoto A, Kinoshita K (1997) Development of concrete bridge rating prototype expert system with machine learning. J Comput Civil Eng (ASCE) 11(4):238–47

Kwon SJ, Song HW (2010) Mechanism of carbonation behavior in concrete using neural network algorithm and carbonation modeling. Cem Concr Res 40:119–127

Lazarevska M, Knezevic M, Cvetkovska M (2014) Application of artificial neural network in civil engineering. J Tehnicki Vjesnik 21(6):126–142

Li H, Shen LY, Love PDE (1999) ANN-based mark-up estimation system with self-explanatory capacities. J Constr Eng Manag 125(3):185–189

Liu W, Cui H, Dong Z, Xing F, Zhang H, Lo TY (2016) Carbonation of concrete made with dredged marine and sand and its effect on chloride binding. Constr Build Mater 120:1–9

Lu C, Liu R (2009) Predicting carbonation depth of prestressed concrete under different stress states using artificial neural network. Adv Artif Neural Syst 2009:1–8

Maekawa K, Ishida T, Kishi T (2003) Multi-scale modeling of concrete performance. J Adv Concr Technol 1:1–126

Martins AR, Monticelli I, Camarini G (2001) Carbonatação em concretos submetidos a diferentes procedimentos de cura. In: Congresso Brasileiro do Cimento, 43º, Foz do Iguaçu, 2001. Anais. São Paulo: Instituto Brasileiro do Concreto

Masri SF, Smyth AW, Chassiakos AG, Caughey TK, Hunter NF (2000) Application of neural networks for detection of changes in nonlinear systems. J Eng Mech 126(7):666–676

McCulloch WS, Pitts WH (1943) A logical calculus of the ideas immanent in nervous activity. Bull Math Biophys 5:115–133

Mehta PK, Monteiro PJ (2013) Concrete: microstructure, properties and materials, 4th ed. McGraw-Hill Professional Publishing

Meira GR, Padaratz IJ, Alonso MC, Andrade MC (2003) Effect of distance from sea and chloride aggressiveness in concrete structures Brazilian coastal site. Mater Constr 53:179–188

Meira GR, Padaratz IJ, Borba Junior JC (2006) Carbonatação natural de concretos: resultados de cerca de quatro anos de monitoramento. In: XI Encontro Nacional de Tecnologia do Ambiente Construído—ENTAC, 2006

Moselhi O, Hegazy T, Fazio P (1991) Neural networks as tools in construction. J Constr Eng Manage. 117(4):606–625

Muqeem S, Idrus A, Khamidi MF, Zakaria SB (2011) Development of construction labour productivity estimation model using artificial neural network. J Constr Eng Manag 16:713–726

Nassr A, Javadi A (2018) Developing constitutive models from EPR-based self-learning finite element analysis. Int J Numer Anal Meth Geomech 42(3):401–417

Ni HG, Wang JZ (2000) Prediction of compressive strength of concrete by neural networks. Cement Concr Res 30(8):1245–1250

Oztas A, Pala M, Ozbay E, Kanca E, Caglar N, Bhatti MA (2006) Predicting the compressive strength and slump of high strength concrete using neural network. Constr Build Mater 20(9):769–775

Papadakis VG, Vayenas CG, Fardis MN (1991) Fundamental modeling and experimental investigation of concrete carbonation. ACI Mater J 88:363–373

Papadrakakis M, Papadopoulos V, Lagaros ND (1996) Structural reliability analysis of elastic-plastic strutures using neural networks and Monte Carlo simulation. Comput Methods Appl Mech Eng 136:145–63

Parthiban T, Ravi R, Parthiban GT, Srinivasan S, Ramakrishnan KR, Raghavan M (2005) Neural network analysis for corrosion of steel in concrete. Corros Sci 47(7):1625–1642

Possan E, Andrade JJO (2014) Markov Chains and reliability analysis for reinforced concrete structure service life. Mater Res 17(3):593–602

Poon CS, Kou SC, Lam L (2007) Influence of recycled aggregate on slump and bleeding of fresh concrete. Mater Struct 40:981–988

Rogers JL (1994) Simulating structural analysis with neural network. J Comput Civil Eng (ASCE) 8(2):252–65

Rosenblatt F (1958) The perceptron: a probabilistic model for information storage and organization in the brain. Psychol Rev 65(6):386–408

Rumelhart DE, Hinton GE, Williams RJ (1986) Learning internal representation by error propagation. In: Rumelhart DE et al (eds) Parallel distributed processing. MIT Press, Cambridge, MA, pp 318–362

Shafabakhsh G, Talebsafa M, Motamedi M, Badroodi S (2015) Analytical evaluation of load movement on flexible pavement and selection of optimum neural network algorithm. KSCE J Civil Eng 19(4):709–715

Silva ANR, Ramos RAR, Souza LCL, Rodrigues DS, Mendes JFG (2004) SIG: uma plataforma para introdução de técnicas emergentes no planejamento urbano, regional e de transportes: uma ferramenta 3D para análise ambiental urbana, avaliação multicritério, redes neurais artificiais. São Carlos, SP: Ed. dos Autores

Smets HMG, Bogaerts WFL (1992) SCC analysis of austenitic stainless steels in chloride-bearing water by neural network techniques. Corros Sci 48(8):618–623

Sonmez R, Rowings JE (1998) Construction labor productivity modeling with neural networks. J Constr Eng Manag 124(6):498–504

Stavroulakis GE, Antes H (1998) Neural crack identification in steady state elastodynamics. Comput Methods Appl Mech Eng 165:129–146

Taffese WZ, Sistonen E (2013) Service life prediction of repaired structures using concrete recasting method: state-of-the-art. Proc Eng 45:1138–1144

Topçu İB, Saridemir M (2007) Prediction of properties of waste AAC aggregate concrete using artificial neural network. Comput Mater Sci 41:117–125

Topçu İB, Boga AR, Hocaoglu FO (2009) Modeling corrosion currents of reinforced concrete using ANN. Autom Constr 18(2):145–152

Trasatti SP, Mazza F (1996) Crevice corrosion, a neural network approach. Br Corros J 31(2):105–112

Ukrainczyk N, Ukrainczyk V (2008) A neural network method for analysing concrete durability. Mag Concr Res 60(7):475–486

Vafaei M, Adnan AB, Rahman ABA (2013) Real-time seismic damage detection of concrete shear walls using artificial neural networks. J Earthquake Eng 17(1):137–154

Williams TP, Gucunski N (1995) Neural networks for backcalculation of moduli from SASW tests. J Comput Civil Eng (ASCE) 9(1):1–8

Wu X, Ghaboussi J, Garrett JH (1992) Use of neural networks in prediction of structural damage. Comput Struct 42(4):649–59

Zhang L (2017) Artificial neural network model design and topology analysis for FPGA implementation of Lorenz chaotic generator. In: 2017 IEEE 30th Canadian conference on electrical and computer engineering (CCECE), Windsor, ON, pp 1–4

Zhu X, Zi G, Cheng X (2016) Combined effect of carbonation and chloride ingress in concrete. Constr Build Mater 110:369–380

Pre-diagnosis Protocol for Large Residential Building Stock. The Case of Barcelona's Vulnerable Areas

C. Cornadó, S. Vima-Grau, and P. Garcia-Almirall

Abstract The large-scale evaluation of buildings is an important tool to guarantee that our cities are in good condition. This chapter presents the experience of a pre-diagnosis protocol applied to the most socially vulnerable neighborhoods in Barcelona. The protocol was specifically designed for this purpose and proposes a methodology in several elimination phases, in which attention is gradually focused on buildings that may be damaged and could lead to risk situations. The protocol was used to evaluate buildings in 16 neighborhoods of Barcelona. The original characteristics of the buildings varied widely, but all of them had suffered from a lack of building maintenance over decades. The results provide extensive information about the constructed reality of these neighborhoods and general and specific knowledge about the state of conservation of the buildings and their actual damage.

Keywords Refurbishment · Building assessment · Housing refurbishment · Pre-diagnosis protocol

C. Cornadó (✉) · S. Vima-Grau
Grupo de Investigación Rehabilitación y Restauración Arquitectónica (REARQ), Departament de Tecnologia de l'Arquitectura, Universitat Politècnica de Catalunya - Barcelona Tech (UPC), Barcelona, Spain
e-mail: cossima.cornado@upc.edu

S. Vima-Grau
e-mail: sara.vima@upc.edu

P. Garcia-Almirall
Grupo Consolidado de investigación Calidad de vida urbana: sostenibilidad, rehabilitación e innovación IQURB, VIMAC Lab, Departament de Tecnologia de l'Arquitectura, Universitat Politècnica de Catalunya - Barcelona Tech (UPC), Barcelona, Spain
e-mail: pilar-garcia.almirall@upc.edu

1 Introduction

Proper maintenance and updating of buildings are essential to maintain the building stock, and consequently cities, in good condition. One tool to guarantee good condition is the establishment of diagnostic protocols for existing buildings (Díaz et al. 1993). However, this is a challenge when it comes to evaluating large building stock, due to the extent of the work to be done and the mobilization of necessary resources. Diagnosis of large, privately-owned urban developments often entails management difficulties.

In recent years in Spain, building inspection protocols have been established that are mandatory for buildings over 50 years old. These are known as Technical Building Inspections (ITEs) (Ley 2013; Monjo et al. 2002; ITE 2005). ITEs transfer the responsibility for diagnosing buildings and subsequently carrying out refurbishments to private initiative. With this legislation, the preservation and improvement of safety, habitability, accessibility and sustainability of existing buildings are sought.

Unfortunately, in neighborhoods with the most vulnerable economic and social conditions (Castel 1990; Beck 2001; UN 2003), homeowners cannot afford the expense of carrying out inspections to diagnose their building or the subsequent refurbishment that may result from an inspection. It is precisely these neighborhoods that tend to have a greater need for refurbishment, as years have passed without any maintenance due to a lack of financial resources, leading to the progressive deterioration of buildings (Thomsen et al. 2015a, b).

In this context, Barcelona City Council observed that public aid for building refurbishments did not usually reach the most vulnerable sectors of society (Ajuntament de Barcelona 2016; Tapada and Arbaci 2011). There were several reasons for this, including a lack of knowledge of administrative processes, a lack of coordination among residents, situations of late payment and ignorance of the language. Therefore, in 2017, the City Council started a new line of refurbishment grants designed for these vulnerable communities (Ajuntament de Barcelona 2016; DOGC 2018). In this line, the city council had to take a proactive position, and identify buildings in poor condition in the most vulnerable areas of Barcelona, through a multidisciplinary team that communicates with the community and facilitates the procedures and resources required to complete the refurbishment of buildings as necessary.

To identify buildings that are a priority for refurbishment grant programs, Barcelona City Council commissioned the Universitat Politècnica de Catalunya (UPC) to design and apply a pre-diagnosis protocol for the buildings (Cornadó and Garcia-Almirall 2017). This protocol should be applied to areas that were previously identified as especially vulnerable within the residential fabric of the city (Garcia-Almirall et al. 2017), with a large building stock that has a range of technical characteristics and buildings constructed during different periods.

This chapter describes the pre-diagnosis protocol, explains the methodology used and provides the main results of the study to characterize the buildings, their general condition and the main damage observed.

2 Objectives

The main objective is to provide and validate a large-scale diagnostic protocol that can be applied to residential buildings.

The following objectives are established as secondary objectives within the scope of vulnerable residential stock in Barcelona:

- Provide a general understanding of the state of the buildings in relation to potential hazards to people, habitability and accessibility.
- Characterize the construction of vulnerable residential building stock in Barcelona and classify it into building types.
- Systematize the main damage and shortcomings observed in the buildings.
- Establish possible relationships between the construction characteristics of the buildings and the damage found in them.
- Establish priority levels in the need for refurbishment in the study areas.

3 Methodology

3.1 Selection of the Study Areas

A study was carried out in Barcelona in 2017 to create a map of residential vulnerability (Garcia-Almirall et al. 2017). Residential vulnerability is defined as a set of objective conditions in the residential space that indicate situations of social discrimination and structural disadvantage of the population, related to a specific time and context (Castel 1990; Beck 2001; UN 2003). The methodology followed in this study was based on a system of indicators drawn up through the use of statistical data, complemented with very specific data supplied by Barcelona City Council. Overall urban vulnerability within the city of Barcelona was studied in three areas: socio-economic, socio-demographic, and residential and socio-urban (Cornadó et al. 2017). As mentioned above, the result was a general vulnerability map with a vulnerability index on a scale.

It was agreed with the city council that to undertake the pre-diagnosis of buildings in vulnerable areas, three levels of vulnerability should be included in the sample: high, pronounced and extreme.

However, not all areas with these three levels of vulnerability were included in the pre-diagnosis study of buildings. The aim of the study was to start a proactive campaign of refurbishment grants (DOGC 2018) that was applicable to 16 of the neighborhoods included in the areas of maximum vulnerability in Barcelona. Some of the vulnerable areas were excluded. These 16 neighborhoods were included in Barcelona's Neighborhoods Plan (2017) (Ajuntament de Barcelona 2016), a municipal program to reverse inequalities between neighborhoods by promoting, among others, actions and grants for building conservation in complex communities (see Sect. 1, Introduction).
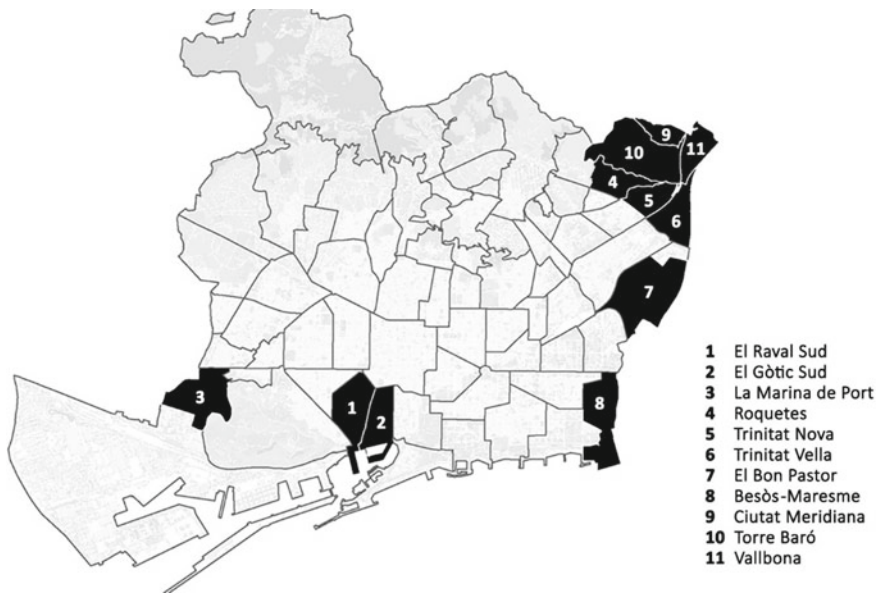
Fig. 1 Location of the studied areas

Figure 1 shows the areas selected for inclusion in the pre-diagnosis study, in which the pre-diagnosis protocol was applied to residential buildings. One of the main challenges was to apply the same protocol to buildings in different neighborhoods and times of construction. The study included areas of the historic center (El Raval Sud and Gotic Sud), large housing estates from the mid-20th century (Trinitat Nova, Besòs-Maresme, Ciutat Meridiana), areas with a combination of suburban growth of the mid-19th century and beginning of the 20th and urban fabrics in closed blocks of the mid-20th century (La Marina de Port, Roquetes, Trinitat Vella, El Bon Pastor) and buildings in originally informal urban developments (Torre Baró and Vallbona).

3.2 Pre-diagnosis Protocol

Faced with the difficulty of covering such vast, diverse building stock, a specific methodology was designed for the pre-diagnosis, with various levels of approximation. The methodology consisted of two inspection phases and an intermediate phase to validate the results (Fig. 2). The first phase consisted of selecting buildings in the study areas (sample) and carrying out an initial pre-diagnosis from the outside. As a result of this first phase, buildings were prioritized according to their state of conservation and need for refurbishment. These results were then discussed with neighborhood and district technicians in various meetings to compare them with the experience of technicians who work every day in the field and thus verify

Fig. 2 Methodological phases of the pre-diagnosis process
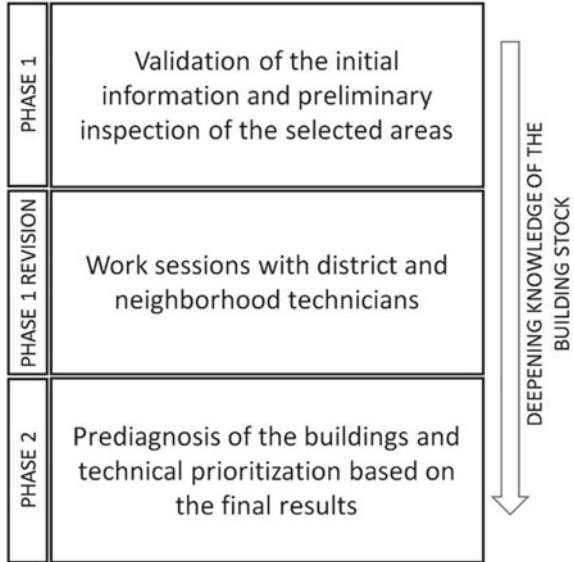
them. In this review phase, consensus was reached on the buildings with the greatest need for refurbishment. Finally, in a second inspection phase, through contact with technicians and neighborhood entities that provided access to the buildings, interior inspections were carried out to further examine the level of severity of the damage in buildings. Figure 2 summarizes the methodological process for the pre-diagnosis protocol of the buildings that were studied. In the following paragraphs, the specific methodology of each of the protocol phases will be described.

3.2.1 Phase 1: Validation of the Information and Preliminary Inspection

As mentioned above, this phase consisted of two stages. A first stage of work with the available data and initial selection of the buildings to be studied (establishment of the sample), and a second stage of on-site inspection.

(a) *Preliminary phase before the inspection*

To limit the study sample, residential buildings within the study areas were selected and the following were discarded:

- buildings that had been refurbished in the last 10 years
- buildings built after 1980

Table 1 List of the areas and number of residential buildings included in the study

District	Neigborhood	Studied buildings
1st district: Ciutat Vella	El Raval Sud	671
	El Gòtic Sud	328
3rd district: Sants Montjuic	La Marina de Port	124
8th district: Nou Barris	Roquetes	583
	Trinitat Nova	109
	Ciutat Meridiana	54
	Torre Baró	355
	Vallbona	94
9th district: Sant Andreu	Trinitat Vella	345
	Bon Pastor	254
10th district: Sant Martí	Besòs-Maresme	188

The final sample consisted of a total of 3633 buildings in 16 neighborhoods (Table 1). Although the protocol was applied to all buildings in the sample, it was decided to deliver the results separately by type of ownership, i.e. vertical or horizontal, as this affects the type of refurbishment policy to be applied.

(b) *Inspection phase*

All the buildings in the sample were inspected from the outside. The inspections were carried out by technicians with experience in building assessment. The following actions were carried out:

- Data was collected on observed visible damage. The focus was points of the façades that could accumulate damage and could denote a poor state of conservation of the building. The indicators that were considered were: cracks in façade walls, façade buckling, unstable façade elements, presence of security nets, rusty metal elements, cracks in the facing, dampness, windows without frames and/or glass or bricked-up windows, degraded woodwork, lack of maintenance, stains and dirt, absence of elevator installation and height of the building.
- Assessment of the conservation state of each building and its need for refurbishment. Five indexes were established according to the state of conservation of the buildings. All buildings were given a rating according to their need for refurbishment on a scale of 5:1 urgent, 1.5 high, 2 necessary, 2.5 low and 3 very low. Buildings with urgent or high need for refurbishment have structural damage and/or risk of detachment of elements or materials from the façades, while buildings with a need for refurbishment have other non-risk evident damage. Buildings with low and very low need for refurbishment should only be maintained regularly. Figure 3 shows examples of buildings according to the need for refurbishment index. Indexing provides a sense of the urgency and need for refurbishment, to prioritize policy making.

Fig. 3 Need for refurbishment rating: 1 urgent, 1.5 high, 2 necessary, 2.5 low and 3 very low

The first exterior inspection phase also included the collection of data on the context of the neighborhood, its uses and activities.

The results of this phase are provided in georeferenced maps, building listings and databases.

3.2.2 Phase 1: Revision

After all the inspections that were carried out on the sample buildings, several meetings were scheduled with district technicians, neighborhood technicians and appropriate social agents in each case, some in the study areas directly, to:

- Verify the buildings to be included in the study areas.
- Compare the results of Phase 1 with local technicians' knowledge.
- Extend and complement the preliminary prioritization of buildings for the development of Phase 2 of the study.
- Facilitate contact with residents and entities and collect useful information for the development of Phase 2 of the study, which consisted of interior inspections of buildings.

In this phase, the detection of buildings that could be included in future refurbishment programs was communicated to the entities and the local government and consensus was reached on each case.

3.2.3 Phase 2: Pre-diagnosis and Technical Prioritization

This phase was based on a series of technical visits to the interior of buildings that were identified as having a higher index of need for refurbishment. To apply the protocol in the city of Barcelona, the study was limited to a total of 200 interior inspections. This did not include all buildings with the maximum level of need on the refurbishment index.

These buildings underwent an inspection similar to the Technical Building Inspections (ITE) that are mandatory in Spain and focus mainly on aspects of safety, accessibility and energy performance of buildings (Ley 2013). The information on the state of conservation and use of buildings was systematized on a card that was designed specifically for this research and reflected the characterization of the building from

the perspective of structure, habitability, accessibility and energy consumption; its pathological state (conservation and maintenance); and the gathering of information from users about use and coexistence in the building. Such data had to pave the way for further refurbishment in these buildings. Physical information included in the inspection card was:

- Building technical description

    Description of the structural system (vertical structure, horizontal structure, roof structure, foundation)
    Building envelope description (façades and roofs)
    Installations
    Sketch of the building

- Diagnosis of the building:

    Visible damage to the structure, envelope and facilities
    Accessibility conditions
    Sustainability
    As the pre-diagnosis protocol was applied to implement public refurbishment programs in buildings that house the most vulnerable communities in Barcelona, in this phase of the study, data of a social nature were collected from the buildings' neighborhood associations. This information focused on use and coexistence in the building: uses and activities, community, user profiles, usage habits, perception and satisfaction about the state of the building and the dwellings, etc.

4 Results

4.1 Characterization of Construction Building Types

A first distinction of building types can be established within the study areas according to their main morphological and construction characteristics.

Type 1: Historical buildings in closed blocks

Buildings of this group were built before 1940 using traditional techniques, with a structural system that consists of load bearing walls made from varying materials and with different widths depending on the date of construction and with unidirectional slabs (Giol et al. 1995; Arquitectura popular et al. 1988; Torres 2010; Busquets et al. 2004). We can find thick load bearing walls built with rubble masonry or rammed earth (pre-nineteenth century) and slender brick masonry walls (nineteenth and first half of the twentieth century). Floor slabs and deck slabs are usually unidirectional structures built with wood or metal beams, depending on the date of construction.

The façade of this type of buildings is a structural element with generally small openings, whether they are windows or balconies. Consequently, in terms of thermal

behavior effects, façades are continuous walls without thermal bridges and without thermal insulation. These buildings are in historical urban fabrics, meaning they are usually included in the protected heritage catalogue (Catàleg del patrimoni arqui-tectònic històrico-artístic de la ciutat de Barcelona 1987). This protection usually affects façades and common elements to a greater or lesser extent. In addition, the urban configuration of very narrow parcels and considerable building depth tends to compromise the habitability of housing units, due to insufficient ventilation and illumination in some rooms (Spain 2008).

This type of buildings (Figs. 4 and 5) can be found in: the historical center of Barcelona (El Raval and El Barri Gòtic), areas of suburban growth of the mid-19th century and beginning of the 20th century (Busquets et al. 2004) and economic housing "Cases Barates" in the El Bon Pastor neighborhood (1929).

Type 2: Buildings from the second half of the twentieth century in closed urban blocks

The buildings in this group have concrete structures. Most of them are made from concrete slabs and columns. However, some load bearing brick masonry walls combined with concrete slabs can be found (Azpilicueta 1939; Planells et al. 1950).

Fig. 4 Examples of Type 1 buildings. Top row: El Raval and El Barri Gòtic. Middle row: Areas of suburban growth. Bottom row Cases Barates in El Bon Pastor neighborhood

Fig. 5 Type 1 buildings' façades

The façade wall is not usually load bearing and this results in higher flexibility and larger openings. In many cases, floor slabs interrupt the façade walls, which generates thermal bridges. Galleries, setbacks and irregularities in the façade plane are common. Galleries are usually built with very thin walls that are not insulated and contain large openings, which generate very big surfaces where heat losses are considerable. Façade cladding can be continuous or discontinuous (including many cases of brickwork façades and plating).

Building typologies included in this group are highly variable, according to each urban fabric and morphology, although interior ventilation, illumination and circulation are better than in the case of traditional constructions. However, it is common to find rooms with insufficient surface area, and very highly partitioned housing types that were created for the traditional family of the twentieth century.

This type of buildings (Figs. 6 and 7) can be found in: Roquetes, Trinitat Vella, La Marina de Port and El Bon Pastor.

Type 3: Buildings in originally informal urban developments

Buildings included in Type 3 were created with construction techniques that are very similar to those of Type 2 buildings because the period of construction is the same. However, the structural configurations are sometimes similar to Type 1 buildings, with masonry bearing walls and unidirectional slab structures. Type 3 buildings were originally constructed in marginal urbanization areas, and most of them were self-constructed. In this kind of buildings, the quality of the construction techniques and systems cannot be guaranteed, because construction took place outside of any regulation framework. This type of buildings (Fig. 8) can be found within the study areas: in Torre Baró, Vallbona and an area of Roquetes.

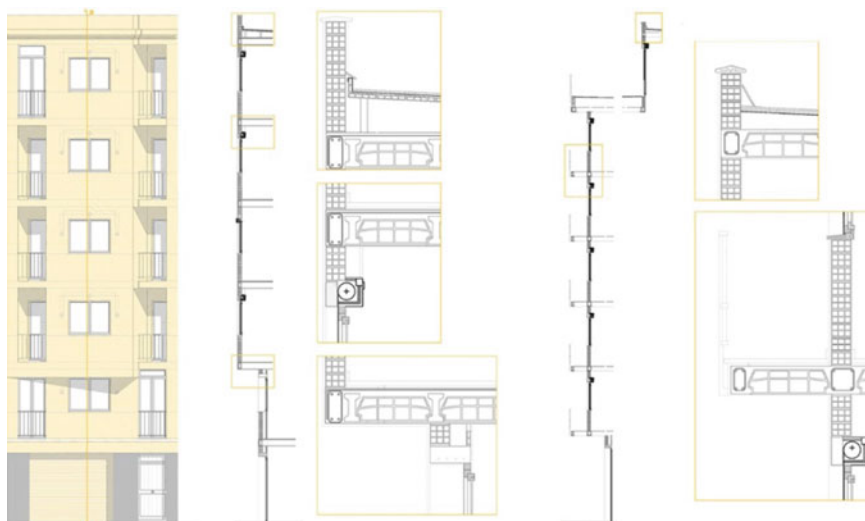**Fig. 6** Examples of Type 2 buildings. Top row: El Bon Pastor. Bottom row: Trinitat Vella

Fig. 7 Type 2 buildings' façades

Fig. 8 Examples of Type 3 buildings in Torre Baró and Vallbona

Type 4: Large housing estate buildings

This type of building is specific to open block urban fabrics, such as those of modern mass housing in large housing estates of the mid-20th century. These buildings are usually built with similar construction techniques to those of Type 2, usually in combination with the use of concrete in large complex systems and prefabricated panels for structural elements (Dutch tunnel system, prefabricated structures) and for the rest of construction systems (façade panels, balcony rails, cladding, etc.) (Díaz 1954; Ferrer 1996; Rosello 2011).

Type 4 buildings correspond to housing typologies that are specifically designed according to the needs of the conventional twentieth century family and are systematically repeated in large housing estates in linear block configuration. The functional layout of the housing units provides a systematic configuration for wet rooms and ventilation. The construction quality varies widely among the cases, depending on the urgency at the time of construction and the political economy that promoted the construction in each case.

This type of buildings (Figs. 9 and 10) can be found in: Ciutat Meridiana, El Sud-oest del Besòs, Trinitat Nova, and certain sectors of Roquetes, Trinitat Vella and La Marina de Port (Fig. 11).

Fig. 9 Examples of Type 4 buildings. From top to bottom: Ciutat Meridiana and Sud-oest del Besòs, Les Marines and Roquetes, Ciutat Meridiana and Trinitat Nova, and, finally Sud-oest del Besòs
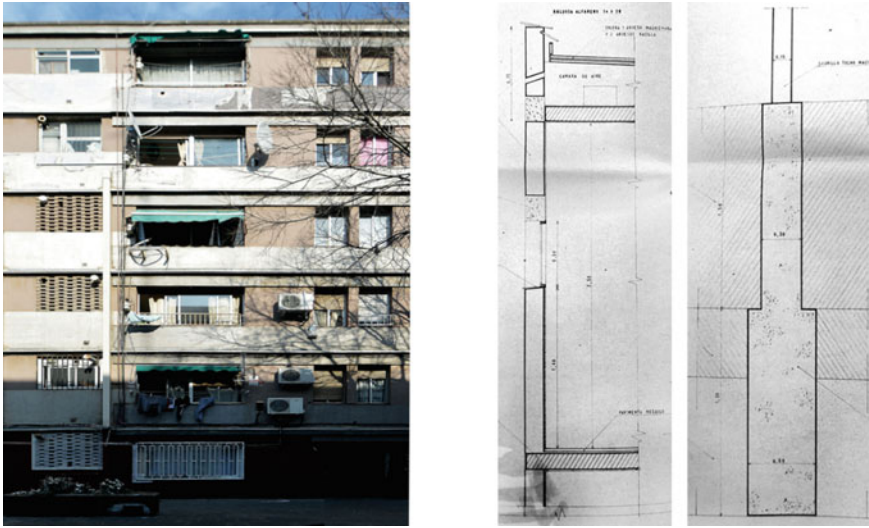
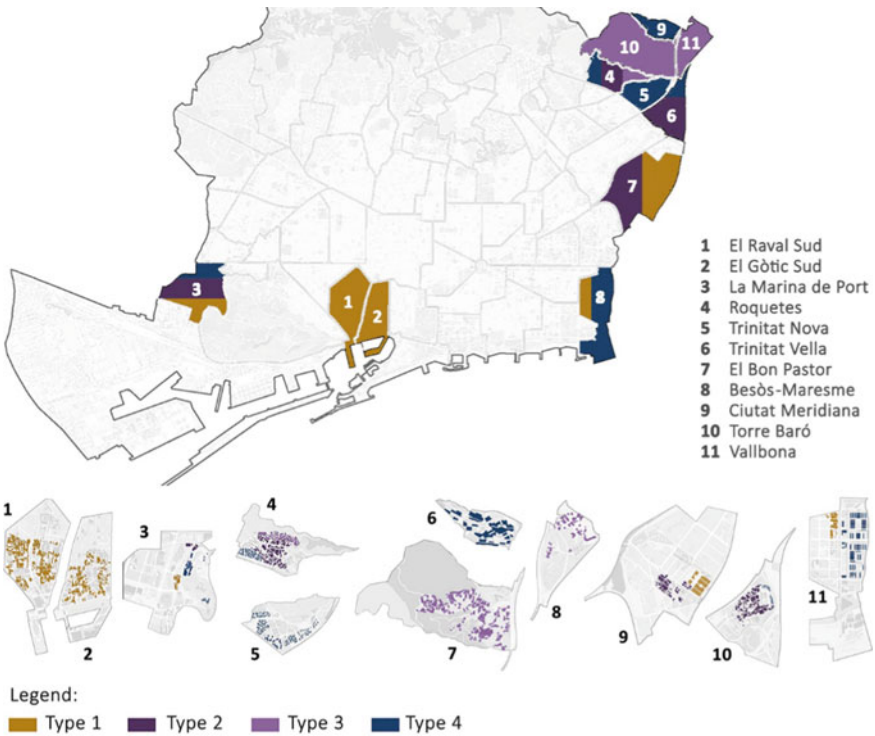**Fig. 10** Examples of Type 4 buildings' façade details (Rosello 2011)

1 El Raval Sud
2 El Gòtic Sud
3 La Marina de Port
4 Roquetes
5 Trinitat Nova
6 Trinitat Vella
7 El Bon Pastor
8 Besòs-Maresme
9 Ciutat Meridiana
10 Torre Baró
11 Vallbona

Legend:
■ Type 1   ■ Type 2   ■ Type 3   ■ Type 4

Fig. 11 Barcelona map where the different building types are indicated within the study areas

4.2 Description of Main Damage Observed

In this section, the main damage observed during the inspection campaigns in Phase 1 of the pre-diagnosis protocol is explained and grouped. These data were validated in the interior inspections. They can be grouped as follows:

(1) **Damage of mechanical, structural origin: cracks in façade walls and façade buckling**

This type of damage (Fig. 12) was observed in 13% of the cases, with different levels of risk according to its impact on the overall structural system or to the severity of rather localized damage.

A considerable percentage of cracks in façade walls were horizontal or slightly inclined and were found at the point of contact between the roof slabs and the façade. Thus, they can be attributed to the fact that the roof slab has different hygrothermal behavior, and expands more during the summer, which causes considerable thrusts to the façade's continuous wall. In cases in which façades are bearing walls subject to compressive stress, some vertical or 45° cracks were observed around window or door lintels. Another commonly observed type of damage was found in balcony slabs, where we observed cracks that could mostly be associated with corrosion of metal reinforcements. This very common damage, especially when it appears to be widespread in the building, was particularly severe in many cases. In only a very few cases, we could observe either a pattern of vertical continuous cracks in bearing façades subject to compression stress or a clear pattern of inclined cracks that can be associated with the wrong behavior of the foundations or the terrain causing differential settlements. In addition, the amount of observed buckling of façade bearing walls is very low, and in most cases some kind of repair had already taken place.

(2) **Unstable façade elements and risk of material detachment**

This group includes damage that could result in material detachment, with different levels of risk, although the severity is usually quite high, particularly in the case of

Fig. 12 Presence of damage of mechanical and structural origin and percentage within the total sample

high buildings that do not have any elements to prevent detachment. This damage was observed in 25% of the studied buildings and was one of the most typical types.

Some of the observed damage in these groups corresponded to unstable elements detaching from discontinuous cladding (especially ceramic tile cladding, vitreous coating and gresite, among others) located either in the ground floor cladding, on the entire façade surface, or in the frames of openings (parapets, jambs or less frequently lintels) and balcony flooring. In addition, observed damage included the risk of detachment of metal elements from 'brise soleils' or other metal elements attached to the façades, for instance, as protection for the fitting of installations. In another large group of cases, the risk of material detachment was associated with the presence of cracks or other damage caused mainly by humidity. Humidity can affect the main materials in façade walls (bricks, air-bricks, stone or mud, mortar or concrete), mortar or concrete in balcony slabs or continuous cladding materials, causing their deterioration and detachment.

Finally, the risk of material detachment has been observed in many cases in cornice elements affected by other damage such as dampness, cracks or even plant growth (Fig. 13).

In contrast with the high percentage of damage of considerable severity, prevention measures (Fig. 14) were only found in 5% of cases. Sometimes, they were associated with localized damage (a balcony, a part of the façade or the cornice), sometimes they were widespread and affected many elements of the building skin or even the

Fig. 13 Presence of unstable façade elements and risk of material detachment and percentage within the total sample

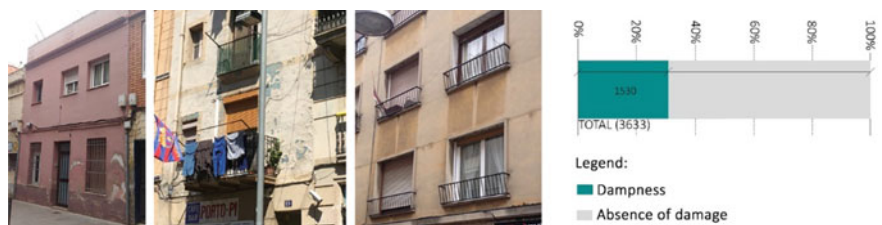**Fig. 14** Buildings with prevention measures applied

Fig. 15 Presence of dampness and percentage within the total sample

entire façade. An increase in the implementation of ITE inspections in Barcelona is leading to a rise in the percentage of prevention measures in buildings that need urgent refurbishment actions.

(3) **Presence of dampness**

Dampness is the most common type of damage that affected 30% of the studied buildings (Fig. 15) and is usually linked to corrosion of metal elements, stains and dirt, or even risks of material detachment and cracks, which generally damage elements or parts of the building.

A first group of dampness damage was observed in the base of the façade and interior walls as rising damp due to capillarity (Fig. 16). Basement continuous claddings usually have dirt, stains or detachments because of rising damp, and discontinuous claddings tend to detach. Wall materials such as mud, stone masonry or brick masonry are usually affected with considerable intensity up to 1 m, with salt crystallization and dissolution of joint material such as lime mortar.

In addition, some dampness damage was observed in locations that are exposed to rainwater leaking, such as cornices, balconies and elements in contact with openings (especially the walls of interior courtyards) (Fig. 17). In the case of cornices, the presence of discontinuous cladding or irregularities in material such as decorative elements, material alterations or cracks contributes to a greater impact in the presence of water leaks. Humidity is very common on the lower side of balcony slabs, while its severity increases to the degree that it affects metal reinforcements.

Fig. 16 Cases of rising damp due to capillarity

Fig. 17 Buildings with cornices, balconies and sills in poor condition

Fig. 18 Examples of water filtrations from interior services or water installations

Finally, some other types of dampness damage were observed at points of the façade in relation to possible water filtrations from interior services or water installations (rainwater or wastewater downspouts or water facilities) (Fig. 18).

(4) **Deficiencies in openings (glass enclosures and carpentry)**

Except for the few buildings that were not previously excluded from this study and that have been refurbished previously, all studied buildings were constructed prior to the first regulation that established the obligation of building with thermal insulation in Spain in 1979. Thus, energy efficiency shortfalls were found in all cases, which is why this section of damages includes more severe lacks of air and water tightness, usually due to damage of varying severity on windows, glass enclosures and carpentry that contributes to water filtration, lack of air tightness and thus very bad energy behavior. These kind of shortcomings were observed in 15% of cases.

A considerable number of buildings have severe observable deficiencies in the openings (Fig. 19). In some cases, the corresponding dwellings are empty. This was the case of bricked-up or blocked openings, and windows without any kind of glass or carpentry enclosure. There were also some cases of dwellings with signs of occupancy and serious damage too, such as windows with some broken glass, without glass enclosures, or very degraded woodwork. Nevertheless, in most cases it could be seen that the carpentry had not been renovated, the woodwork was degraded and the glass was single pane.
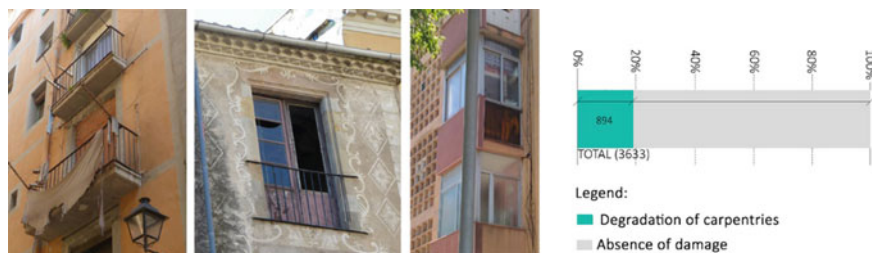
Fig. 19 Examples of deficiencies in the openings and percentage within the total sample

(5) **Deficiencies in accessibility**

As explained in the previous section, several deficiencies in accessibility (CTE 2018) within floors and accesses were widespread among the studied buildings (Fig. 20). Corridors and accesses to the dwellings as well as vestibules and access doors are not big enough. In addition, generally there are one or two steps at the exterior entrance to the building. In some cases, there are over five steps.

These shortcomings are widespread and affect almost the entire sample. Figure 20 includes only cases of considerable height (buildings over four stories) in which a lack of vertical accessibility (no elevator installation) is combined with the rest of the accessibility deficiencies. With a percentage of over 45% of cases, the lack of an elevator when it is needed is by far the most common shortfall in the building stock. In some cases, when the inner dimensions of the staircase or the courtyards are big
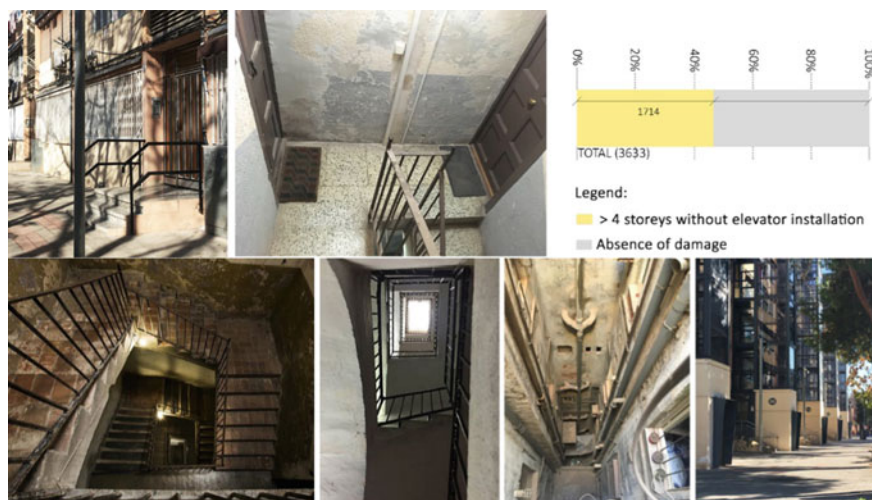

Fig. 20 Deficiencies in accessibility and percentage of 4 or more story buildings without elevator within the total sample

enough, an elevator could be installed. When these dimensions are too small (more commonly in Type 1 buildings) it is very complicated improve vertical accessibility.

4.3 State of Conservation and Need for Refurbishment

Observation of the state of conservation in the analyzed sample of cases (Fig. 21) shows how the proportion of cases in a reasonably good state (low or very low need of refurbishment) corresponded to 60% of cases. In contrast, the proportion of cases with urgent need of refurbishment (evidence of risk) corresponded to a fifth of the total sample.

The proportion of buildings that required refurbishment with some degree of urgency (urgent, high or necessary) was greater in the neighborhoods of El Bon Pastor, Torre Baró and La Marina de Port. This proportion was lower in the neighborhoods of Ciutat Meridiana and El Besòs.

However, if we focus on the highest level of urgency, the neighborhoods of El Bon Pastor, Torre Baró, El Raval (southern area), El Barri Gòtic (southern area), La Marina de Port and surprisingly Ciutat Meridiana had a higher percentage of cases, while the neighborhoods of Roquetes, Trinitat Vella, Vallbona and El Besòs had a lower proportion of cases in urgent need of refurbishment.

Taking into account that a quantitatively larger sample was analyzed in El Bon Pastor, Torre Baró and particularly El Raval and El Barri Gòtic, this high proportion of cases with an urgent need of refurbishment translates into a high number of affected buildings in those areas, particularly in El Bon Pastor.
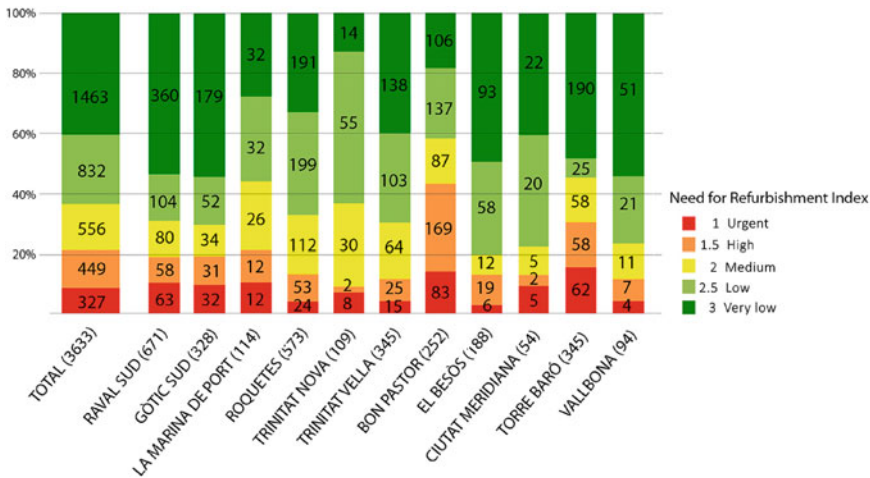

Fig. 21 Need of refurbishment index comparison between neighborhoods

In some neighborhoods, the proportion of cases that needed some refurbishment with a lower degree of urgency (no evident risk) was much higher than the proportion of cases in urgent need of refurbishment. This was the case of Trinitat Nova, Roquetes, La Marina de Port, Trinitat Vella and Vallbona.

Although the variability between neighborhoods in the percentage of buildings requiring some refurbishment measure at different levels was quite small (with few exceptions), the percentage of buildings in a very good state was much more variable. The areas with the highest proportion of buildings in such a state were El Raval, El Barri Gòtic, El Besòs, Torre Baró and Vallbona, while the neighborhoods of Trinitat Nova, El Bon Pastor, Roquetes and La Marina de Port had a much lower proportion. If we take into account the quantitative differentiation of the sample per neighborhood, the number of cases in a very good state of conservation according to an exterior inspection was higher in El Raval, Torre Baró, Roquetes, El Barri Gòtic, Trinitat Vella and El Besòs.

Finally, mapping of refurbishment need results shows how the observed variety in states of conservation within each of the neighborhoods translated into considerable geographic variability of results (Fig. 22). It was impossible to identify areas of a certain scale that were uniformly well-conserved, or areas of a certain scale that were uniformly deprived. In addition, it was common to observe how cases that required urgent refurbishment appeared to be adjacent to cases in a very good state of conservation.

4.4 Cross Analysis of Damage and Building Types Per Neighborhood

In this section, Figs. 23, 28, 30, 32 and 34 show how each of the previously described types of damage had a similar presence in the studied buildings. Close to 20% of mechanical structural damage, 25% risk of material detachments, 30% dampness, close to 20% degraded carpentry, and over 45% of severe deficiencies in accessibility. This balance, as well as the proportion of each kind of damage, varied widely depending on the neighborhood and therefore in relation to the construction building types that mainly characterized each neighborhood.

Firstly, mechanical structural damage appeared to be found quite uniformly in the neighborhoods, regardless of the construction building type, in 15–20% of cases (Fig. 23). The highest percentages were in El Bon Pastor, Torre Baró, El Besòs and El Barri Gòtic. In the first case, the observed damage corresponded mainly to cracks in cornices and lintels of mostly abandoned and very poorly maintained buildings (Fig. 24) in the area of 'Cases Barates' (economic housing) (Type 1). This repetition of the same kind of damage was generally quite unique to this area, although similar damage was observed in some cases of low Type 1 buildings, such as typologies of suburban growth of the nineteenth century in La Marina de Port.
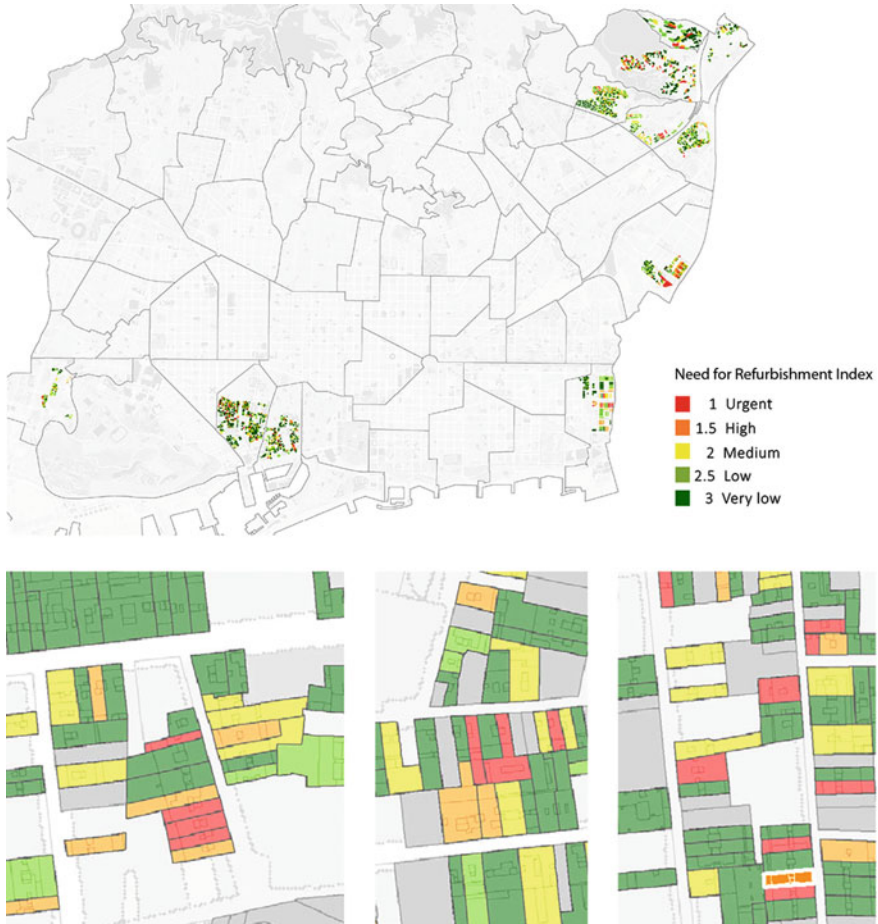
Fig. 22 Need for refurbishment index in the studied areas (top) and close up views in different neighborhoods (bottom)

In the case of Torre Baró (Type 3), the observed deficiencies were much more varied, and differed between considerable structural deficits in precarious self-constructions to other less relevant cracks in bearing walls around window or door lintels (Fig. 25). This combination of damage characterized, to a lesser extent, other areas with the same construction building types (Roquetes and Vallbona, Type 3).

Cracks observed in high linear block buildings in El Besòs (Type 4) were associated with old, mostly repaired serious damage in bearing walls with insufficient foundations (Díaz 1954), and other currently ongoing problems associated with deterioration in balconies and other slab elements built with aluminous cement (Fig. 26). Even though El Besòs was very specific for this problem, similar concrete pathology and damage associated with the deterioration of balcony slabs were observed in both
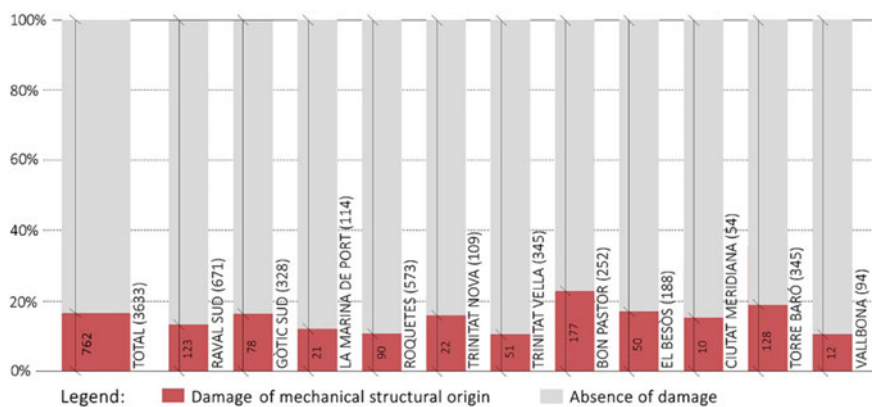
Fig. 23 Percentage of damage of mechanical structural origin and risk of material detachment within the sample

Fig. 24 Cracks in cornices and lintels in type 1 buildings

Fig. 25 Damage in type 3 buildings

neighborhoods with buildings of Type 2, Type 3 and particularly Type 4 (Ciutat Meridiana and Trinitat Nova).

Finally, observed damage in El Barri Gòtic (Type 1) (Fig. 27) differed from processes of buckling of load bearing façade walls that had mostly been repaired, cracks around window and door lintels, cracks in balcony slabs due to the corrosion

Fig. 26 Damage in balcony slabs

Fig. 27 Cracks and damage in load bearing façades

of metal elements and, in occasional cases, widespread structural damage observable with cracks that affected the whole length of the façade. Similar damage was observed in El Raval and other construction buildings of Type 1, with the exception of façade buckling that was more specific to El Barri Gotic, where buildings are older.

Notably, Types 2 and 3 buildings, with the exception of Torre Baró, had a lower percentage of damage of mechanical structural origin, as observed in the exterior inspection.

Secondly, unstable elements (Figs. 28 and 29) were observed in much more variable proportions among the neighborhoods (between 20 and 60%). Trinitat Nova was a distinctive case in which there was a very high percentage of buildings with unstable elements in the façade. This damage was greater in neighborhoods where Type 1 and Type 2 are predominant. In the first (Type 1), damage was mainly observed in balconies, cornices and continuous cladding, while in buildings from Type 2, these types of damage mostly appeared in façade plating and other elements besides balconies, and was similar to the observed damage in Trinitat Nova and linear blocks in El Besòs (Type 4). Curiously, in neighborhoods where Type 3 buildings are predominant, the amount of damage was considerably lower (Roquetes, Vallbona, and relatively low in Torre Baró).

Figure 30 presents damage related to bad hygrothermal behavior of the envelope due to the presence of humidity. These percentages were quite variable among neighborhoods. The percentage of buildings affected by dampness varied from just under
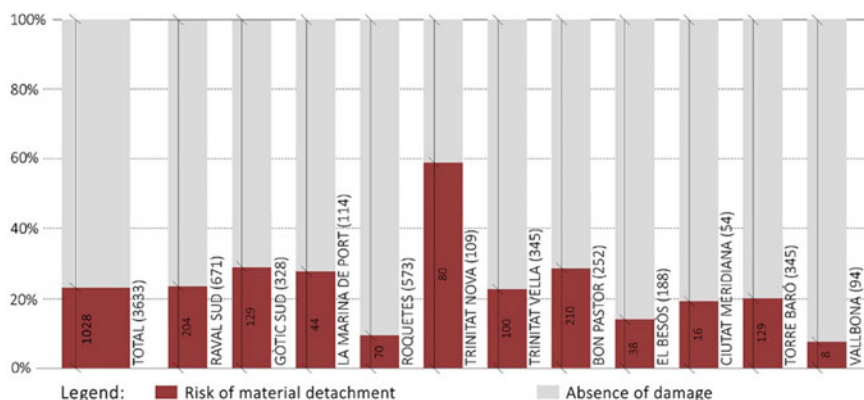
Fig. 28 Percentage of risk of material detachment

Fig. 29 Material detachment in façades

20% in Trinitat Vella, El Raval and El Barri Gòtic, and Vallbona and slightly over 20% in Torre Baró, to around 40% in La Marina de Port, Roquetes, Trinitat Nova, El Besòs and Ciutat Meridiana, and 60% in El Bon Pastor. Since the presence of dampness is associated with other observed types of damage, it is indicative of the general state of maintenance of the façade.

As mentioned above, it can be assumed that some of the single family buildings in Torre Baró and Vallbona have carried out refurbishment and maintenance actions, while the public programs to improve building façades in the historical center may have contributed to a lower percentage of damage in El Raval and El Barri Gòtic.
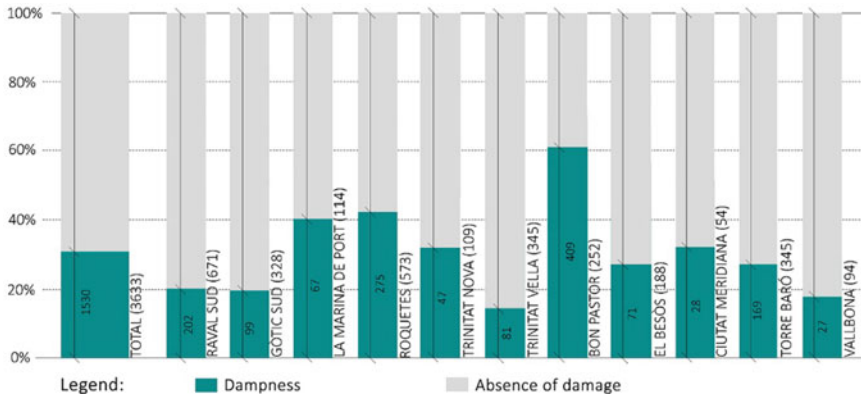
Fig. 30 Percentage of buildings with damage due to dampness

Other neighborhoods have significant percentages of damage, at around 40%, regardless of the building construction type (Types 1, 2 and 4) (Fig. 31). The concentration of damage in El Bon Pastor was, once again, specific to the 'Cases Barates' area.

Regarding damage to carpentry and woodwork (Figs. 32 and 33), the percentages were considerably higher in Type 1 buildings (El Raval, El Barri Gòtic and La Marina de Port), mostly due to aging and deformation of woodwork. Percentages were also high in some neighborhoods characterized by Type 2 buildings (Trinitat Vella) and 4 (Ciutat Meridiana), where the carpentry is mostly old aluminum frames, sometimes with deteriorated sliding windows containing single-pane or non-transparent glass.

Finally, severe deficiencies in accessibility was the type of damage that varied most widely by neighborhood and was greater in many neighborhoods (Fig. 34). Logically, the variation can be explained by the fact that high buildings with no elevator installation depended strictly on building type and urban morphology.

The highest percentages were observed in the historical neighborhoods of El Raval and El Gòtic, with Type 1 buildings in which the installation of elevators is extremely complex due to the small dimension of inner courtyards and staircases (Fig. 35), but the buildings are higher than 4 stories.

This problem is also common in large housing estates (Type 4), although in these cases it usually affects only linear block buildings, while tower blocks and other higher buildings usually have elevators installed at the time of construction. This explains the small percentage of deficiencies in El Besòs, where the coexistence of different typologies (higher blocks with elevators, lower blocks with no elevators and single family houses) distorts the relevance of the number of dwellings with no elevator access (a percentage that would be more similar to that of Ciutat Meridiana) (Fig. 36).

Neighborhoods in which this damage is less significant usually consist of lower buildings, as in the case of urbanization areas that were originally marginal (Type 3) or the unique typology of 'Cases barates' in El Bon Pastor.

Fig. 31 Damage due to dampness observed in façades. Buildings of Type 1, Type 2 and Type 4
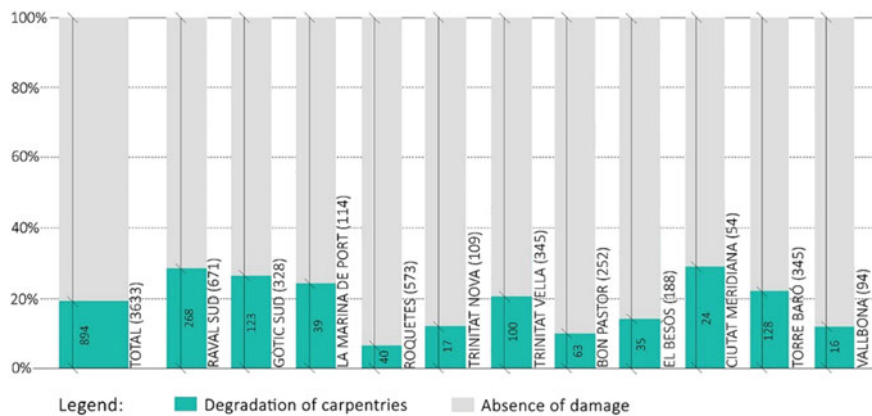

Fig. 32 Percentage of buildings with damage to carpentry and woodwork

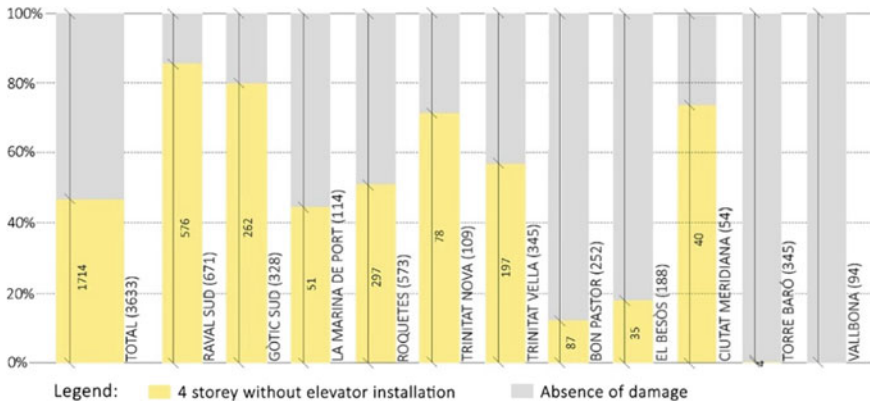**Fig. 33** Damage to carpentry and woodwork in buildings of Type 1 and Type 2 and 4

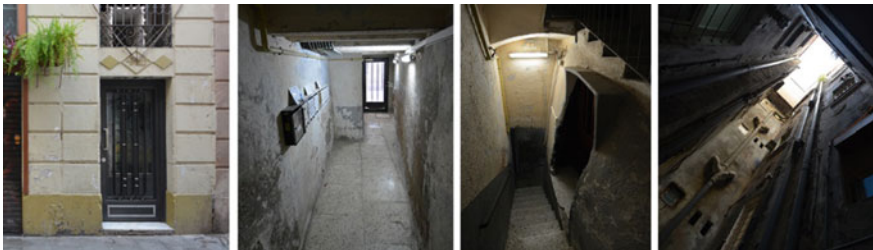**Fig. 34** Percentage of 4 or more story buildings without elevator

Fig. 35 Accessibility deficiencies in buildings of Type 1, in El Raval neighborhood

Fig. 36 Accessibility deficiencies in linear blocks of Type 4, in El Besòs neighborhood

Regarding the state of conservation (Fig. 21), the highest proportion of cases in urgent need of refurbishment correspond to the area of 'Cases barates' in El Bon Pastor (Type 1), followed by the neighborhood of Torre Baró (Type 3), and the neighborhoods of the historical center of the city, El Raval and El Barri Gòtic (Type 1).

El Bon Pastor and Torre Baró have particularly high percentages of cases with an urgent need of refurbishment, both quantitatively and in proportion. El Bon Pastor has a very large area that is affected by ongoing urban transformation that prevents some buildings from being refurbished, while the second corresponds to an urban development that was originally marginal and consists of mostly self-constructed buildings.

The proportion of cases in a very bad state of conservation was much lower in neighborhoods characterized by construction and building types 2 and 4. Surprisingly, 50% of buildings were in a very good state in the two neighborhoods of the historical center (Type 1), and in the two neighborhoods that were originally marginal and self-constructed (Type 3), while it was much lower in neighborhoods with buildings that were constructed between the 1950s and 1970s (Types 2, 3 and 4). This may be related with the public façade refurbishment programs carried out particularly in the historical neighborhoods of Ciutat Vella in Barcelona (Giol et al. 1995; Ripoll 1988), which had an impact on the good state of the building envelopes. In the case of buildings in a very good state in areas of originally marginal urbanization, their uniqueness in terms of property and typology (single family housing owned by tenants in building types that are usually not higher than two floors) may have made it more feasible to carry out improvements in many cases.

Finally, regarding the mapping and forms of aggregation of cases with a need for refurbishment, the aforementioned variation was, logically, common to all neighborhoods regardless of the building types and characteristics.

In neighborhoods comprised of clearly differentiated areas in terms of urban form and building types, the mapping showed remarkably different results according to building type. For example, the north-western area of El Besòs, comprised of Type 1 buildings, clearly had a higher concentration of buildings in a very good state, and cases with considerable evidence of risk were nonexistent. Similarly, the area of 'Cases barates' in El Bon Pastor (type 1) had the highest concentration of cases with

Fig. 37 Need for refurbishment index in El Bon Pastor (left) and Roquetes (right)

an urgent, high need for refurbishment, and could clearly be distinguished from other areas in El Bon Pastor with 3 and 4 type buildings. Finally, the south-western area of Roquetes, comprised of linear blocks and tower blocks built between the 1950s and 1970s (Type 4) was uniformly in a very good state of conservation according to the exterior inspection, while the northern part of the neighborhood comprised of an originally marginal urbanization of mostly self-constructed buildings had the highest concentration of buildings that need refurbishment with some degree of urgency, and the highest number of cases with evidence of risk in the neighborhood. Figure 37 shows the need of refurbishment index in El Bon Pastor and Roquetes.

Despite the differentiation in the mapping results in specific zones, it clear that on a smaller scale, per zone and within the same construction and building type, there was wide variety in the results and a dispersion of cases that had an urgent need for refurbishment. The most evident cases were probably those mapped in El Besòs and Ciutat Meridiana (Type 4) (Fig. 38), in which one building type of a linear block had cases in a very good state of conservation and cases with urgent need of refurbishment.

5   Conclusions

Once the pre-diagnosis protocol had been applied to residential buildings in the most vulnerable areas of Barcelona, the following conclusions were drawn on aspects of the characterization and assessment of the buildings.

The characterization of the buildings' construction was consistent with the year of construction and the urban context. Four building types were differentiated considering their morphological and construction characteristics. One type corresponds to historical buildings built with historical construction techniques, while three types built with modern construction techniques were distinguished: buildings from the

Fig. 38 Need for refurbishment index in El Besòs (left) and Ciutat Meridiana (right)

second half of the twentieth century in closed urban blocks, buildings that were originally in informal urban developments and buildings in large housing estates.

In terms of the general state of conservation of the buildings and their need for refurbishment, a low percentage of buildings urgently required refurbishment to guarantee safety (between 5 and 10%). The highest percentages of buildings with urgent need of refurbishment correspond to historical buildings (Type 1) or self-constructed buildings (Type 3). However, in construction types built with modern construction techniques (Types 2, 3 and 4), the percentage of buildings that need some type of refurbishment, regardless of severity, was greater than in types built with historical techniques (Type 1). No correlation was found between the amount of damage observed and its severity. In other words, there was no correspondence between the amount or diversity of damage in a building and its need for refurbishment. This contributes to validating the methodology that was used, and proves the need for the use of a global qualitative index to assess the need for refurbishment, in addition to the damage quantitative analysis.

Regarding the geographical distribution of the state of conservation of the buildings, wide variation was observed in all neighborhoods in the sample, regardless of building type. It was not possible to delimit areas on a large scale where the results were uniform. This makes it difficult to establish perimeters in which specific measures could be implemented. The design of refurbishment programs needs to incorporate tools that consider the existing variation, to achieve interventions that are flexible enough to address the very different nature of small delimitated areas while, at the same time, attempting to reach an extensive scope that can address the large dispersion of damage and degraded cases.

In general, the pathological states of the buildings studied can be associated with a prolonged lack of maintenance for years, which reflects the vulnerable social situation of the inhabitants. However, a relationship can be established between the type of

damage present and the building types. In traditional construction building types (Type 1), the damage observed in façades was concentrated in cornices and balconies, while more modern buildings had more damage related to unstable façade elements such as plating. In contrast, the presence of cracks or other damage of mechanical structural origin, and the presence of dampness, were common types of damages that appeared uniformly in all building types, regardless of their age and construction techniques.

In terms of accessibility, the building types with the most deficiencies were historical buildings (Type 1) and mid-rise buildings on large housing estates (Type 4).

Finally, some conclusions should be made about the methodology used in the pre-diagnosis protocol. It is confirmed that the methodology used in Phase 1 is consistent with the results obtained in Phase 2, thereby validating the results of Phase 1 on the total sample. It is also verified that the accompaniment and support of neighborhood technicians and entities is very important to obtain higher quality results. Likewise, contact with neighborhood agents and technicians facilitates access to the buildings for a second phase and paves the way with neighbors for the implementation of future refurbishment programs. Likewise, it is verified that large building stock can be assessed using a protocol of this type, with the methodology in several phases to deepen knowledge of the buildings.

References

Ajuntament de Barcelona (2016) Pla pel Dret a l'Habitatge de Barcelona 2016–2025. Resum executiu

Ajuntament de Barcelona: Pla de Barris. https://pladebarris.barcelona/ca

Azpilicueta E (2004) La construcción de la arquitectura de postguerra en España (1939–1962). Doctoral Thesis, Universidad Politécnica de Madrid

Beck U (2001) The society of risk. On the road to another modernity. Aubier, Paris, France

Busquets J et at (2004) The old town of Barcelona: a past with a future. Ajuntament de Barcelona ed., Barcelona, Spain

Castel R (1990) Disaffiliation: work and relational vulnerability. Hébergeur, Paris, France

Catàleg del patrimoni arquitectònic històric-artístic de la ciutat de Barcelona. Ajuntament de Barcelona (1987). http://hdl.handle.net/11703/101775

Código Técnico de la Edificación (CTE) (2018) Documento Básico de Seguridad de utilización y accesibilidad (SUA). DB-SUA/2: Adecuación efectiva de las condiciones de accesibilidad en edificios existentes

Cornadó C, Garcia-Almirall P, Vima-Grau S (2017) Prediagnosi de l'edificació residencial en els àmbits de vulnerabilitat de la ciutat de Barcelona. Ajuntament de Barcelona

Cornadó C, Garcia-Almirall P, Vima-Grau S, Vila G, Uzqueda A (2017) Methodology for the detection of residential vulnerable areas—the case of Barcelona. In: IOP conference series materials science and engineering, vol 245. https://doi.org/10.1088/1757-899x/245/4/042062

Diari Oficial de la Generalitat de Catalunya (DOGC): Anunci de la Convocatòria del Programa de Finques d'Alta Complexitat. Núm 7642-14.6.2018. CVE-DOGC-A-18157071-2018 (2018)

Díaz C (1986) Aproximación a la evolución y el comportamiento derivado de las técnicas constructivas utilizadas en los tipos edificatorios exentos destinados a la vivienda económica en Cataluña (período 1954–1976). Doctoral thesis, Universitat Politècnica de Catalunya

Díaz C, Ferrer A, García R, Ulla A (1993) Els teixits edificats: transformació i permanencia. PAPERS. Regió Metropolitana de Barcelona 15

Ferrer A (1996) Els polígons a Barcelona. Edicions UPC, Barcelona, Spain

Garcia-Almirall P, Vila G, Vima-Grau S, Uzqueda A (2017) Estudi i detecció a la ciutat de Barcelona d'àmbits de vulnerabilitat residencial. Ajuntament de Barcelona

Giol P (1995) La casa de veins del segle XIX a Barcelona. Doctoral thesis, Universitat Politècnica de Catalunya, Barcelona, Spain

ITE (2005) Protocolo de Inspección Técnica de Edificios. Colegio Oficial de Arquitectos de Sevilla, Fundación FIDAS, Sevilla, Spain

Ley 8/2013, de 26 de junio, de rehabilitación, regeneración y renovaciones urbanas. Gobierno de España (2013)

Monjo J (2002) Manual para la inspección técnica de edificios. Ed. Munilla-Leria, Madrid, Spain

Planells A, Cornadó C, Díaz C (2013) Housing Typology in Santa Coloma de Gramanet (Barcelona) 1950–75. A methodology for analysis and further improvement of common housing. In: XXXIX IAHS World Congress on Housing. Milano, Italy. https://doi.org/10.13140/2.1.2855.9684

Ripoll R (1988) Arquitectura popular, reflexions vers una nova lectura. Quaderns de la Selva 2. Centre d'estudis selvatans **2**, 217–223. Santa Coloma de Farners, Barcelona, Spain

Rosello M (2011) Las técnicas de construcción utilizadas en la construcción del polígono residencial del Sud-Oest del Besós. Barcelona 1959–1961. In: Séptimo congreso nacional de historia de la construcción. Santiago de Compostela, Spain, pp 1233–1245 http://hdl.handle.net/2117/81450

Tapada MT, Arbaci S (2011) Proyectos de regeneración urbana en Barcelona contra la segregación socioespacial (1986-2009): solución o mito? ACE Archit City Environ 6(17):187–222. https://doi.org/10.5821/ace.v6i17.2534

Tarragó S, Barrionuevo A, Martí C (2008) Exigencias de la Habitabilidad de los Centros Históricos. In: Habitabilidad y Ciudad. Escuela Técnica Superior de Arquitectura de Sevilla ed., Sevilla, Spain, pp 31–34

Thomsen A, Van der Flier K, Nieboer N (2015a) Analyising obsolescence, an elaborated model for residential buildings. Struct Surv 33(3):210–227. https://doi.org/10.1108/SS-12-2014-0040

Thomsen A, Nieboer N, Van der Flier K (2015) Obsolescence—understanding the underlying processes. In: ENHR 2015 conference Lisbon

Torres C, Díaz C (2010) Técnicas de Intervención para la recuperación de los sistemas constructivos en los edificios del centro Histórico de Barcelona. In: CINPAR-2010 VI Congreso Internacional sobre Patología y Recuperación de Estructuras

UN (2003) Report on the social situation of the world 2003. Social vulnerability: sources and challenges. United Nations Publications, New York, US